PHILOSOPHICAL MAGAZINE

eBook

Investigating magnetism with Monte Carlo simulations

Taylor & Francis
by informa

eBook

Investigating magnetism with Monte Carlo simulations

Contents

Taylor & Francis
by informa

Philosophical Magazine

ISSN: 1478-6435 (Print) 1478-6443 (Online) Journal homepage: www.tandfonline.com/journals/tphm20

Monte Carlo simulation study comparing the magnetic hysteresis of graphene and fullerene C_{60}

Z. Fadil, Chaitany Jayprakash Raorane, R. El Fdil, Khaled H. Mahmoud, Abdulrahman A. Alsayyari & Seong-Cheol Kim

To cite this article: Z. Fadil, Chaitany Jayprakash Raorane, R. El Fdil, Khaled H. Mahmoud, Abdulrahman A. Alsayyari & Seong-Cheol Kim (2026) Monte Carlo simulation study comparing the magnetic hysteresis of graphene and fullerene C_{60}, Philosophical Magazine, 106:4, 366-379, DOI: 10.1080/14786435.2025.2557562

To link to this article: https://doi.org/10.1080/14786435.2025.2557562

PHILOSOPHICAL MAGAZINE
2026, VOL. 106, NO. 4, 366–379
https://doi.org/10.1080/14786435.2025.2557562

Taylor & Francis
Taylor & Francis Group

Monte Carlo simulation study comparing the magnetic hysteresis of graphene and fullerene C_{60}

Z. Fadil[a]*, Chaitany Jayprakash Raorane[b]*, R. El Fdil[a], Khaled H. Mahmoud[c], Abdulrahman A. Alsayyari[d] and Seong-Cheol Kim[b]

[a]Laboratoire de Matière Condensée et Sciences Interdisciplinaires (LaMCScI), Faculty of Sciences, URL-CNRST, Mohammed V University in Rabat, Rabat, Morocco; [b]School of Chemical Engineering, Yeungnam University, Gyeongsan, Republic of Korea; [c]Department of Physics, College of Khurma University College, Taif University, Taif, Saudi Arabia; [d]Department of Radiologic Technology, College of Applied Medical Sciences, Qassim University, Buraydah, Saudi Arabia

ABSTRACT

This study uses Monte Carlo simulations to provide a comparative analysis of the magnetic hysteresis behaviours of graphene and fullerene C_{60} nanostructures, focusing on the influence of structural geometry and parameter variations on their magnetic behaviour. The magnetic hysteresis behaviours of graphene and fullerene C_{60} were compared, focusing on the effects of linear (J) and biquadratic (K) exchange coupling interactions, as well as temperature (T). Fullerene C_{60}, with its 3D spherical structure, exhibits a higher coercive field (H_C) than planar 2D graphene. The study demonstrates how adjustments to structural and coupling parameters can fine-tune the magnetic properties of nanostructures, offering valuable insights for applications in nanotechnology and magnetic data storage.

ARTICLE HISTORY
Received 23 May 2025
Accepted 30 August 2025

KEYWORDS
Graphene; fullerene C_{60}; magnetic hysteresis cycles; Monte Carlo simulations; coercive field

1. Introduction

Two-dimensional (2D) materials have significantly impacted nanotechnology by providing remarkable physical and chemical properties [1–3]. These materials, characterised by their high surface-area-to-volume ratios, excellent electronic conductivity, and adjustable magnetic properties, are highly promising for various applications [2,4–6]. They are particularly useful in developing sensors, flexible electronics, and magnetic data storage devices [7,8]. Among the 2D materials, graphene and fullerene C_{60} are noteworthy due to their distinct shapes and properties. Graphene is a planar sheet where carbon atoms are interconnected in a honeycomb-like array, while fullerene C_{60} forms a spherical structure [9,10]. These different geometries lead to unique magnetic and structural characteristics. For example, graphene-based materials have been shown to enhance the performance of magnetic storage systems by increasing durability and reducing

CONTACT Z. Fadil fadilzakaria604@gmail.com Laboratoire de Matière Condensée et Sciences Interdisciplinaires (LaMCScI), Faculty of Sciences, URL-CNRST, Mohammed V University in Rabat, P.O. Box 1014, Rabat, Morocco; Chaitany Jayprakash Raorane chaitanyaraorane22@ynu.ac.kr; Seong-Cheol Kim sckim07@ynu.ac.kr School of Chemical Engineering, Yeungnam University, Gyeongsan 38541, Republic of Korea
*Authors contributed equally

friction, which is crucial for creating high-density magnetic media [11–13]. On the other hand, functionalised fullerene structures have demonstrated potential in incorporating spin-carrying units on graphitic substrates, broadening their use in nanotechnology [14–16]. The magnetic hysteresis properties of these nanomaterials are particularly critical for their integration into storage devices, as they determine their ability to retain magnetic states under varying external conditions [17,18]. Magnetic hysteresis, characterised by coercive field strength (H_C) and magnetic anisotropy, not only reflects intrinsic material stability but also informs practical design choices in data storage systems [19,20]. Recent advances in Monte Carlo simulations have significantly deepened our understanding of magnetic properties and hysteresis behaviour in a variety of nanostructures. Comparative studies of borophene β_{12}, χ^3 and striped geometries, have provided valuable insights into the magnetic properties of two-dimensional materials and enriched our understanding of structure-dependent magnetic responses [21]. Further simulations have focused on borospherene and Buckminsterfullerene structures, revealing unique magnetic properties in these novel structures [22]. Comparative study between honeycomb, kagome and triangular nanolattices have revealed the crucial role of lattice symmetry and topology in shaping magnetic and hysteresis behaviour [23]. In addition, research on graphene-like bilayer systems has revealed intriguing compensation temperature and hysteresis phenomena that open up a deeper perspective on layered magnetic materials. Monte Carlo simulations have also helped analyse specific nanostructures such as CrI_3 monolayers, hexacene-like frameworks, and perylene-like nanostructures, revealing compensation temperatures, ground state characteristics, and hysteresis properties that are closely related to their molecular design [24–26]. Hexagonal core–shell nanowires analysed within the Blume–Emery–Griffiths framework have further elucidated the critical and hysteresis behaviour, especially in systems with complex spin interactions [27]. These computational studies highlight the versatility of Monte Carlo methods in the study of nanoscale magnetism. By providing detailed insights into phase transitions, critical phenomena, and structure-dependent behaviour, this research underscores the importance of computational techniques for the development of magnetic materials for next-generation technologies, including spintronics and memory devices.

To enhance our understanding of these phenomena, this study utilises Monte Carlo simulations grounded in the Blume-Emery-Griffiths model [28,29]. By replacing carbon atoms with spin-1 sites, we examine how structural and coupling parameters – specifically linear (J) and biquadratic (K) exchange interactions – affect the magnetic hysteresis behaviour of graphene and fullerene C_{60}. These simulations enable a systematic exploration of how material properties can be optimised for improved magnetic stability in data storage applications. Notably, the integration of two-dimensional materials as functional supports for magnetic systems has been shown to enhance hysteresis and minimise thermal disruptions, making them suitable for high-density storage technologies [11,14]. By offering a comparative analysis of graphene and fullerene C_{60}, this research bridges the gap between theoretical modelling and practical applications. The results emphasise the significant roles of geometry, coupling interactions, and temperature on magnetic behaviour, underscoring the utility of Monte Carlo methods and the Blume-Emery-Griffiths model in guiding the development of next-generation magnetic storage systems [30–32]. The paper is structured as follows: Section 2 describes the model

and method, Sect. 3 details the Monte Carlo simulation results, and Section 4 provides the concluding insights.

2. Model and method

This study explores the comparative magnetic hysteresis behaviours of graphene and fullerene C_{60} nanostructures, consisting of N_T (graphene) = 54 and N_T (fullerene) = 60 atoms, respectively, as shown in Figure 1. Since carbon atoms are intrinsically non-magnetic, a commonly used theoretical approach was adopted to study the magnetic properties of graphene and fullerene: each carbon site was substituted with a spin variable 1, thus allowing the effective magnetic responses to be examined. Such spin representations are widely used in theoretical work on non-magnetic nanostructures to describe collective behaviours and explore possible magnetic analogies [33–39]. Monte Carlo simulations are used to study the magnetic properties of nano-graphene bilayers [33] under longitudinal magnetic fields, while the bilayer graphene systems [34,35] using similar computational approaches. For fullerene structures [36,37], examined mixed-spin configurations in C_{30}, and conducted a comparative study of the magnetic properties between graphene and C_{60} nanostructures. Further Monte Carlo studies on the magnetic properties of various fullerene nanostructures [38,39] have been reported, demonstrating the wide applicability of this theoretical framework. Moreover, this spin-1 substitution approach, while modelling induced non-magnetic carbon systems, captures the emergent magnetic behaviour observed experimentally in doped graphene (e.g. Fe/N-doped) [40,41] or by defect engineering [42] and in functional fullerenes (e.g. Gd-encapsulated in C_{60}) [43] or radical-adducted fullerenes exhibiting localised magnetic moments [44], where structural modifications or chemical functionalization induce localised magnetic moments. This provides a physical rationale for this widely used theoretical framework allowing the study of magnetic analogies in carbon nanostructures.

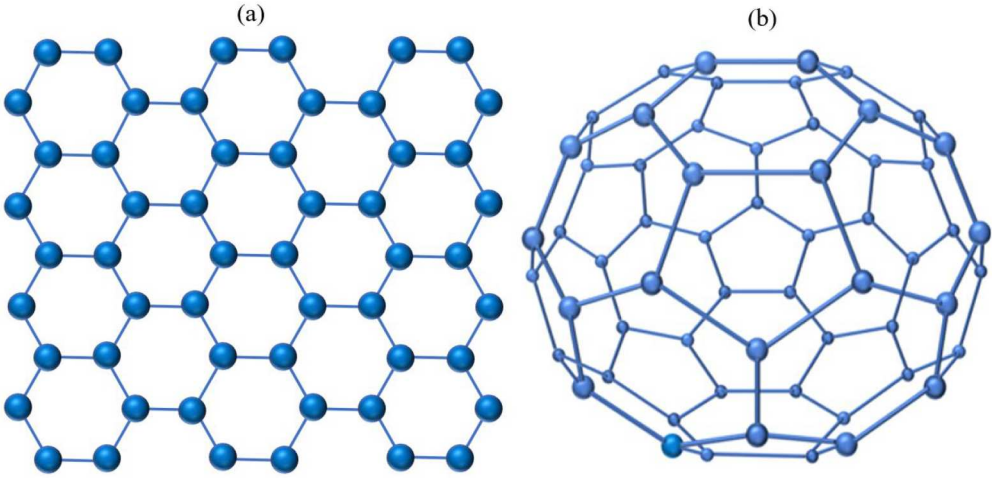

Figure 1. Graphene (a) and fullerene C_{60} (b) nanostructures illustrated, with each atom having a spin of 1.

In this study, Monte Carlo simulations were then performed using the Metropolis algorithm in the Blume–Emery–Griffiths model [45,46]. To ensure statistical reliability, each simulation included 10^6 Monte Carlo steps per rotation, of which the first 10^5 were discarded to ensure thermal equilibration.

Hamiltonian governing the graphene and fullerene C_{60} nanostructures:

$$\mathcal{H} = -J \sum_{\langle i,j \rangle} S_i\, S_j - K \sum_{\langle i,j \rangle} (S_i\, S_j)^2 - H \sum_i S_i, \tag{1}$$

The bilinear J and biquadratic K exchange interactions are associated with neighbouring spins S_i and S_j in each nanostructure, with the index $\langle i, j \rangle$ representing the summation over the nearest neighbours. An external magnetic field H also influences the atoms in both nanostructures.

The energy associated with each individual site:

$$E = \frac{1}{N_{T(graphene)}} \langle \mathcal{H} \rangle, \tag{2}$$

$$E = \frac{1}{N_{T(fullerene)}} \langle \mathcal{H} \rangle, \tag{3}$$

Formulas for calculating magnetisation in graphene and fullerene C_{60}:

$$M_{graphene} = \frac{1}{N_{T(graphene)}} \sum_i S_i, \tag{4}$$

$$M_{fullerene} = \frac{1}{N_{T(fullerene)}} \sum_i S_i. \tag{5}$$

In this study, the parameters J, K, H, and T are expressed in reduced and dimensionless units, which is common practice in Monte Carlo simulations of spin systems. This approach allows us to highlight qualitative behaviours without aiming for a material-specific quantitative description. Similar modelling strategies have been adopted in previous theoretical works [47–51].

3. Results of Monte Carlo simulations

This part emphasises the comparison of magnetic hysteresis of graphene and fullerene C_{60} using Monte Carlo simulations, with a particular emphasis on the effects of linear (J) and biquadratic (K) exchange coupling interactions, as well as temperature (T).

Table 1. List of symbols and definitions.

Symbol	Definition	Remarks
J	Bilinear exchange interaction	Controls ferromagnetic/antiferromagnetic alignment
K	Biquadratic exchange interaction	Accounts for higher-order correlations
H	External magnetic field	Applied to spins at each site
Si	Spin variable at site *i*	Each atom carries a unit spin
T	Temperature	Controls the transition to the paramagnetic phase
Hc	Coercive field	Decreases with *T*

Table 1 illustrates the list of symbols representing the parameters used in this study and their definitions. Moreover, Figure 2 compares magnetic hysteresis for graphene (a) and fullerene C_{60} (b) nanostructures, evaluated with parameters $J = 1$, $K = 0$ and $T = 1$. The results indicate that the fullerene C_{60} nanostructure exhibits a higher H_C than the graphene nanostructure when analysed using the same method, identical spin values, and identical parameter settings. This difference in magnetic behaviour, particularly in H_C, is attributed to the distinct geometries of the two nanostructures. Indeed, the spherical form of C_{60} fullerene creates unique angular spin arrangements, enhancing stability in certain magnetic configurations and resulting in a higher H_C due to the energy required for spin reorientation. Unlike the planar structure of graphene with uniform 2D spin interactions, the 3D lattice of C_{60} allows for multiple spin-coupling directions, enhancing magnetic anisotropy and increasing the H_C field.

Figure 3 presents the hysteresis loops for graphene (a) and fullerene C_{60} (b) nanostructures, evaluated with varying J and fixed parameters $K = 0$ and $T = 1$. As J increases, the area of the magnetic hysteresis loop expands considerably in both nanostructures, causing the H_C to rise. This increase in H_C is more pronounced in the fullerene C_{60} nanostructure than in graphene. The curvature of fullerene C_{60} stabilises spin configurations and creates larger resistance to magnetic reversal, resulting in higher H_C as J increases. In contrast, graphene's flat, two-dimensional structure exhibits simpler, more uniform spin interactions, resulting in it being less resistant to magnetisation changes. In fact, fullerene C_{60} is more rigid than graphene due to its 3D structure, which stabilises spins and increases resistance to magnetic reversal, resulting in a larger increase in H_C as J increases. In opposition, the 2D structure of graphene allows for more flexible reorientation of the spins, resulting in a smaller increase in H_C.

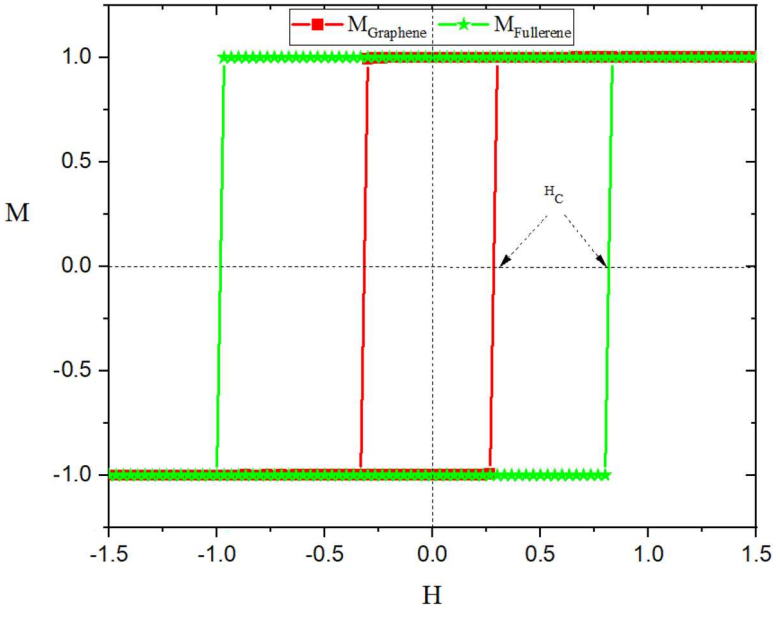

Figure 2. Hysteresis loops for graphene (a) and fullerene C_{60} (b) nanostructures, evaluated with parameters $J = 1$, $K = 0$ and $T = 1$.

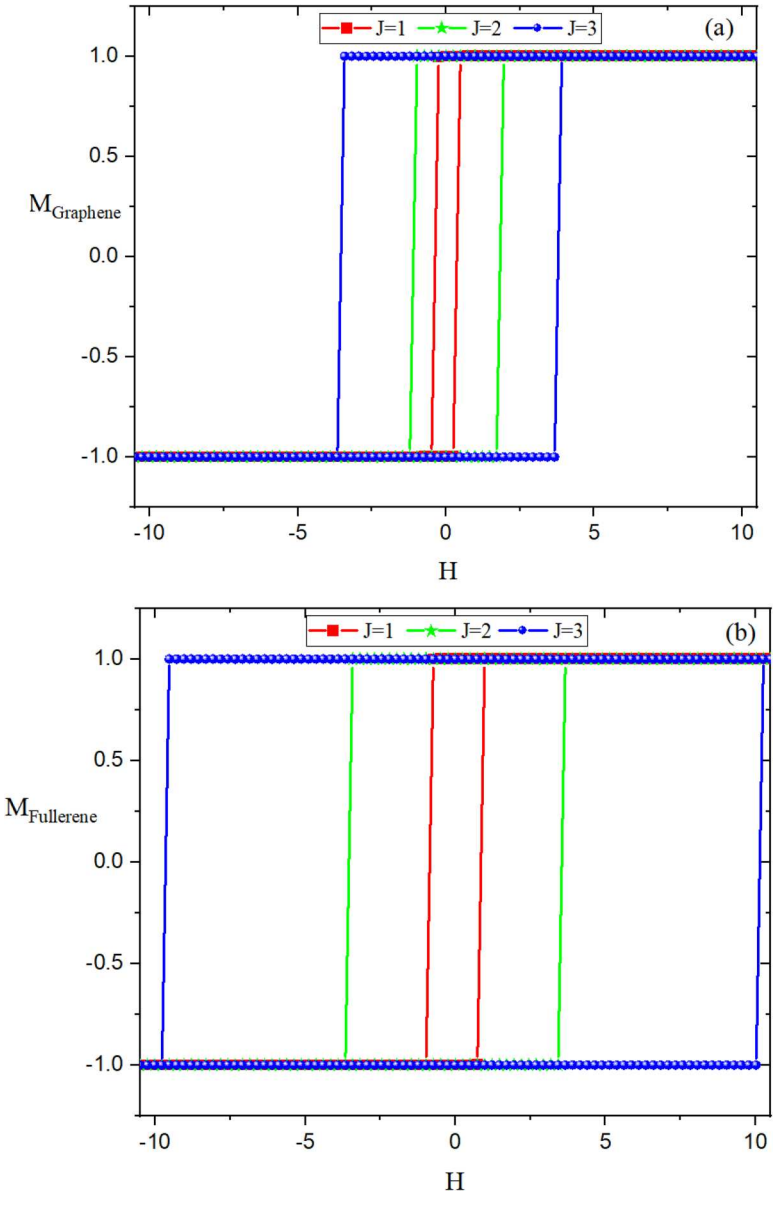

Figure 3. Hysteresis loops for graphene (a) and fullerene C_{60} (b) nanostructures, evaluated with varying J and fixed parameters $K = 0$ and $T = 1$.

Guided by the same approach, Figure 4 investigates the hysteresis loops for graphene (a) and fullerene C_{60} (b) nanostructures, evaluated with varying K and fixed parameters $J = 1$ and $T = 1$. As K increases, both nanostructures show a substantial widening of the hysteresis loop, contributing to a higher H_C. This increase in H_C is more pronounced in the fullerene C_{60} nanostructure than in graphene, and the influence of K on H_C is stronger for both nanostructures compared to that of J. Indeed, the biquadratic parameter K impacts magnetic hysteresis more strongly as it introduces both stronger

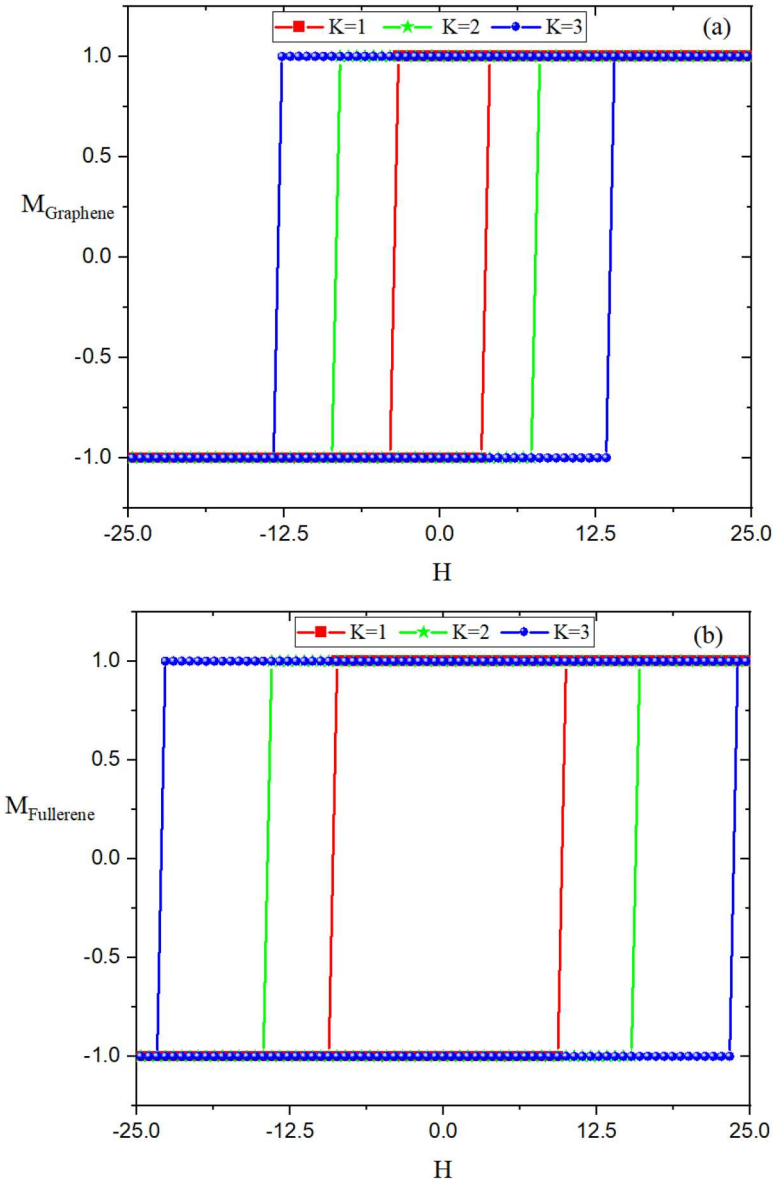

Figure 4. Hysteresis loops for graphene (a) and fullerene C_{60} (b) nanostructures, evaluated with varying K and fixed parameters $J = 1$ and $T = 1$.

coupling and further anisotropy, resulting in a higher energy threshold for spin inversion and a higher H_C than the linear parameter J.

Figure 5 investigates the hysteresis loops for graphene (a) and fullerene C_{60} (b) nanostructures, evaluated with varying T and fixed parameters $J = 1$ and $K = 0$. As T increases, both nanostructures show a substantial reduction in the area of the magnetic hysteresis loop, resulting in a decrease in the H_C. Additionally, graphene transitions to the paramagnetic phase at $T \geq 1.5$, where $H_C = 0$, while fullerene transitions to the paramagnetic phase at $T \geq 2.5$. Indeed, as T increases, thermal fluctuations disrupt spin alignment in

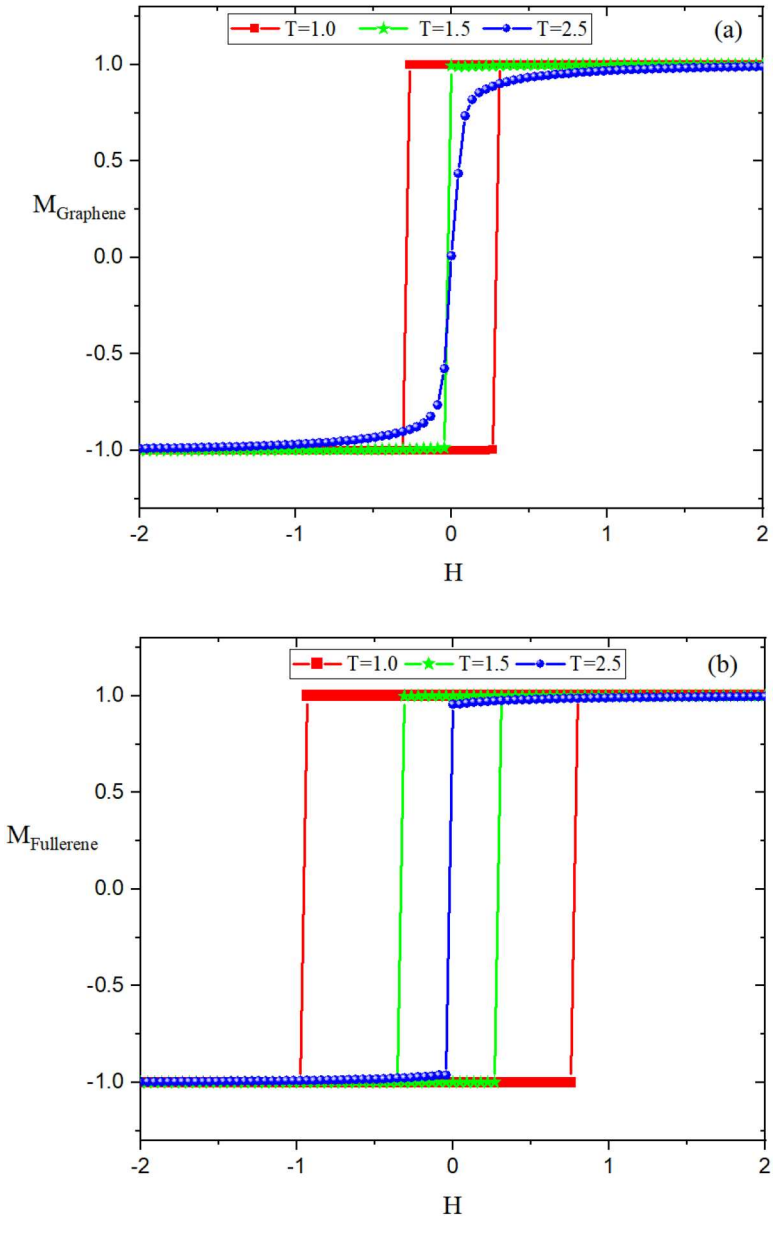

Figure 5. Hysteresis loops for graphene (a) and fullerene C_{60} (b) nanostructures, evaluated with varying T and fixed parameters $J = 1$ and $K = 0$.

both graphene and fullerene C_{60}, reducing the area of the magnetic hysteresis loop and lowering the H_C. Graphene, with its simpler 2D structure, transitions to a paramagnetic phase where spin alignment is random (giving $H_C = 0$) at a lower temperature ($T \geq 1.5$) due to weaker planar spin interactions. In contrast, the 3D spherical structure of fullerene C_{60} offers greater magnetic stability and requires more thermal energy to reach the

paramagnetic phase, occurring at $T \geq 2.5$. This structural stability of fullerene delays the reduction of H_C, which explains the higher temperature threshold than graphene.

Finally, Figure 6 investigates H_C for graphene (a) and fullerene C_{60} (b) nanostructures, evaluated under different conditions with varying parameters. Specifically: (a) $K = 0$ and $T = 1$ with varying J; (b) $J = 1$ and $T = 1$ with varying K; (c) $J = 1$ and $K = 0$ with varying T. All parameter variations significantly affect both nanostructures. Increasing J and K results in an almost linear increase in H_C for both types of nanostructures, while decreasing T leads to an exponential decay in H_C, which approaches zero when $T \geq 1.5$ for graphene and $T \geq 2.5$ for fullerene. Particularly, K has a more substantial effect on H_C than either J or T.

Increasing J in fullerene and graphene shows a strong positive correlation with H, described by the equations $H_C = -5.733 + 5.365 \times J$ for fullerene and $H_C = -3.711 + 3.005 \times J$ for graphene, allowing for the prediction of H_C values based on J. Similarly, increasing K in fullerene and graphene results in a strong positive correlation with H_C, given by $H_C = 1.326 + 7.606 \times K$ for fullerene and $H_C = -0.977 + 4.699 \times K$ for graphene. Moreover, increasing T in both fullerene and graphene follows an exponential decay model: $H_C = -0.00863 + 2.29471 \times \exp((-T - 0.50093)/0.46169)$ for fullerene and H_C

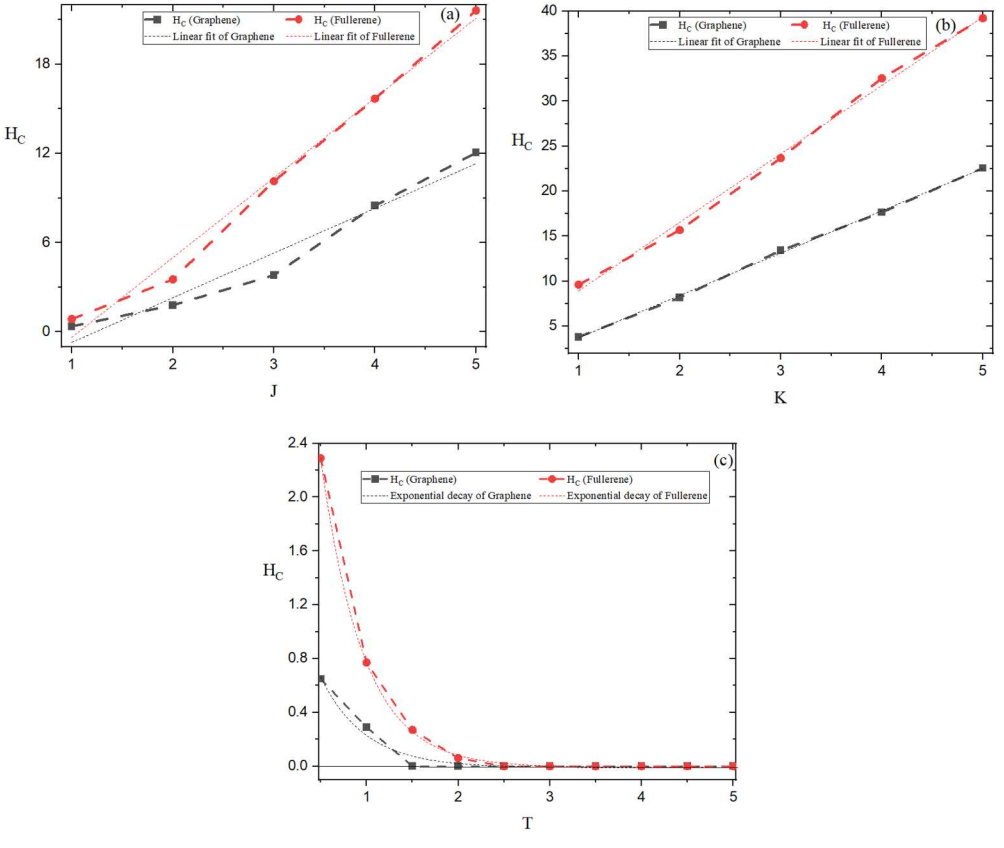

Figure 6. H_C for graphene (a) and fullerene C_{60} (b) nanostructures, evaluated under different conditions with varying parameters. Specifically: (a) $K = 0$ and $T = 1$ with varying J; (b) $J = 1$ and $T = 1$ with varying K; (c) $J = 1$ and $K = 0$ with varying T.

$= -0.01051 + 0.80768 \times \exp\left((-T - 0.41039)/0.48589\right)$ for graphene, both showing a clear exponential decay of H_C as T increases.

Moreover, although no experimental or DFT studies have investigated systems with exactly the geometry and spin configuration examined in our work under the influence of the considered parameters, our Monte Carlo results demonstrate magnetic behaviours – including hysteresis characteristics, especially the H_C under different parameters – that show qualitative agreement with established Monte Carlo studies on similar carbon nanostructures. The observed phenomena correspond to the hysteresis of graphene bilayers under longitudinal fields [31], finite size effects [32,33], as well as to fullerene systems including mixed-spin C_{30} [34], comparative studies on C_{60} [35], and various X_n nanostructures [36,37]. This consistency across different carbon architectures (graphene vs. fullerene) and spin models validates both our dimensionless parameterisation approach and the broader applicability of these magnetic analogies in carbon materials, despite the lack of *Ab initio* parameters specific to our exact system.

Finally, as a perspective, it should be noted that the effects of magnetic fields on pure or doped graphene have been extensively studied using advanced theoretical models, such as the tight-binding model and the Kubo-Greenwood formula [52,53], which reveal significant changes in the electronic structure, band gap opening, and thermoelectric properties. In parallel, recent advances in the study of fullerenes [54] have highlighted their unique potential among carbon nanomaterials, both for fundamental aspects and practical applications, with a particular focus on their mechanical characteristics [54] and sensing capabilities [55].

In this context, our work, based on Monte Carlo simulations, contributes by focusing on the magnetic response and spin-related phenomena in graphene nanostructures. Therefore, it would be highly relevant for future research to integrate these complementary approaches to achieve a more comprehensive understanding that links the electronic and spintronic properties of graphene and its derivatives.

In the future, these simulations could be extended by including defects, different spin amplitudes, or modulated magnetic fields to assess their influence on hysteresis and H_C. These extensions complemented existing studies based on tight-binding and the Kubo–Greenwood formula [52,53], drawing on the electronic and spintronic responses of carbon nanostructures.

4. Conclusions

This study provided a comparative analysis of the magnetic hysteresis properties of graphene and C_{60} fullerene using Monte Carlo simulations. The 3D spherical geometry of C_{60} fullerene resulted in a higher coercive field H_C and greater thermal stability than planar graphene, due to enhanced magnetic anisotropy and resistance to spin reorientation. The exchange parameters J and K strongly influenced H_C, with K having the most marked effect, while increasing the temperature caused an exponential decay of H_C, with graphene becoming paramagnetic for $T \geq 1.5$ and fullerene for $T \geq 2.5$. These differences have allowed to propose guidelines for the design of spintronic and magnetic storage devices: fullerene-based nanostructures have proven to be better suited for applications requiring high coercive field and high thermal stability, while graphene has shown a tunable H_C via parameter tuning, allowing to optimise the performance for specific

needs. Future work could extend these simulations by including defects, different spin amplitudes or modulated magnetic fields, paving the way for the design of nanostructures with tailored electronic and spintronic properties, by combining the magnetic results of Monte Carlo simulations with electronic models such as tight-binding and Kubo–Greenwood.

Acknowledgements

The authors extend their appreciation to Taif University, Saudi Arabia, for supporting this work through project number (TU-DSPP-2024 -51).

Disclosure statement

No potential conflict of interest was reported by the author(s).

Funding

This research was funded by Taif University, Saudi Arabia, Project No. (TU-DSPP-2024 -51). Also, this research was supported by the National Research Foundation of Korea (NRF) grant funded by the Korea government (MSIT) (RS-2025-22222973) and with the support of the "2024 System Semiconductor Technology Development Support Project" of Chungbuk Technopark.

Data availability statement

All data that support the findings of this study are included within the article.

References

[1] N. Baig, *Two-dimensional nanomaterials: a critical review of recent progress, properties, applications, and future directions*. Compos. Part A Appl. Sci. Manuf. 165 (2023), p. 107362.
[2] K. Khan, A.K. Tareen, M. Aslam, R. Wang, Y. Zhang, A. Mahmood, Z. Ouyang, H. Zhang, and Z. Guo, *Recent developments in emerging two-dimensional materials and their applications*. J. Mater. Chem. C. 8 (2020), pp. 387–440.
[3] A. Hayat, M. Sohail, A.E. Jery, K.M. Al-Zaydi, S. Raza, H. Ali, Z. Ajmal, A. Zada, T.A. Taha, I.U. Din, M.A. Khan, M.A. Amin, Y. Al-Hadeethi, A.Z. Barasheed, Y. Orooji, J. Khan, and M.Z. Ansari, *Recent advances, properties, fabrication and opportunities in two-dimensional materials for their potential sustainable applications*. Energy Storage Mater. 59 (2023), p. 102780.
[4] T. Das, B.K. Sharma, A.K. Katiyar, and J.-H. Ahn, *Graphene-based flexible and wearable electronics*. J. Semicond. 39 (2018), p. 011007.
[5] A. Armano and S. Agnello, *Two-dimensional carbon: a review of synthesis methods, and electronic, optical, and vibrational properties of single-layer graphene*. C. 5 (2019), p. 67.
[6] S.Z. Butler, S.M. Hollen, L. Cao, Y. Cui, J.A. Gupta, H.R. Gutiérrez, T.F. Heinz, S.S. Hong, J. Huang, A.F. Ismach, E. Johnston-Halperin, M. Kuno, V.V. Plashnitsa, R.D. Robinson, R.S. Ruoff, S. Salahuddin, J. Shan, L. Shi, M.G. Spencer, M. Terrones, W. Windl, and J.E. Goldberger, *Progress, challenges, and opportunities in two-dimensional materials beyond graphene*. ACS Nano. 7 (2013), pp. 2898–2926.
[7] M. Donarelli and L. Ottaviano, *2D materials for gas sensing applications: a review on graphene oxide, MoS2, WS2 and phosphorene*. Sensors 18 (2018), p. 3638.

[8] K. Rajkumar and R.T.R. Kumar, *Gas sensors based on two-dimensional materials and its mechanisms*, in *Fundamentals and Sensing Applications of 2D Materials*, Elsevier, 2019. pp. 205–258.
[9] M.J. Allen, V.C. Tung, and R.B. Kaner, *Honeycomb carbon: a review of graphene*. Chem. Rev. 110 (2010), pp. 132–145.
[10] M. Bühl and A. Hirsch, *Spherical aromaticity of fullerenes*. Chem. Rev. 101 (2001), pp. 1153–1184.
[11] N. Dwivedi, A.K. Ott, K. Sasikumar, C. Dou, R.J. Yeo, B. Narayanan, U. Sassi, D.D. Fazio, G. Soavi, T. Dutta, O. Balci, S. Shinde, J. Zhang, A.K. Katiyar, P.S. Keatley, A.K. Srivastava, S.K.R.S. Sankaranarayanan, A.C. Ferrari, and C.S. Bhatia, *Graphene overcoats for ultra-high storage density magnetic media*. Nat. Commun. 12 (2021), p. 2854.
[12] C. Casiraghi, J. Robertson, and A.C. Ferrari, *Diamond-like carbon for data and beer storage*. Mater. Today 10 (2007), pp. 44–53.
[13] R. Kumar, P. Bharti, C. Dhand, R.J. Yeo, M. Zhang, and N. Dwivedi, *"It's team work": multi-layered wear-resistant and lubricating overcoats derived from the synergy of ultrathin carbon surface and interface chemistry*. Appl. Surf. Sci. 641 (2023), p. 158485.
[14] L. Spree, F. Liu, V. Neu, M. Rosenkranz, G. Velkos, Y. Wang, S. Schiemenz, J. Dreiser, P. Gargiani, M. Valvidares, C. Chen, B. Büchner, S.M. Avdoshenko, and A.A. Popov, *Robust single molecule magnet monolayers on graphene and graphite with magnetic hysteresis up to 28 K*. Adv. Funct. Mater. 31 (2021), p. 2105516.
[15] M.A. Lebedeva, T.W. Chamberlain, E.S. Davies, B.E. Thomas, M. Schröder, and A.N. Khlobystov, *Tuning the interactions between electron spins in fullerene-based triad systems*. Beilstein J. Org. Chem. 10 (2014), pp. 332–343.
[16] M. Liedtke, A. Sperlich, H. Kraus, A. Baumann, C. Deibel, M.J.M. Wirix, J. Loos, C.M. Cardona, and V. Dyakonov, *Triplet exciton generation in bulk-heterojunction solar cells based on endohedral fullerenes*. J. Am. Chem. Soc. 133 (2011), pp. 9088–9094.
[17] G. Mörée and M. Leijon, *Review of hysteresis models for magnetic materials*. Energies 16 (2023), p. 3908.
[18] M.D. Hossain, M.A. Hossain, and S.S. Sikder, *Hysteresis loop properties of rare earth doped spinel ferrites: a review*. J. Magn. Magn. Mater. 564 (2022), p. 170095.
[19] J.-S. Suen, M.H. Lee, G. Teeter, and J.L. Erskine, *Magnetic hysteresis dynamics of thin Co films on Cu(001)*. Phys. Rev. B. 59 (1999), pp. 4249–4259.
[20] Ö Özdemir and D.J. Dunlop, *Hysteresis and coercivity of hematite*. J. Geophys. Res. Solid Earth 119 (2014), pp. 2582–2594.
[21] R. El Fdil, H. Sabbah, D. Kabouchi, Z. Fadil, A. Mhirech, C.J. Raorane, E. Salmani, A. El-marghany, P. Rosaiah, and H. Ez-Zahraouy, *Comparative Monte Carlo study on magnetic characteristics in β12, χ^3 and striped borophene structures*. Phys. B. 683 (2024), p. 415934.
[22] Z. Fadil,, C.J. Raorane, D. Kabouchi, R. El Fdil, A.A. Alsayyari, S. Saadaoui, S.-C. Kim, A. Mhirech, and E. Salmani, *Exploring magnetic attributes: borospherene-like and buckminsterfullerene-like lattices in Monte Carlo simulations*. ECS J. Solid State Sci. Technol. 13 (2024), p. 081001.
[23] H. Sabbah, Z. Fadil, R. El Fdil, S.C. Kim, C.J. Raorane, D. Kabouchi, A. Mhirech, E. Salmani, B. Kabouchi, A.A. Alsayyari, K.H. Mahmoud, and A.S.A. Alsubaie, *Monte Carlo simulations unveil magnetic differences in honeycomb, kagome, and triangular nanolattices*. Phys. B. 695 (2024), p. 416566.
[24] Z. Fadil, C.J. Raorane, R.E. Fdil, A.A. Alsayyari, S.-C. Kim, S.K. Rajasekharan, K.H. Mahmoud, and A.S.A. Alsubaie, *Investigating magnetic behavior in Crl3 monolayer nanostructure via Monte Carlo simulations*. Appl. Phys. A. 130 (2024), p. 493.
[25] N. Saber, Z. Fadil, A. Mhirech, B. Kabouchi, L. Bahmad, and W. Ousi Benomar, *Magnetic properties and compensation temperature behaviors in the hexacene-like nanostructure: A Monte Carlo study*. J. Low Temp. Phys. 210 (2023), pp. 310–324.
[26] Z. Fadil, R. Haldhar, C.J. Raorane, N. Saber, R.E. Fdil, S. Karam, P. Rosaiah, M. Ouladsmane, and S.-C. Kim, *Monte Carlo simulations revealing ground state characteristics and magnetic hysteresis in perylene-like nanostructure*. J. Low Temp. Phys. 214 (2024), pp. 314–330.

[27] G.B.A. Goguin, T.D. Oke, R.A.A. Yessoufou, and E. Albayrak, *Critical and hysteresis behaviors for a hexagonal core-shell structure nanowire in the Blume–Emery–Griffiths model*. Physica A. 624 (2023), p. 128927.
[28] W. Selke and J. Yeomans, *Interface properties of the two-dimensional Blume-Emery-Griffiths model*. J. Phys. A: Math. Gen. 16 (1983), p. 2789.
[29] Z. Fadil, N. Saber, H. Eraki, A. Mhirech, B. Kabouchi, and L. Bahmad, *Study of the Blume–Emery–Griffiths model for mixed carbon-like nanotube: Monte Carlo study*. J. Low Temp. Phys. 210 (2023), pp. 285–296.
[30] E.M. Jalal, H. Saadi, A. Hasnaoui, A. Lafhal, N. Hachem, and M. El Bouziani, *Critical and reentrant phenomena in the Blume–Emery–Griffiths model with attractive biquadratic interaction*. Eur. Phys. J. B. 97 (2024), p. 126.
[31] S.S. Ahmed, L. Bahmad, A. Benyoussef, and A.E. Kenz, *Mixed spin-1 and spin-1/2 Blume-Emery-Griffiths model on the Bethe lattice: Monte Carlo simulation*. Superlattices Microstruct. 109 (2017), pp. 841–851.
[32] Y. Al Qahoom, R. Aharrouch, K. El Kihel, H. Saadi, M. Madani, and M. El Bouziani, *Blume–Emery–Griffiths model for mixed spin (1, 5/2) calculated by mean-field approximation*. Eur. Phys. J. B. 96 (2023), p. 142.
[33] W. Wang, R. Liu, D. Lv, and X. Luo, *Monte Carlo simulation of magnetic properties of a nanographene bilayer in a longitudinal magnetic field*. Superlattices Microstruct. 98 (2016), pp. 458–472.
[34] R. Masrour and A. Jabar, *Magnetic properties of bilayer graphene: a Monte Carlo study*. J. Comput. Electron. 16 (2017), pp. 12–17.
[35] R. Masrour and A. Jabar, *Magnetic properties of bilayer graphene armchair nanoribbons: A Monte Carlo study*. J. Magn. Magn. Mater. 426 (2017), pp. 225–229.
[36] O. Abounachit, A. Jabar, S. Idrissi, and L. Bahmad, *Investigation of the magnetic properties of the fullerene C30 with mixed spins: A Monte Carlo study*. J. Magn. Magn. Mater. 589 (2024), p. 171604.
[37] Z. Fadil, C.J. Raorane, S. Karam, A. Samih, S.C. Kim, E. Salmani, A.A. Alsayyari, and K.H. Mahmoud, *Comparative study of magnetic properties in graphene and fullerene C_{60} nanostructures via Monte Carlo simulations*. J. Magn. Magn. Mater. 622 (2025), p. 172962.
[38] S. Aouini, A. Mhirech, A. Alaoui-Ismaili, and L. Bahmad, *Magnetic properties in different fullerenes Xn nano-structures: Monte Carlo study*. Chin. J. Phys. 56 (2018), pp. 1640–1647.
[39] A. Mhirech, S. Aouini, A. Alaoui-Ismaili, and L. Bahmad, *Monte Carlo study of magnetic properties of mixed spins in a fullerene X30 Y30-like structure*. J. Low Temp. Phys. 192 (2018), pp. 65–74.
[40] M. Sepioni, et al., *Limits on intrinsic magnetism in graphene*. Phys. Rev. Lett. 105 (2010), p. 207205.
[41] Y. Wang, Y. Huang, Y. Song, X. Zhang, Y. Ma, J. Liang, and Y. Chen, *Room-temperature ferromagnetism of graphene*. Nano Lett. 9 (2009), pp. 220–224.
[42] J. Fernández-Rossier and J.J. Palacios, *Magnetism in graphene nanoislands*. Phys. Rev. Lett. 99 (2007), p. 177204.
[43] J. Lu, W.N. Mei, Y. Gao, X. Zeng, M. Jing, G. Li, R. Sabirianov, Z. Gao, L. You, J. Xu, D. Yu, and H. Ye, *Structural and electronic properties of Gd@C60: All-electron relativistic total-energy study*. Chem. Phys. Lett. 425 (2006), pp. 82–84.
[44] V. Georgakilas, J.A. Perman, J. Tucek, and R. Zboril, *Broad family of carbon nanoallotropes: classification, chemistry, and applications of fullerenes, carbon dots, nanotubes, graphene, nanodiamonds, and combined superstructures. Chem*. Rev. 115 (2015), pp. 4744–4822.
[45] W. Hoston and A.N. Berker, *Multicritical phase diagrams of the Blume-Emery-Griffiths model with repulsive biquadratic coupling*. Phys. Rev. Lett. 67 (1991), pp. 1027–1030.
[46] A. Jabar, A. Belhaj, H. Labrim, L. Bahmad, N. Hassanain, and A. Benyoussef, *Mixed spin thin films in the Blume–Emery–Griffiths model with biquadratic exchange interaction: A Monte Carlo study*. Superlattices Microstruct. 78 (2015), pp. 171–182.
[47] A. Jabar and R. Masrour, *Magnetic properties of Kekulene structure: A Monte Carlo study*. Physica A. 514 (2019), pp. 974–981.

[48] A. Jabar and R. Masrour, *Magnetic properties of magnetic bilayer Kekulene structure: a Monte Carlo study*. Physica B. 539 (2018), pp. 21–28.
[49] A. Jabar and R. Masrour, *Monte Carlo simulations of magnetic properties of Kekulene structure bilayers separate by a nonmagnetic with RKKY interactions*. Chem. Phys. Lett. 700 (2018), pp. 130–137.
[50] R. Masrour and A. Jabar, *Mixed spin-3/2 and spin-2 ising model on diamond-like decorated square: A Monte Carlo simulation*. Physica A. 539 (2020), p. 122878.
[51] M. Jerrari, R. Masrour, and T. Sahdane, *Monte Carlo study of magnetic and magnetocaloric properties of the graphene alternate layers of a ferrimagnetic mixed spins S=3/2 and σ=2*. MRS. Commun. 13 (2023), pp. 1171–1179.
[52] R. Chegel, *Magneto-electronic and thermopower properties of B, N and Si doped monolayer graphene*. Diamond Relat. Mater. 137 (2023), p. 110154.
[53] R. Chegel, *Tuning temperature-dependent of thermal conductivity and heat capacity of two-dimensional GeC compared to graphene and germanene: effects of magnetic field*. Physica B. 638 (2022), p. 413921.
[54] E. Ghavanloo, H. Rafii-Tabar, A. Kausar, G.I. Giannopoulos, and S.A. Fazelzadeh, *Experimental and computational physics of fullerenes and their nanocomposites: synthesis, thermo-mechanical characteristics and nanomedicine applications*. Phys. Rep. 996 (2023), pp. 1–116.
[55] G.I. Giannopoulos, *Fullerenes as mass sensors: a numerical investigation*. Physica E. 56 (2014), pp. 36–42.

Philosophical Magazine

ISSN: 1478-6435 (Print) 1478-6443 (Online) Journal homepage: www.tandfonline.com/journals/tphm20

Magnetic ordering, thermal stability, and hysteresis behaviour in a nested fullerene C_{24} system: a Monte Carlo study

A. Jabar, Z. Fadil, Mohamed Sheikh, Ayman A. Ghfar, Chaitany Jayprakash Raorane & Seong-Cheol Kim

To cite this article: A. Jabar, Z. Fadil, Mohamed Sheikh, Ayman A. Ghfar, Chaitany Jayprakash Raorane & Seong-Cheol Kim (2026) Magnetic ordering, thermal stability, and hysteresis behaviour in a nested fullerene C_{24} system: a Monte Carlo study, Philosophical Magazine, 106:13-14, 1318-1330, DOI: 10.1080/14786435.2026.2622741

To link to this article: https://doi.org/10.1080/14786435.2026.2622741

PHILOSOPHICAL MAGAZINE
2026, VOL. 106, NOS. 13–14, 1318–1330
https://doi.org/10.1080/14786435.2026.2622741

Taylor & Francis
Taylor & Francis Group

Magnetic ordering, thermal stability, and hysteresis behaviour in a nested fullerene C_{24} system: a Monte Carlo study

A. Jabar[a,b], Z. Fadil[c], Mohamed Sheikh[d], Ayman A. Ghfar[d], Chaitany Jayprakash Raorane[e] and Seong-Cheol Kim[e]

[a]LMHEP, Faculty of Sciences, Hassan II University of Casablanca, Casablanca, Morocco; [b]LPHE-MS, Science Faculty, Mohammed V University in Rabat, Rabat, Morocco; [c]Laboratoire de Matière Condensée et Sciences Interdisciplinaires (LaMCScI), Faculty of Sciences, URL-CNRST, Rabat, Morocco; [d]Department of Chemistry, College of Science, King Saud University, Riyadh, Saudi Arabia; [e]School of Chemical Engineering, Yeungnam University, Gyeongsan, Republic of Korea

ABSTRACT

This work investigates the magnetic behaviour of a nested C_{24} fullerene system featuring mixed spins ($S = 2$ and $\sigma = 5/2$) using Monte Carlo simulations based on the Blume-Capel Ising model. The ground state, identified from an analysis of 30 spin configurations, is primarily governed by the competition between the crystal field (d) and the external magnetic field (h). Thermal analyses reveal a stable ferrimagnetic phase characterised by two first-order transitions: a reentrant transition (t_r) followed by a paramagnetic transition at the Néel temperature (t_N). The presence of field-induced first-order transitions is corroborated by step-like magnetisation hysteresis loops. Increasing the magnitudes of the exchange couplings ($|r|$ and p) enhances both the magnetic rigidity and coercivity of the system. Conversely, the ferrimagnetic order is suppressed either by sufficiently negative crystal fields or elevated temperatures. This study provides detailed insight into the ordering mechanisms and thermal stability of the system, highlighting its potential for novel applications in spintronics.

ARTICLE HISTORY
Received 8 December 2025
Accepted 22 January 2026

KEYWORDS
Nested fullerene C_{24}; Monte Carlo study; magnetic properties; reentrant transition

1. Introduction

The year 1985 marked the discovery of fullerenes by Kroto, Curl, and Smalley, a finding that turned out to be crucial in the realm of material science. As Smalley recalls in his personal account, this discovery opened the way to 'an infinite new class of carbon molecules' [1]. Early systematic research, such as the comprehensive review by Dresselhaus et al. [2], established the structural and electronic foundations of these cage molecules, while also identifying the exceptional potential of alkali–metal-doped fullerenes as superconducting materials.

CONTACT Z. Fadil fadilzakaria604@gmail.com Laboratoire de Matière Condensée et Sciences Interdisciplinaires (LaMCScI), Faculty of Sciences, URL-CNRST, P.O. Box 1014, Rabat, Morocco; Chaitany Jayprakash Raorane chaitanyaraorane22@ynu.ac.kr School of Chemical Engineering, Yeungnam University, Gyeongsan 38541, Republic of Korea; Seong-Cheol Kim seongcheol2025@gmail.com School of Chemical Engineering, Yeungnam University, Gyeongsan 38541, Republic of Korea

The extremely fast development of the field has permitted to anticipate to Smalley and Yakobson [3], two main axes of development: the incorporation of C_{60}-type cages in organic chemistry and the use of carbon nanotube materials for future electronic and structural applications. Basic characterisation further proceeded with the work of Yadav and Kumar [4], which reviewed detailed information concerning the sp^2 hybridised structure with icosahedral symmetry of C_{60}, while astrophysical studies by García-Hernández et al. [5] showed that fullerenes naturally exist in interstellar space, including molecules such as C_{70} and possibly C_{24}.

Theoretical investigations have been pursued further by the DFT study of Chang et al. [6], where a systematic analysis of the geometry versus stability relation of carbon cages between C_{24} and C_{70} was performed, confirming the remarkable stability of C_{60}. In parallel, another research field was opened to Monte Carlo simulations on magnetic properties: after pioneering work by Benyoussef et al. on the C_{24} [7], comparative studies on C_{60} with graphene were performed by Fadil et al. [8,9], then on C_{36} by Idrissi et al. [10].

Further work on other fullerenes continued to study the properties of C_{20}, C_{60}, and C_{70} by Aouini et al. [11], while complex systems such as C_{18} [12] and C_{30} [13] received detailed analyses. Sabzevar et al. inspected the effect of structural defects [14], and Kabouchi et al. studied the C_{60} dimers [15]. Finally, in this process of growing system complexity, Wang et al. presented the compensation characteristics and hysteresis loops for large fullerenes [16].

This methodological development was sustained by parallel achievements in the application of the Blume-Capel model, represented by the investigations on multilayer systems [17–24]. All of these works have thus provided a sound theoretical framework for investigations into the magnetic properties of carbon nanomaterials. With such a diversity of approaches and systems studied, there is a real need for a unifying study that will enable the systematic comparison of magnetic properties of different fullerene structures. The present work, therefore, seeks to determine structure-magnetic property relationships by applying a consistent Monte Carlo simulation methodology to a representative series of fullerenes, ranging from small cages like C_{24} [5,7] to more complex systems like C_{60} [8,9,11,15], while relying on the theoretical framework of the Blume-Capel model [17–24] for an explanation of the basic mechanism governing the magnetic behaviour of these exceptional materials.

Recent Monte Carlo simulations have modelled magnetic and magnetocaloric effects in nanomaterials. Studies on core–shell NPs, bilayer fullerenes, graphene nanoribbons, and MBene-like systems [25–32] modelled dynamic and thermodynamic phenomena. Simultaneously, some compounds have been investigated for magnetic refrigerants: $LaCr_2Si_2C$, with the transition temperature $Tt = 18.5$ K and relative cooling power $RCP = 13.03$ J/kg at 5 T [33], MnAs and MnBi with the *ab initio*/Monte Carlo approach [34,35], and Kekulene with expected high magnetocaloric performance [36], as well as the hexagonal nanostructure Dendrimer with an $RCP = 115$ J/mol at 0.6 T [37].

Moreover, the nested fullerene C_{24} system consists of two concentric carbon shells with strong interlayer coupling and rich magnetic behaviour. Due to its highly symmetric and spatially confined structure, this fullerene represents an ideal model for studies on spin interaction, reentrant transitions, and temperature effects relevant for nanoscale magnetic and spintronic applications [38].

Contrary to single-cage fullerenes, the nested (core–shell) C_{24} structure introduces a competition between the intra-layer and inter-layer exchange interactions, which substantially enriches the magnetic behaviour of the system. The mixed-spin core–shell configuration stabilises intermediate magnetic states and gives rise to reentrant phase transitions and multi-step hysteresis loops associated with the layer-selective spin reversal. This nested geometry effectively enhances magnetic rigidity and thermal stability due to increased local coordination and underlines the important role of core–shell and mixed-spin architectures in shaping complex magnetic responses at the nanoscale.

In the present work, it is demonstrated that geometrical topology dominates magnetic behaviour at the nanoscale. We show that radial confinement in nested core–shell nanostructures enhances interlayer connectivity, stabilises ferrimagnetic order at an elevated temperature, and induces controllable metastability manifested as staircase-like hysteresis. The transition from a simple to a nested geometry thus converts a binary magnetic system into a multi-state one, enabling fine nanoscale control of magnetic order with direct implications for multilevel spintronic applications [38].

The paper is organised as follows. Section 2 describes the details of the computational method. Results of the calculated magnetic properties of the studied material are presented and discussed in Section 3. Finally, the main conclusions are given in Section 4.

2. Model and method

We use the Blume-Capel Ising model to study the nested fullerene C_{24} system, made up of mixed spins $S = 2$ and $\sigma = 5/2$, where free boundary conditions are imposed. It is composed of two atomic sublattices, each one containing 24 atoms (see Figure 1). The mixed high spins $S = 2$ and $\sigma = 5/2$ were taken to model nanostructures containing transition-metal or rare-earth ions with large magnetic moments, as commonly considered in Refs. [39–41]. Such a choice increases the number of accessible spin states leading to a rich energy spectrum and complex phase behaviour [39,40]. The high-spin configuration strengthens the competition between exchange interactions and crystal-field effects that drives the

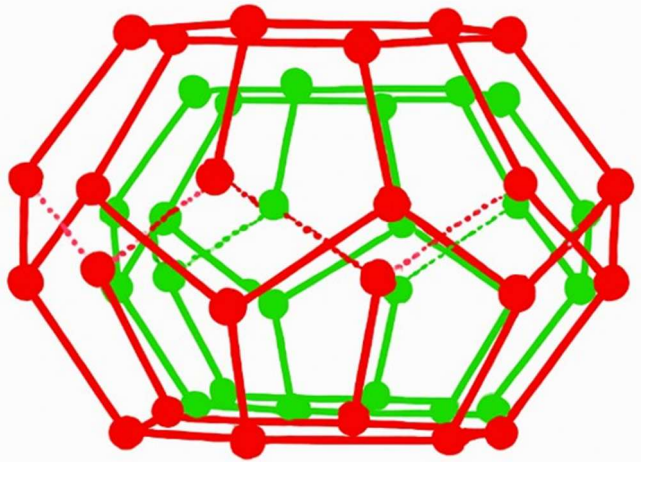

Figure 1. The nested fullerene C_{24} system made up of mixed spins: S = 2 (green) and σ = 5/2 (red).

appearance of intermediate phases and reentrant transitions and also naturally explains the staircase-like hysteresis loops arising due to successive spin-state reversals [41].

Moreover, physical quantities were averaged over 10^5 Monte Carlo steps per spin after discarding 10^6 Monte Carlo steps to ensure that the system was in the equilibrium state.

The system's Hamiltonian, is presented by:

$$\mathcal{H} = -J_{S\sigma}\sum_{\langle i,j\rangle} S_i\sigma_j - J_{\sigma\sigma}\sum_{\langle j,k\rangle}\sigma_j\sigma_k - J_{SS}\sum_{\langle i,l\rangle} S_iS_l - D\left(\sum_i S_i^2 + \sum_i \sigma_i^2\right) - H\left(\sum_i S_i + \sum_j \sigma_j\right) \tag{1}$$

The spin moment values are as follows, where S and σ are the spins of the two sublattices of the system, $\sum_{\langle ij\rangle}$ is the sum over nearest neighbours of sites i and j, and the notations $\langle i, j\rangle$ represent the initial nearest neighbour association between sites i and j. S can be ±2, 0, or ±1, while σ can be ±5/2, ±3/2, and ±1/2.

The system includes three kinds of exchange interactions: between spins S and σ ($J_{S\sigma}$), between identical σ spins ($J_{\sigma\sigma}$), and between identical S spins (J_{SS}). Besides the above coupling terms, there exist an external magnetic field h and a crystal field D to which the spin sites are subjected. The last two terms depend on the parameters D_σ and D_S and describe the effects of crystal anisotropy. In the given study, we will assume that the anisotropy is uniform, $D = D_\sigma = D_S$ for simplicity.

The spin moment values are as follows: S can be ±2, 0, and ±1, and σ can be ±5/2, ±3/2, and ±1/2. In this paper, we follow a standard normalisation convention commonly used in statistical physics to simplify the analysis and to enable the generalisation of results. The intra-sublattice exchange energy is set equal to unity, $J_{SS} = 1.0$, and serves as the reference energy scale. Then all other physical parameters are dimensionless quantities with respect to that scale: the inter-sublattice and secondary exchange couplings are $r = J_{S\sigma}/J_{SS}$ and $p = J_{\sigma\sigma}/J_{SS}$, respectively; the crystal field anisotropy is $d = D/J_{SS}$; the external magnetic field is $h = H/J_{SS}$; while the reduced temperature is $t = T/J_{SS}$. Such unit-free representation makes the following material much more compact, and our phase diagrams apply universally to a whole class of materials possessing identical interaction ratios.

We will begin by studying the internal energy per site:

$$E = \frac{H}{N} \tag{2}$$

The total and partial magnetisations are:

$$M_S = \frac{1}{N_S}\sum_i S_i \tag{3}$$

$$M_\sigma = \frac{1}{N_\sigma}\sum_i \sigma_i \tag{4}$$

$$M_{tot} = \frac{N_S \times M_S + N_\sigma \times M_\sigma}{N_S + N_\sigma} \tag{5}$$

The total and partial susceptibilities are:

$$\chi_S = \beta\left(\left\langle M_S^2\right\rangle - \langle M_S\rangle^2\right) \tag{6}$$

$$\chi = \beta\left(\left\langle M^2\right\rangle - \langle M\rangle^2\right) \tag{7}$$

$$\chi_{tot} = \frac{N_S\chi_S + N_\sigma\chi_\sigma}{N_S + N_\sigma} \tag{8}$$

Where T is the absolute temperature, $k_B = 1$ is the Boltzmann's constant, and $\beta = 1/(k_B T)$.

3. Results and discussions

This section is organised as follows: The ground-state phase diagrams are shown in Section 3.1 while Section 3.2 describes the magnetic properties.

3.1. Ground state phase diagrams

In this section, we present an analysis of the ground state phase diagrams of nested fullerene C_{24} system at absolute zero temperature, $t = 0$.

Figure 2 presents the ground state phase diagrams of the nested fullerene C_{24} system: (a) in the (r, p) plane for $d = 0$ and $h = 0$, (b) in the (d, p) plane for $r = -1$ and $h = 0$, (c) in the (p, h) plane for $r = -1$ and $d = 0$, and (d) in the (d, h) plane for $r = 1$ and $p = 1$. These four diagrams (a–d) map the ground state configurations (at $t = 0$) of a mixed-spin two-sublattice magnetic system (S, σ) as a function of the inter-sublattice coupling ($r = J_{S\sigma}/J_{SS}$), intra-sublattice coupling ($p = J_{\sigma\sigma}/J_{SS}$), crystal field ($d = D/J_{SS}$), and external magnetic field ($h = H/J_{SS}$). The total number of possible spin configurations at the ground state is 30 (S $\in \{\pm 2, \pm 1, 0\} \rightarrow 6$ values; $\sigma \in \{\pm 5/2, \pm 3/2, \pm 1/2\} \rightarrow 5$ values; thus $6 \times 5 = 30$). However, only a fraction of these configurations are energetically stable and appear as distinct phases in the diagrams. Figures (a) and (b) illustrate the influence of internal couplings (r and p, or d and p), while Figures (c) and (d) highlight the effect of h and d. The analysis reveals that the intra-sublattice coupling (parameter p) plays a dominant role in determining the spin configurations at $h = 0$: large positive p values (strong ferromagnetic coupling) stabilise saturated states (±2, ±5/2), whereas negative p values (strong antiferromagnetic coupling) promote intermediate or partially compensated phases such as (±2, ±1/2) to minimise the system energy. The crystal field d, particularly for large negative values ($d \ll 0$), tends to suppress the S spin ($S = 0$), leading to compensated phases like (0, ±3/2) or (0, ±1/2) along the $h = 0$ axis. The external magnetic field h exhibits its classical role by polarising the phases towards positive saturation for $h \gg 0$ and negative saturation for $h \ll 0$, thereby simplifying the phase structure at high field intensities. These diagrams illustrate the global picture; the ground state is primarily determined by the opposing contributions d and h, rather than by the exchange couplings. The last point to discuss is that the perfect symmetry observed in Figure (c) and (d) for the cuts along the $h = 0$ axis results from the invariance of the exchange energy and crystal field under simultaneous inversion of the spins at $h = 0$.

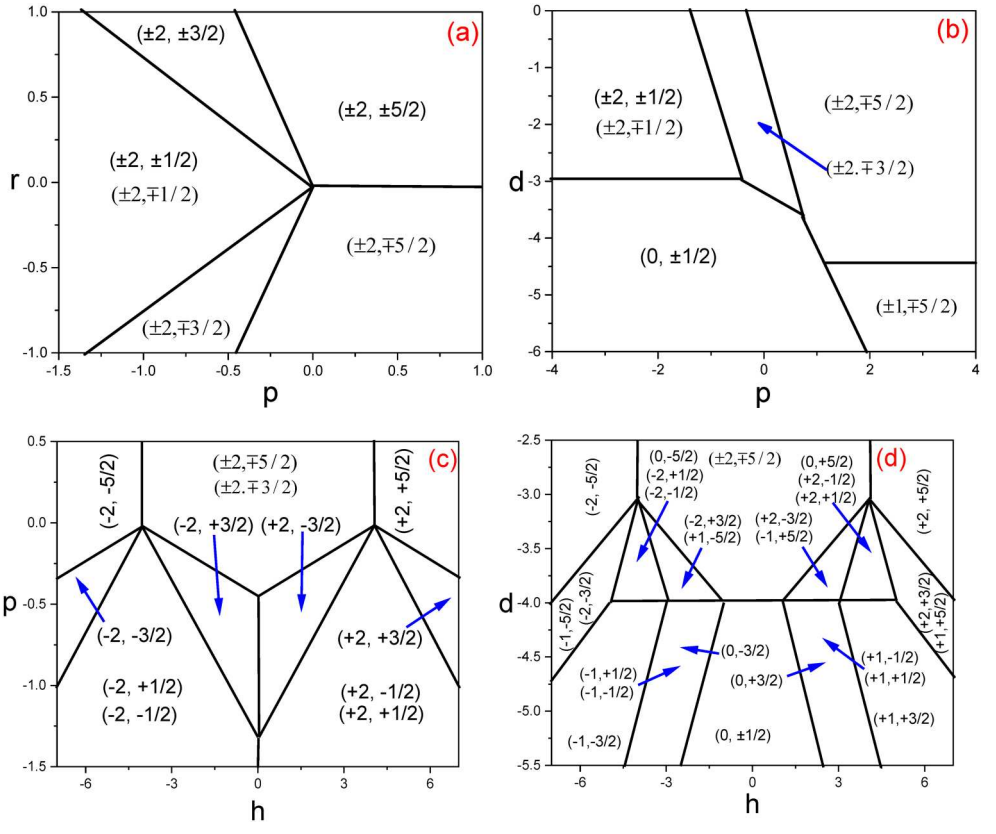

Figure 2. Ground state phase diagrams of the nested fullerene C_{24} system. (a) In the plane (r, p) for $d = 0$ and $h = 0$, (b) in the plane (d, p) for $r = -1$ and h = 0 (c) in the plane (p, h) for $r = -1$ and $d = 0$, and (d) in the plane (d, h) for r = −1 and $p = 1$.

In summary, phase stabilisation is the result of the competition between intra- and inter-sublattice couplings (p, r), the crystal field d, and the external field h. Positive p favours ferrimagnetic saturated states, negative p stabilises partially compensated phases, and strong negative d promotes compensated states with $S = 0$. Field h polarises the system at high values, whereas the symmetry around $h = 0$ reflects the invariance of exchange and crystal-field energies. Therefore, ferrimagnetic, compensated, and saturated phases naturally come out of the energetic hierarchy in this mixed-spin core–shell system.

3.2. Magnetic behaviour

In this section, we explain the influence of the physical parameters on magnetisations, susceptibilities, and hysteresis cycles.

Figure 3 illustrates the partial and total magnetisations (M_S, M_σ, M_{tot}) together with the total susceptibility (χ_{tot}) versus the reduced temperature (t), for fixed coupling parameters $r = -1$, $p = 1$, $h = 0$, and $d = 0$. At very low temperatures, the σ sublattice reaches positive saturation ($M_\sigma = +2.5$), while the S sublattice is negatively saturated ($M_S = -2$),

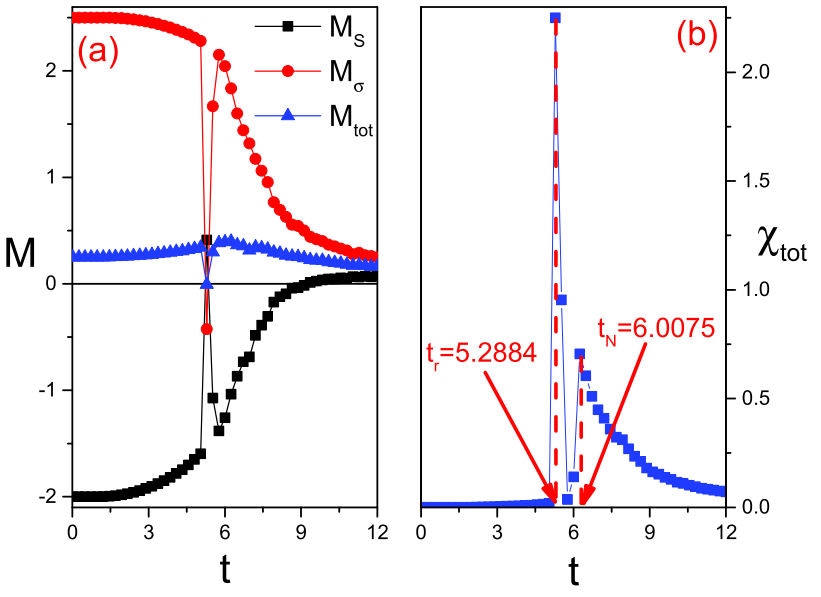

Figure 3. M (a) and χ (b) of the nested fullerene C_{24} system for $r = -1$, $p = 1$, $h = 0$ and $d = 0$.

confirming a ferrimagnetic ground state induced by the antiferromagnetic inter-sublattice coupling ($r = -1$). The total magnetisation (M_{tot}) remains positive (+0.25) due to the dominant contribution of the σ (5/2) compared to S (2). Around $t_r \approx 5.28$, a sharp discontinuity occurs where M_S drops abruptly while M_σ rises rapidly, leading to a local minimum in M_{tot}. This behaviour indicates a reentrant point (t_r), corresponding to a first-order phase transition or a sudden spin reorientation resulting from the competition between exchange and thermal energies. As the temperature further increases, all magnetisations collapse to zero near $t_N \approx 6$, marking the Neel temperature, where the system loses its ferrimagnetic order and becomes paramagnetic. Additionally, the total susceptibility χ_{tot} has two distinct peaks around the re-entrant transition (t_r) and the Néel transition (t_N), which indicates the first-order nature of the transitions. In the absence of the magnetic field ($h = 0$) and the crystal field ($d = 0$), the ferrimagnetic state for the lower-temperature phases is sustained by the rivalry between the intra- (p) and the inter-sublattice (r) exchange interactions. The re-entrant transition around $t_r \approx 5.3$ results due to thermal fluctuations that cause the preferential disruption of the magnetic order of the individual sublattices. This results in the partial reconstruction of the ferrimagnetic state and the negative sign of the magnetisation of the sublattices in some regions of the parameter space. This is then followed by the dominance of the thermal disruption in the exchange interactions as the temperature increases to trigger the transition to the paramagnetic state at $t_N \approx 6$. As seen from Figure 3, the system exhibits a ferrimagnetic ground state followed by two first-order phase transition points due to the competition in the exchange interaction and the role of the temperature.

Figure 4 presents the dependence of the reentrant temperature (t_r) and Neel temperature (t_N) on the inter-sublattice coupling parameter (r) at $p = 1$, $h = 0$, and $d = 0$. One can see from this figure that the thermal stability of the ferrimagnetic order strongly depends on the magnitude of the antiferromagnetic inter-sublattice exchange coupling ($|r|$). Both

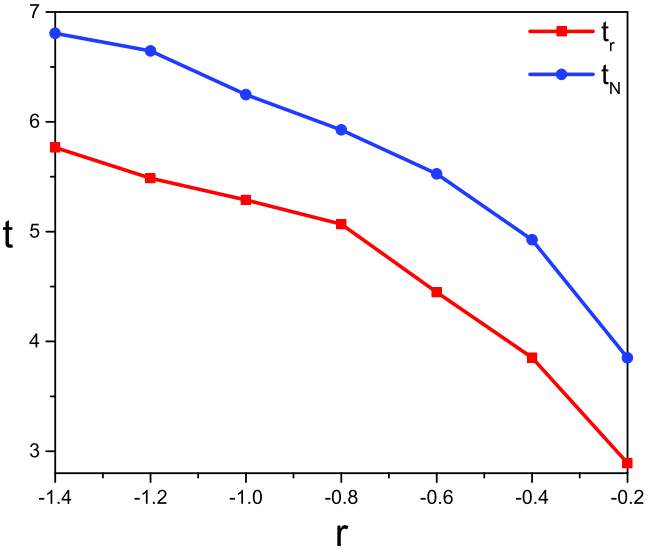

Figure 4. t_r and t_N vs. r of the nested fullerene C_{24} system for $p = 1$, $h = 0$ and $d = 0$.

critical temperatures t_r and t_N monotonically decrease by weakening the coupling strength $|r|$ from $r = -1.4$ to $r = -0.2$. Hence, the long-range magnetic order is more stable and persists up to higher temperatures if the antiferromagnetic interaction between the S and σ sublattices is stronger. Moreover, the Neel temperature (t_N) is always higher than the reentrant temperature (t_r), indicating that the spin reorientation transition at t_r systematically precedes the complete loss of magnetic order at t_N.

Figure 5 shows total magnetisation as a function of the reduced crystal field d for low temperature, $t = 1.0$ of the nested fullerene C_{24} system under zero magnetic field. In panel (a), the inter-sublattice coupling r changes from -0.2 to -1.0, -1.5, -2.0, and -2.5 by taking $p = 1$, while in panel (b), intra-sublattice coupling p changes from 0.5, 0.8, 1.0, 1.3 to 1.5 by considering $r = -1.0$. From this figure, it is observed that crystal field d acts as a magnetic switch that causes first-order phase transitions with sudden jumps in the total magnetisation. With an increase in the strength of exchange couplings, which may be inter-sublattice $|r|$ or intra-sublattice p, magnetic order becomes more rigid. Due to this rigidity, stronger coupling values need large negative crystal fields $|d|$ for the inversion or extinction of spins, shifting therefore, the transition points at lower d. From the above observations, it concludes that magnetisation stability depends not only on anisotropy but also on competition and/or cooperation provided by internal exchange energies within the system.

Figure 6 presents the hysteresis cycles of the nested fullerene C_{24} system for $t = 1.0$, i.e. the behaviour of the total magnetisation M_{tot} to the external magnetic field h under the influence of internal parameters r, p, d and temperature t. In panel (a), the coupling parameter r varies from -0.2, -1.0, -1.5 to -2.0 with $p = 1$, $t = 1$ and $d = 0$; in panel (b), p varies from 0.3, 0.5, 1.0 to 1.2 with r = -1, $t = 1$ and d = 0; in panel (c), d varies from 0.0, -1.0, -1.5 to -2.0 with $p = 1$, $t = 1$ and $r = -1$; and in panel (d), t increases from 1, 3, 5 to 6 with $r = -1$, $p = 1$ and $d = 0$. These hysteresis loops present a staircase-shaped (multi-step) profile, which reflects field-induced first-order phase transitions due to field-induced spin transitions between local states separated by energy barriers that these

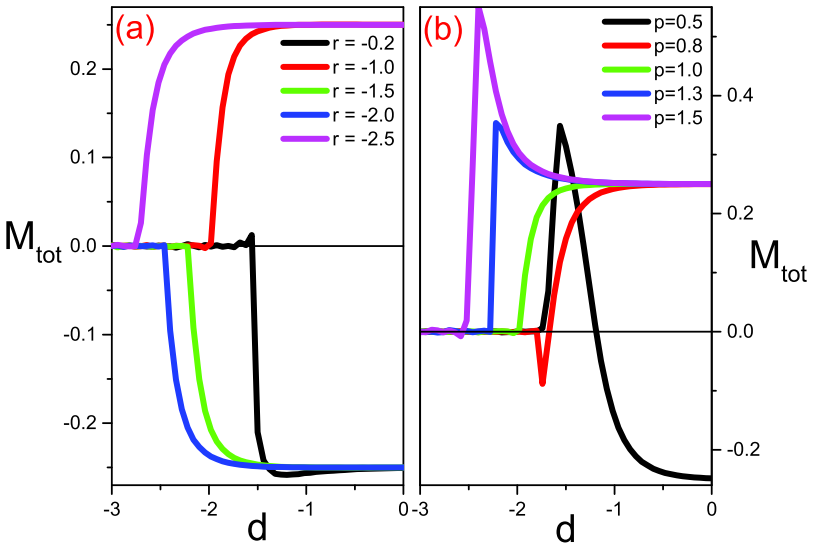

Figure 5. M_{tot} vs. d: in (a) for $p = 1$; in (b) for $r = -1$ of the nested fullerene C_{24} system with $h = 0$ and $t = 1$.

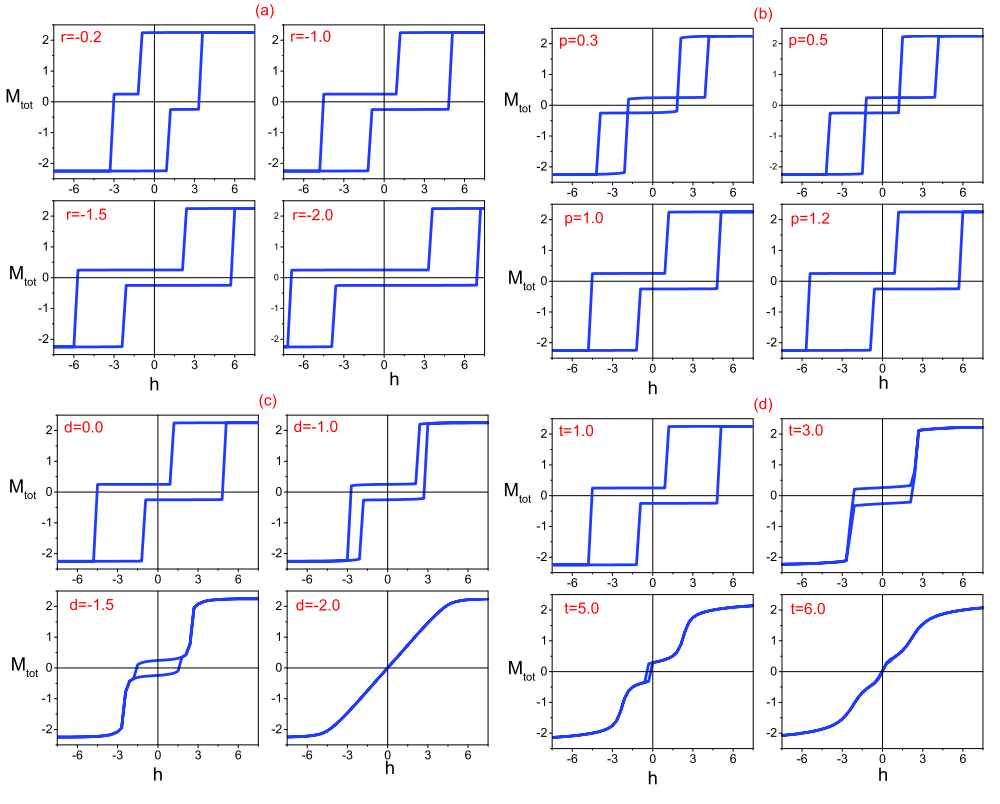

Figure 6. Magnetic hysteresis cycle: In (a) for $t = 1$, $p = 1$ and $d = 0$. In (b), for $t = 1$, $r = -1$ and $d = 0$. In (c) for $t = 1$, $p = 1$ and $r = -1$. In (d) for $r = -1$, $p = 1$ and $d = 0$.

multi-steps exactly represent. These multi-steps, far from being due only to numerical inaccuracies, actually mark transitions across these energy barriers separating different metastable configurations of spins localised in free energy convergence valleys. Within this triple C_{24} arrangement, due to the differing spin values ($S = 2$, $\sigma = 5/2$) as well as their environments, these magnetic sub-lattices switch in a layer-by-layer fashion, as shown in panels a and b, where an increased strength of sub-lattice coupling values $|r|$ and intra-lattice coupling value p, respectively, reflects increased potential energy barriers across which spins would have to switch, therefore producing a stiffer magnetic arrangement that requires larger coercive forces to reverse. Additionally, we also see that a strongly negative value of crystal field strength ($d<<0$, as in panel c) lowers the ferrimagnetic arrangement because a vanishing state ($S = 0$) becomes more favoured from a free energy consideration, producing a near-reversible hysteresis cycle implying a vanishing coercive force and remanent magnetisation.

As the temperature t increases (panel d), thermal activation becomes sufficient to cross these barriers in lower fields, resulting in a blurring and elimination of these sharp features at the Néel temperature, $t_N \approx 6$, signalling the onset of the thermally disordered paramagnetic state.

Furthermore, the staircase hysteresis in the nested C_{24} system is brought about by the discretisation of high spins, such as $S = 2$ and $\sigma = 5/2$, allowing discontinuous transitions between quantised states; sequential switching of its concentric cages due to their distinct spin magnitudes and coordination gives rise to metastable intermediate plateaus; and metastability controlled by energy barriers from the competition of the exchange (r, p) and crystal field (d) interactions. These tunable steps allow multi-level magnetic storage, wherein the plateau widths are directly controlled by the stiffness of exchange and temperature.

The hysteresis behaviour obtained in this paper is in good agreement with the recent Monte Carlo simulations on the mixed-spin nanostructures, which have also presented similar dynamic magnetic properties and hysteresis loops for the X540@Y540 structure [25], for bilayer fullerene-like structures [26,27], for a ferrimagnetic core–shell nanoparticle [28], for the bilayer graphene nanoribbons [29], for hexagonal core/double-shell nanowires [30], for the core–shell nanoparticles in an oscillating field [31], and for the mixed-spin Ising model with an MBene-like structure [32].

Moreover, though the actual model presented uses generic exchange and crystal field interactions to decouple the geometric factor, the observed magnetic phenomena show natural structural stability. When considered in a more realistic context, the actual variations of such interactions, such as anisotropies, can, as a practical effect, result only in the broadening of the peaks in the susceptibility and a rotation of the magnetisation plateaus. Whereas the basic physical processes, such as the step-by-step switching of the layers, as well as the re-entrance transitions, remain naturally secured through the shell-shaped structure and the high-spin characterisation with (2, 5/2). This suggests that the multi-step ordering and thermal stability properties are highly probable to be maintained in the nanostructured realisation, even in the presence of structural imperfections.

4. Conclusions

Based on the Blume-Capel Ising model, Monte Carlo simulations were performed in order to study the magnetic characteristics of the nested fullerene system C_{24} comprised

of two sublattices with mixed spins S = 2 and σ = 5/2, respectively. The ground-state phase diagrams analysed for t = 0 showed that due to 30 possible spin configurations, the ground state was determined mainly by competition between the crystal field and the magnetic field, and not due to the exchange couplings. The thermal behaviour exhibited a stable ferrimagnetic phase at low temperature, characterised by two consecutive first-order transitions: a reentrant transition ($t_r \approx 5.3$) caused by spin reorientation, succeeded by a transition to the paramagnetic phase at the Neel temperature ($t_N \approx 6.0$). The hysteresis cycles confirmed the occurrence of field-induced first-order phase transitions (staircase-like loops). The results showed that increasing the exchange couplings ($|r|$) and (p) enhanced the magnetic rigidity and coercivity, while a strongly negative crystal field ($d << 0$) or an increase in temperature towards (t_N) suppressed the zero-field ferrimagnetic order, leading to the disappearance of the hysteresis and remanence. This work provided a detailed understanding of the ordering mechanisms and thermal stability, and hence the potential of such architectures for applications in spintronic devices.

Disclosure statement

No potential conflict of interest was reported by the author(s).

Funding

This work was supported by this research was also supported by the National Research Foundation of Korea (NRF) grant funded by the Korea government (MSIT) [Grant Number (RS-2025-22222973)]; This research was supported by the Regional Innovation System & Education (RISE) programme through the Gyeongbuk RISE CENTER, funded by the Ministry of Education (MOE) and the Gyeongsangbuk-do, Republic of Korea [Grant Number (2025-RISE-15-115)].

Data and code availability

The investigation was conducted using Monte Carlo simulations employing the Metropolis algorithm through a Fortran code.

References

[1] M.S. Dresselhaus, G. Dresselhaus, and P.C. Eklund, *Fullerenes*. J. Mater. Res. 8(8) (1993), pp. 2054–2097.
[2] R.E. Smalley, *Discovering the fullerenes*. Rev. Mod. Phys. 69(3) (1997), pp. 723–730.
[3] R.E. Smalley and B.I. Yakobson, *The future of the fullerenes*. Solid State Commun. 107(11) (1998), pp. 597–606.
[4] B.C. Yadav and R. Kumar, *Structure, properties and applications of fullerenes*. Int. J. Nanotechnol. Appl. 2(1) (2008), pp. 15–24.
[5] D.A. García-Hernández, S. Iglesias-Groth, J.A. Acosta-Pulido, A. Manchado, P. García-Lario, L. Stanghellini, E. Villaver, R.A. Shaw, and F. Cataldo, *The formation of fullerenes: clues from new C_{60}, C_{70}, and (possible) planar C_{24} detections in magellanic cloud planetary Nebulae*. Astrophys. J. 737(2) (2011), pp. 7.
[6] Y.F. Chang, J.P. Zhang, H. Sun, B. Hong, Z. An, and R.S. Wang, *Geometry and stability of fullerene cages: C_{24} to C_{70}*. Int. J. Quantum Chem. 105(2) (2005), pp. 142–147.
[7] S. Benyoussef, A. Jabar, and L. Bahmad, *Monte Carlo study of magnetic properties of the fullerene C_{24} structure*. Phase Transitions 97(7-8) (2024), pp. 474–483.

[8] Z. Fadil, C.J. Raorane, S. Karam, A. Samih, S.C. Kim, E. Salmani, A.A. Alsayyari, and K.H. Mahmoud, *Comparative study of magnetic properties in graphene and fullerene C_{60} nanostructures via Monte Carlo simulations*. J. Magn. Magn. Mater. 622 (2025), pp. 172962.
[9] Z. Fadil, C.J. Raorane, R. El Fdil, K.H. Mahmoud, A.A. Alsayyari, and S.C. Kim, *Monte Carlo simulation study comparing the magnetic hysteresis of graphene and fullerene C $_{60}$*. Philos. Mag. (2025), pp. 1–14.
[10] S. Idrissi, A. Jabar, and L. Bahmad, *Study of magnetic properties of the fullerene C_{36} structure by Monte Carlo simulations*. Indian J. Phys. 98(10) (2024), pp. 3453–3460.
[11] S. Aouini, A. Mhirech, A. Alaoui-Ismaili, and L. Bahmad, *Magnetic properties in different fullerenes Xn nano-structures: Monte Carlo study*. Chin. J. Phys. 56(4) (2018), pp. 1640–1647.
[12] S. Idrissi, A. Jabar, and L. Bahmad, *Magnetism and critical behavior of the fullerene C_{18} studied by Monte Carlo simulations*. J. Supercond. Novel Magn. 38(1) (2025), pp. 27.
[13] O. Abounachit, A. Jabar, S. Idrissi, and L. Bahmad, *Investigation of the magnetic properties of the fullerene C_{30} with mixed spins: a Monte Carlo study*. J. Magn. Magn. Mater. 589 (2024), pp. 171604.
[14] M. Sabzevar, M. Solaimani, M.H. Ehsani, and D.H.T. Tehrani, *The effect of vacancy-defects on the magnetic properties of Ising fullerene-like nano-structures: a Monte Carlo study*. J. Magn. Magn. Mater. 502 (2020), pp. 166573.
[15] D. Kabouchi, Z. Fadil, R. El Fdil, C.J. Raorane, B. Kabouchi, A. Mhirech, E. Salmani, A.M. Tighezza, P. Rosaiah, and S.C. Kim, *Investigation of the magnetic features of the fullerene-dimer-like nanostructure (C_{60}) 2: a Monte Carlo Study*. ECS J. Solid State Sci. Technol. 13(5) (2024), pp. 051002.
[16] W. Wang, B.C. Li, T.L. Wang, J. Liang, and F.G. Zhang, *Compensation characteristics and hysteresis loops of a fullerene-like (XY) 540: a Monte Carlo study*. J. Mater. Sci. 59(20) (2024), pp. 8874–8893.
[17] T. Sahdane, R. Masrour, and A. Jabar, *Dielectric properties of the mixed spins ($S = 5/2$, $\sigma = 2$) and ($\sigma = 5/2$ and $S = 2$) in nanotube system: a Monte Carlo study*. Solid State Commun. 310 (2020), pp. 113851.
[18] N. Tahiri, A. Jabar, and L. Bahmad, *Monte Carlo study of the magnetic properties of a bi-layer decorated graphene structure*. Phys. Lett. A 381(4) (2017), pp. 189–193.
[19] A. Jabar and R. Masrour, *Monte Carlo simulations of magnetic properties of Kekulene structure bilayers separate by a nonmagnetic with RKKY interactions*. Chem. Phys. Lett. 700 (2018), pp. 130–137.
[20] R. Masrour and A. Jabar, *Magnetic properties in stacked triangular lattice: Monte Carlo approach*. Physica A 491 (2018), pp. 926–934.
[21] A. Jabar and R. Masrour, *Magnetic properties of armchair graphene nanoribbons: a Monte Carlo study*. Chin. J. Phys. 64 (2020), pp. 1–8.
[22] R. Masrour, A. Jabar, A. Benyoussef, and M. Hamedoun, *Comparable studies of magnetic properties of Ising spins-5/2 and 3/2 systems on decorated square and triangular lattices*. J. Magn. Magn. Mater. 410 (2016), pp. 223–225.
[23] A. Jabar and R. Masrour, *Magnetic properties of a graphene with alternate layers*. Superlattices Microstruct. 112 (2017), pp. 541–553.
[24] A. Jabar, R. Masrour, A. Benyoussef, and M. Hamedoun, *Monte Carlo study of alternate mixed spin-5/2 and spin-2 Ising ferrimagnetic system on the Bethe lattice*. J. Magn. Magn. Mater. 397 (2016), pp. 287–294.
[25] B.C. Li, W. Wang, and D. Lv, *Dynamic magnetic characteristics and hysteresis behaviors of X540@ Y540: A Monte Carlo study*. Physica A 662 (2025), pp. 130446.
[26] W. Wang, X.G. Wang, Z.Y. Liu, G.C. Bao, and Z.Y. Xu, Exploration of dynamic thermodynamic properties and hysteresis loops of a bilayer fullerene-like structure. Physica A 675 (2025), pp. 130864.
[27] W. Wang, Z.Y. Liu, X.G. Wang, Y. Xia, and Z.Y. Xu, Exploration of dynamic magnetic properties and magnetocaloric effect of a bilayer fullerene X540-Y540. J. Mater. Sci. 60 (2025), pp. 21338–21356.

[28] W. Wang, Z.Y. Liu, X.G. Wang, S. Zou, and D. Lv, *Magnetic properties of a ferrimagnetic core–shell nanoparticle based on Monte Carlo method*. Appl. Phys. A 131(5) (2025), pp. 351.
[29] M. Mouhib, A.E. Fadl, S. Bri, M.D. Belrhiti, and H. Mounir, *The magnetic and hysteretic characteristics of bilayer graphene nanoribbons: a comparative study by the Monte Carlo method*. Phys. Scr. 100(8) (2025), pp. 085994.
[30] M. Chakir, A. El Ghazrani, and L.B. Drissi, *Magnetic phase transitions and hysteresis in hexagonal multi-layered core/double-shell nanowires*. J. Supercond. Novel Magn. 38(3) (2025), pp. 150.
[31] Z.Y. Liu, W. Wang, D. Lv, and Y.H. Tu, *Dynamic magnetic properties of core-shell nanoparticles in an oscillating magnetic field*. Phys. B 697 (2025), pp. 416707.
[32] B.W. Xiao, S.Y. Huang, Y. An, and W. Wang, *Dynamic magnetic properties of the mixed-spin (5/2, 2) Ising model with an MBene-like structure*. Physica A 663 (2025), pp. 130447.
[33] M. Arejdal, *A computational study of the magnetocaloric effect in the LaCr2Si2C compound*. Polyhedron *183* (2020), pp. 114539.
[34] M. Arejdal, L. Bahmad, and A. Benyoussef, *The calculated magnetic properties and magnetocaloric effect in compound MnAs*. J. Supercond. Novel Magn. *30*(6) (2017), pp. 1565–1574.
[35] M. Arejdal, A. Abbassi, A. Kadiri, A. Slassi, and L. Bahmad, *The magnetic properties and magneto-caloric effect in the compound MnBi: The Monte Carlo study*. J. Magn. Magn. Mater. 466 (2018), pp. 463–468.
[36] M. Arejdal, *Prediction of the magnetocaloric behaviors of the kekulene structure for the magnetic refrigeration*. Results Phys. *18* (2020), pp. 103342.
[37] M. Arejdal, *The theoretical study of the magneto-caloric effect in a nano-structure formed on a Dendrimer structure*. Appl. Phys. A *126*(11) (2020), pp. 829.
[38] O.D. Jayakumar and A.K. Tyagi, *Spintronic materials, synthesis, processing and applications*, Elsevier, Amsterdam, 2012193228.
[39] W. Wang, D. Lv, F. Zhang, J.L. Bi, and J.N. Chen, *Monte Carlo simulation of magnetic properties of a mixed spin-2 and spin-5/2 ferrimagnetic Ising system in a longitudinal magnetic field*. J. Magn. Magn. Mater. *385* (2015), pp. 16–26.
[40] N. De La Espriella, C.A. Mercado, and J.C. Madera, *Spin compensation temperatures in the Monte Carlo study of a mixed spin-2 and spin-5/2 Ising ferrimagnetic system*. J. Magn. Magn. Mater. *401* (2016), pp. 22–29.
[41] A. Jabar, L. Bahmad, and A. Benyoussef, *Phase transitions and magnetic properties of zigzag triangular nanographenes: Monte Carlo simulation*. J. Supercond. Novel Magn. *36*(1) (2023), pp. 111–118.

Philosophical Magazine

ISSN: 1478-6435 (Print) 1478-6443 (Online) Journal homepage: www.tandfonline.com/journals/tphm20

Monte Carlo simulations of magnetisation plateaus of mixed spin 7/2-1 Ising model in a CrI_3-inspired nanostructure

Z. Fadil, Chaitany Jayprakash Raorane, Hussein Sabbah, Gamal A. Shazly & Seong Cheol Kim

To cite this article: Z. Fadil, Chaitany Jayprakash Raorane, Hussein Sabbah, Gamal A. Shazly & Seong Cheol Kim (2025) Monte Carlo simulations of magnetisation plateaus of mixed spin 7/2-1 Ising model in a CrI_3-inspired nanostructure, Philosophical Magazine, 105:23, 1654-1667, DOI: 10.1080/14786435.2025.2539851

To link to this article: https://doi.org/10.1080/14786435.2025.2539851

PHILOSOPHICAL MAGAZINE
2025, VOL. 105, NO. 23, 1654–1667
https://doi.org/10.1080/14786435.2025.2539851

Taylor & Francis
Taylor & Francis Group

Monte Carlo simulations of magnetisation plateaus of mixed spin 7/2-1 Ising model in a CrI_3-inspired nanostructure

Z. Fadil[a]*, Chaitany Jayprakash Raorane[b]*, Hussein Sabbah[c], Gamal A. Shazly[d] and Seong Cheol Kim[b]

[a]Faculty of Sciences, Laboratoire de Matière Condensée et Sciences Interdisciplinaires (LaMCScI), URL-CNRST, Mohammed V University in Rabat, Rabat, Morocco; [b]School of Chemical Engineering, Yeungnam University, Gyeongsan, Republic of Korea; [c]College of Engineering and Technology, American University of the Middle East, Egaila, Kuwait; [d]Department of Pharmaceutics, College of Pharmacy, King Saud University, Riyadh, Saudi Arabia

ABSTRACT

Motivated by recent advances in the study of magnetisation plateaus and their relevance to nanotechnology applications, this research used Monte Carlo simulations using the Blume-Capel model to explore the phase diagrams and magnetisation behaviour in a CrI_3-inspired nanostructure at very low temperatures. Our study reveals that the system exhibits 16 stable configurations symmetrically distributed around the zero magnetic field, which is a characteristic feature of ferrimagnetic systems. Furthermore, the magnetisation plateaus of the CrI_3-inspired nanostructure were strongly influenced by the crystal field D, the ferrimagnetic coupling $J_{S\sigma}$, and the temperature T. These findings enhance our insight into the dynamics of magnetisation of CrI_3-inspired nanostructure, with potential applications in spintronics, by aligning with established theoretical models.

ARTICLE HISTORY
Received 4 December 2024
Accepted 22 July 2025

KEYWORDS
Monte Carlo simulations; ground-state phase diagrams; magnetisation plateaus; CrI_3-inspired nanostructure; Blume-Capel model

1. Introduction

Due to their distinct physical characteristics and a variety of possible uses, 2D materials have been attracting a lot of attention recently. These applications are especially evident in the domains of electronics [1, 2], spintronics [3, 4] and magnetic storage [5, 6] systems. Additionally, layered magnetic semiconductors like chromium trihalides (CrI_3), offer a promising class of van der Waals materials with potential for advancing 2D spintronic technologies. The intrinsic magnetic anisotropy in CrI_3 layers supports ferromagnetism at the monolayer level, while the weak antiferromagnetic interaction between the layers results in remarkably high tunnel magnetoresistance [7]. CrI_3, being a layered and easily exfoliated semiconductor, displays unique magnetic characteristics, including an unexpected temperature-dependent variation in magnetisation [8]. The regulation and

CONTACT Z. Fadil fadilzakaria604@gmail.com Faculty of Sciences, Laboratoire de Matière Condensée et Sciences Interdisciplinaires (LaMCScI), URLCNRST, Mohammed V University in Rabat, P.O. Box 1014, Rabat 10500, Morocco; Seong Cheol Kim sckim07@ynu.ac.kr School of Chemical Engineering, Yeungnam University, Gyeongsan 38541, Republic of Korea
*These authors have contributed equally to this work.

preservation of valley polarisation is essential for valleytronic devices. Ferroelectric polarisation inversion has been proposed to control and stabilise the valley state within a trilayer heterostructure composed of 2D (HfN_2), ferromagnetic (CrI_3) and ferroelectric (In_2Se_3) valleytronic materials. Simulations indicate that polarisation inversion of In_2Se_3 changes the orientation of the magnetisation axis of CrI_3 [9]. The series of 2D materials is expanding, offering new opportunities to explore phenomena and create van der Waals (vdW) heterostructures. Until recently, this family lacked a crucial member: 2D magnets. In the last two years, numerous atomically thin magnetic crystals have been identified. The distinct magnetic properties observed in 2D materials, particularly CrI_3, compared to their bulk counterparts, along with the development of van der Waals heterostructures enabled by 2D magnets, provide exciting new opportunities in this rapidly growing field [10]. The study of magnetism in 2D nanostructures [11,12] is essential for the development of next-generation technologies, particularly in the fields of spintronics [13,14], data storage [15,16] and quantum computing [16,17]. In spintronics, 2D magnetic materials can serve as efficient spin filters [18,19], transistors or even memory devices [20,21], since they may retain long-range magnetic order in small dimensions. Additionally, they are perfect for sensors and other electronic applications due to their high surface-to-volume ratio [22], where nanoscale magnetic interactions are essential. Besides, experimental studies have led to a better understanding of the presence of magnetisation plateaus in various materials. For example, in $SrCu_2(BO_3)_2$, a remarkable series of magnetisation plateaus has been observed and is currently the subject of intensive research [23]. Similarly, in $Cu_3(CO_3)_2(OH)_2$ compound, a 1/3 magnetisation plateau has been clearly detected, with results examined employing exact diagonalization and density matrix renormalisation techniques [24]. On the theoretical front, Monte Carlo simulations using the Blume-Capel model have been applied to study magnetisation plateaus in various nanostructures. For example, zigzag graphene nanoribbons [25] and nano-graphene bilayer [26] structures exhibit multiple magnetisation plateaus due to competition between anisotropies, exchange couplings and external fields. These simulations allow us to better understand complicated magnetic interactions in low-dimensional systems by allowing us to investigate in depth how physical parameters affect magnetisation behaviour. Theoretical research also extends to structures such as the magnetisation plateaus of TbB_4 in a frustrated Ising model [27], honeycomb nanorods [28], and decorated hexagonal nanoparticles [29]. In bi-layer graphyne-like structures [30] and nano-graphene with a sandwich-like structure [31], the Monte Carlo approach has proved effective in optimising magnetic properties. These advances offer significant potential for applications in fields such as spintronics and nanotechnology. Moreover, CrI_3 structure are thermodynamically stable in 2D form, with ferromagnetic order up to ~45 K [7, 10], but require encapsulation due to sensitivity to humidity and oxidation. Their crystal structure belongs to the P-3m1 space group, featuring a hexagonal lattice with *Cr* atoms octahedrally coordinated by six I atoms. Exfoliated from bulk (rhombohedral R-3 or monoclinic C2/m), weak vdW forces enable stable monolayers. Challenges like low Curie temperatures and environmental sensitivity must be addressed for room-temperature applications [7, 10], yet CrI_3 remains promising for spintronics, valleytronics, and quantum technologies. Besides, motivated by recent studies on magnetisation plateaus and their applications in nanotechnology, this work employs Monte Carlo simulations using the Metropolis algorithm and the Blume-Capel model to

investigate the ground-state phase diagrams and magnetisation plateau behaviour in a CrI_3-inspired nanostructure. The growing interest in 2D magnetic materials for spintronics, nanotechnology, and quantum computing has highlighted CrI_3 as a promising candidate due to its intrinsic magnetic anisotropy, which enables ferromagnetism at the monolayer level. The interplay between exchange interactions, crystal field effects, and thermal fluctuations leads to the formation of discrete magnetisation plateaus, whose stability and tunability are enhanced in nanostructures. Using Monte Carlo simulations, we aim to identify and characterise these plateaus, analyse the effects of key parameters such as crystal field strength D, ferrimagnetic coupling $J_{S\sigma}$, and temperature T, and compare our findings with existing theoretical studies on 2D systems. Given their relevance in quantum materials and potential applications in high-density data storage, magnetic sensors, and spintronic devices, the results of this study contribute to the broader exploration of tuneable magnetic states in van der Waals 2D materials.

This study is organised as follows: Section 2 summaries the model and method used. Section 3 explores the ground state phase diagrams, while Section 4 delves into the investigation of magnetisation plateaus. Finally, Section 5 concludes the article with a summary of the key findings.

2. Model and method

This study employs simulations based on the Monte Carlo method with the Metropolis algorithm, based on the Blume-Capel model, to explore the ground state phase diagrams at zero temperature ($T = 0$) and investigate the magnetisation plateau behaviour at very low temperatures ($T = 0.01$) in a mixed CrI_3-inspired nanostructure, consisting of 32 atoms with spin type S ($N_S = 32$), where $S = 1$, and 8 atoms with spin type σ ($N_\sigma = 8$), where $\sigma = 7/2$. The Ising Blume-Capel model is used to study discrete magnetisation plateaus, suitable for systems with out-of-plane anisotropy. Instead of replicating experimental or DFT-derived parameters of CrI_3, the study introduces artificial magnetism to explore basic magnetic behaviour. This model serves as a theoretical framework for other nanosystems, as seen in references [25–30]. In addition, to ensure that the system reached thermal equilibrium and eliminate transient effects, 5×10^5 initial Monte Carlo steps were discarded, as shown in Figure 1. During this equilibration phase, fluctuations in the system's energy and magnetisation were monitored to confirm stabilisation before proceeding with measurements. Once equilibrium was reached, statistical data collection was carried out over 5×10^6 Monte Carlo steps per spin to ensure accurate averaging and minimise statistical errors. This large number of Monte Carlo steps enables precise determination of thermodynamic quantities, reducing noise and improving the reliability of calculated magnetisation plateaus.

In this study, spins of 1 and 7/2 are artificially introduced to model the magnetic properties of the system. Specifically, spin-1 is assigned to Cr atoms (S_i) to model simple magnetic interactions (±1 or 0), while spin-7/2 is assigned to neighbouring atoms (σ_j) to represent more complex magnetic states ($\pm 7/2, \pm 5/2, \pm 3/2, \pm 1/2$), thus enabling a richer exploration of the magnetic behaviour, particularly regarding spin configurations and multiple magnetisation plateaus. This approach, using artificial spins, aims to simulate the magnetic behaviour of the nanostructure. Cr and I atoms are assigned spins that can contribute to magnetisation. The primary objective is to study the magnetic

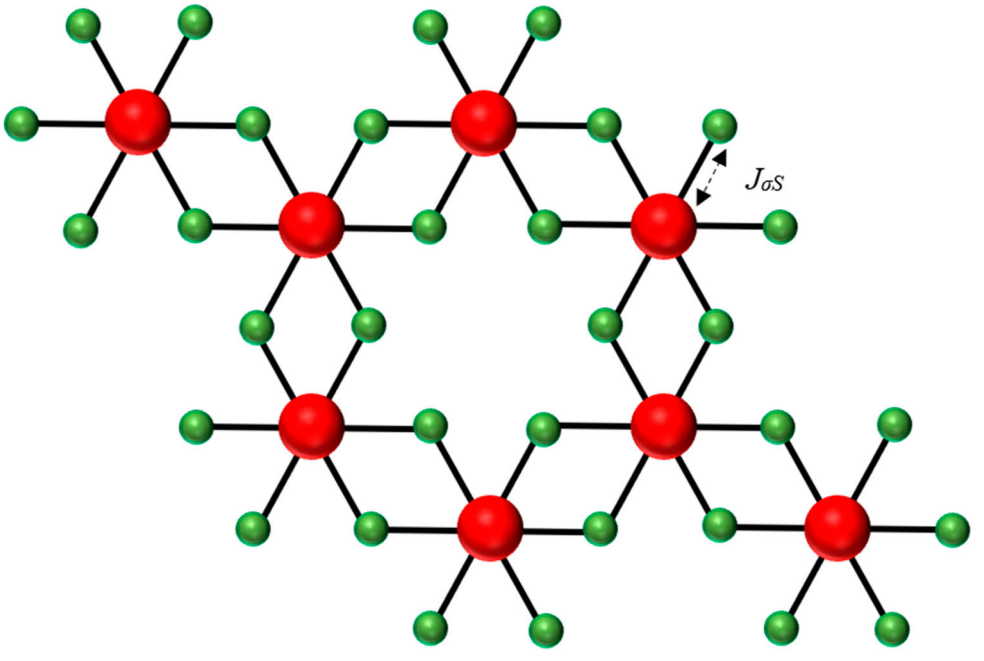

Figure 1. Illustration depicting the CrI_3-inspired nanostructure, highlighting the ferrimagnetic interaction among two distinct atom types: S-1 (green) and σ−7/2 (red).

properties at the nanometric scale of such a structure. Many non-magnetic structures in the literature replace non-magnetic atoms with magnetic atoms; see, for example, references [25, 26, 31]. Furthermore, in the system studied, we used free boundary conditions. To assess the robustness of our results in relation to the size of the system, we doubled the number of spins while maintaining the same model configuration and boundary conditions, and remaining within the framework of a nanostructure, given the numerical feasibility of the calculations. The results show that the magnetisation plateaus remain qualitatively unchanged, indicating that the observed magnetic characteristics are not significantly affected by system size in the nanoscale regime. Therefore, we focused our study on the number of atoms mentioned in the paper. This reinforces the relevance and validity of our results for finite nanostructures.

The governing Hamiltonian of the CrI_3-inspired nanostructure is outlined below:

$$H = -J_{\sigma S}\sum_{\langle i,j\rangle}\sigma_i S_j - H\left(\sum_i \sigma_i + \sum_j S_j\right) - D_\sigma \sum_i (\sigma_i)^2 - D_S \sum_j (S_j)^2, \qquad (1)$$

In this context, $J_{\sigma S}$ represents the interaction between two nearest neighbour atoms with spins σ and S, mediated through ferrimagnetic interaction. The external magnetic field is represented by the symbol H. The spin S can assume values of ±1 and 0, while the spin σ can take values of ±7/2, ± 5/2, ± 3/2, and ±1/2. To simplify the analysis by reducing the number of parameters exhibiting similar behaviour, we unify the crystal fields D_S and D_σ, which influence spins S and σ, into a single parameter D. The crystal fields D_S and D_σ independently influence the spins S and σ, respectively. To simplify the analysis

and reduce complexity, we equate both parameters, defining a unified crystal field parameter D such that $D_S = D_\sigma = D$. This assumption facilitates a more straightforward interpretation of the system's behaviour without compromising generality. $J_{\sigma S}$ is chosen as the characteristic energy scale, serving as a reference for interaction strength and temperature, which may vary depending on the system under study. This is a common practice in theoretical studies. This choice allows all physical quantities to be expressed in dimensionless form, simplifying the analysis and facilitating the generalisation of results to various systems, which may vary depending on the system under study. Such normalisation is standard in Ising model studies, as it enables direct comparisons between different research works and the identification of universal scaling behaviours. See, for example, references [25, 26, 29, 31].

Each site's internal energy is defined as:

$$E_T = \frac{\langle \mathcal{H} \rangle}{N_{tot}}, \tag{2}$$

With $N_{tot} = N_S + N_\sigma = 42$ atoms.

The calculation of sublattices and total magnetisation is performed as follows:

$$M_S = \frac{1}{N_S} \sum_i S_i, \tag{3}$$

$$M_\sigma = \frac{1}{N_\sigma} \sum_i \sigma_i, \tag{4}$$

$$M_{tot} = \frac{N_S M_s + N_\sigma M_\sigma}{N_S + N_\sigma}, \tag{5}$$

3. Ground state phase diagrams

This study focuses on exploring the complex ground-state phase diagrams of a CrI_3-inspired nanostructure, incorporating spins $\sigma = 7/2$ and $S = 1$. Using the Hamiltonian defined in Eq. (1), the ground-state energy was calculated by examining the 24 possible spin configurations, determined from the product $(2\sigma + 1)$ x $(2S + 1) = 8 \times 3 = 24$. This accounts for the different orientations that both spins can assume, considering the discrete states available for each spin type.

In Figure 2, the phase diagram was plotted in the (D, H) plane, where D is the crystal field and H represents the external magnetic field. The phase diagram was generated while fixing the ferrimagnetic coupling constant between σ and S at $J_{\sigma S} = -1$, which imposes an antiparallel alignment of the spins, reflecting a ferrimagnetic interaction.

The results highlight 16 distinct stable configurations, symmetrically distributed around the $H = 0$ axis, where the external magnetic field was zero. This symmetry indicates that the system's behaviour is equally stable for positive and negative values of H, a characteristic common in ferrimagnetic systems due to the opposing spin alignment. Furthermore, it is important to note that all stable configurations occur when the crystal field D takes negative values. This suggests that in this system, the crystal field's

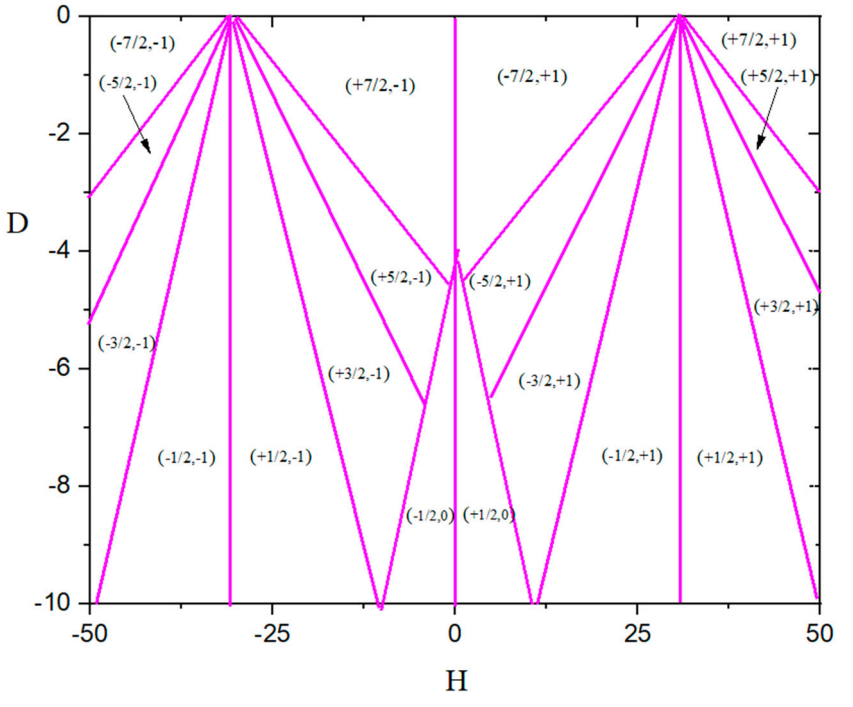

Figure 2. Ground state phase diagrams depicting $J_{S\sigma} = -1$.

influence favours specific spin alignments, leading to these stable configurations under negative D.

4. Magnetisation Plateaus

This section explores the emergence of magnetisation plateaus as various parameters were adjusted. Figure 3 presents the magnetisation plateaus for (a) sublattices and (b) total magnetisation, calculated at very low temperature $T = 0.01$, a crystal field value $D = -15$, and a fixed ferrimagnetic coupling $J_{\sigma S} = -1$. These conditions allow for a detailed investigation of the magnetisation behaviour, emphasising the unique contributions from both sublattices, M_S and M_σ, and their combined effect on the total magnetisation, M_{tot}. The sublattice magnetisation M_σ, associated with spin $\sigma = 7/2$, reveals eight distinct magnetisation plateaus. These plateaus occur at the following values: $M_\sigma = -7/2, -5/2, -3/2, -1/2, +1/2, +3/2, +5/2, +7/2$, corresponding to the possible states of the spin σ. These plateaus reflect the stability of the system as the external magnetic field was varied, showing the quantised steps in magnetisation where the system resists further spin alignment due to the field. On the other hand, the sublattice magnetisation M_S, associated with spin $S = 1$, displays three distinct magnetisation plateaus at $M_S = -1, 0, +1$, corresponding to the possible spin orientations of the $S = 1$ atom. This behaviour demonstrates that the spin S sublattice has fewer possible stable states compared to σ, resulting in fewer plateaus. By summing the contributions from both sublattices, the total magnetisation, Mtot, exhibits eight distinct plateaus. These plateaus were symmetrically distributed across the external magnetic field, with four occurring when $H<0$ and

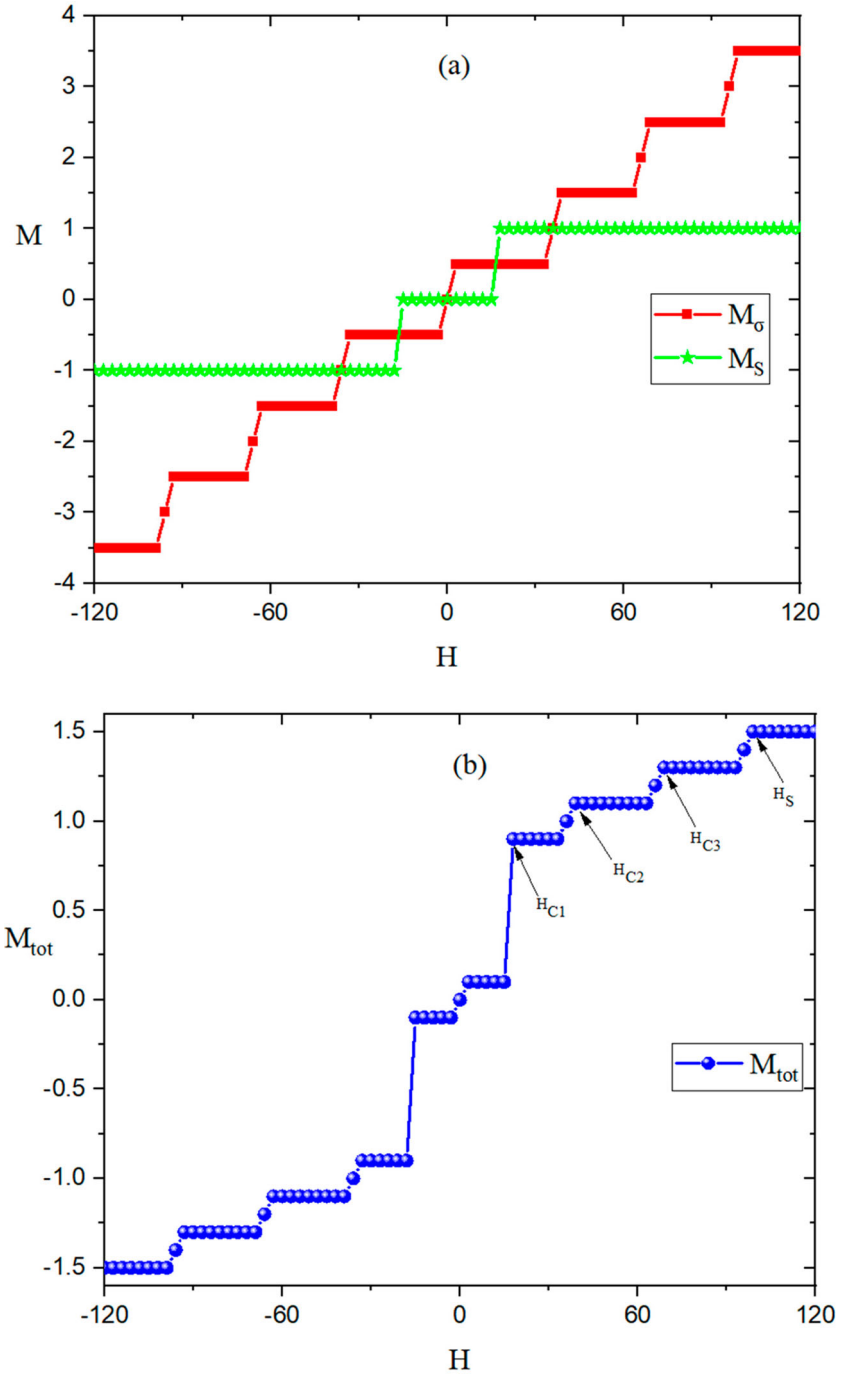

Figure 3. Magnetisation plateaus of (a) sublattices and (b) total magnetisation for $T = 0.01$, $D = -15$ and $J_{S\sigma} = -1$.

four when $H > 0$, a characteristic of systems with ferrimagnetic ordering. The total magnetisation plateaus occur at $M_{tot} = -1.50, -1.30, -1.10, -0.89, +0.89, +1.10, 1.30$ and $+1.50$. This symmetric distribution of plateaus highlights the balance between the spin

sublattices in response to changes in the external magnetic field. Additionally, for $H > 0$, the system reveals two critical fields (H_{c1}, H_{c2}, H_{c3}) and a saturation field H_S. The critical fields correspond to the points where the system undergoes transitions between different magnetisation plateaus, while the saturation field marks the maximum magnetisation, where all spins are aligned with the external field. These critical points and the saturation field are key indicators of the magnetic behaviour of the CrI_3-inspired nanostructure and provide insight into the phase transitions of the system.

Figure 4 illustrates the total magnetisation plateaus at a low temperature of $T = 0.01$ T $= 0.\ 01$, highlighting two distinct cases: (a) the effect of varying crystal field D while keeping ferrimagnetic coupling constant $J_{S\sigma} = -1$, and (b) the effect of varying $J_{S\sigma}$ while keeping D constant at -15.

As the crystal field D was decreased, it was observed that the critical fields, which represent the transitions between different magnetisation plateaus increase (Figure 4a). This behaviour can be explained by the fact that a stronger (more negative) crystal field stabilises certain spin states, making it harder for the external magnetic field to induce transitions between them. As a result, the nanosystem requires a larger external magnetic field to overcome the energy gap created by the crystal field, leading to an increase in the critical and saturation fields. Additionally, this stabilisation effect extends the width of the magnetisation plateaus, as the nanosystem resists further spin reorientation over a larger range of external magnetic field values.

In Figure 4b, a similar trend was observed when the ferrimagnetic coupling $J_{S\sigma}$ was decreased. The ferrimagnetic coupling determines the strength of the interaction between the spins σ and S. A weaker coupling (i.e. more negative values of $J_{S\sigma}$) reduces the influence of the opposing sublattice spin on each individual spin. As a result, each spin becomes more sensitive to the external magnetic field, leading to an increase in the critical and saturation fields. With weaker coupling, the nanosystem also exhibits larger magnetisation plateaus, as the spins are more loosely coupled and can maintain stable orientations over a wider range of magnetic field values.

In both cases, decreasing D or $J_{S\sigma}$ leads to an increase in the critical and saturation fields, which reflects the nanosystem's enhanced resistance to changes in magnetisation. This increased stability was reflected in the larger magnetisation plateaus, where the nanosystem remains in a stable magnetisation state over a broader range of H. These findings demonstrate the significant influence of both the crystal field and the ferrimagnetic coupling on the magnetisation dynamics of the CrI_3-inspired nanostructure.

Figure 5 shows the behaviour of the critical and saturation fields at $T = 0.01$, based on the data in Figure 4. The figure shows two scenarios: (a) varying the crystal field D while preserving the ferrimagnetic coupling $J_{S\sigma} = -1$, and (b) varying $J_{S\sigma}$ with D kept at $-$ 15. The study shows that increasing the absolute values of $|D|$ and $|J_{S\sigma}|$ leads to a nearly linear increase in the critical and saturation fields. This behaviour shows that greater crystal fields and ferrimagnetic couplings enhance the energy barriers between different magnetisation states, making it more difficult for the external magnetic field to cause transitions between them.

Moreover, the second critical field H_{c2} was more sensitive to changes in $|D|$ and $|J_{S\sigma}|$ than the first critical field H_{c1}. Because H_{c2} represents a mid-point transition with more spins reoriented, the system becomes more sensitive to these factors. Similarly, H_{c3} corresponds to higher-energy transitions and was even more sensitive than H_{c2}

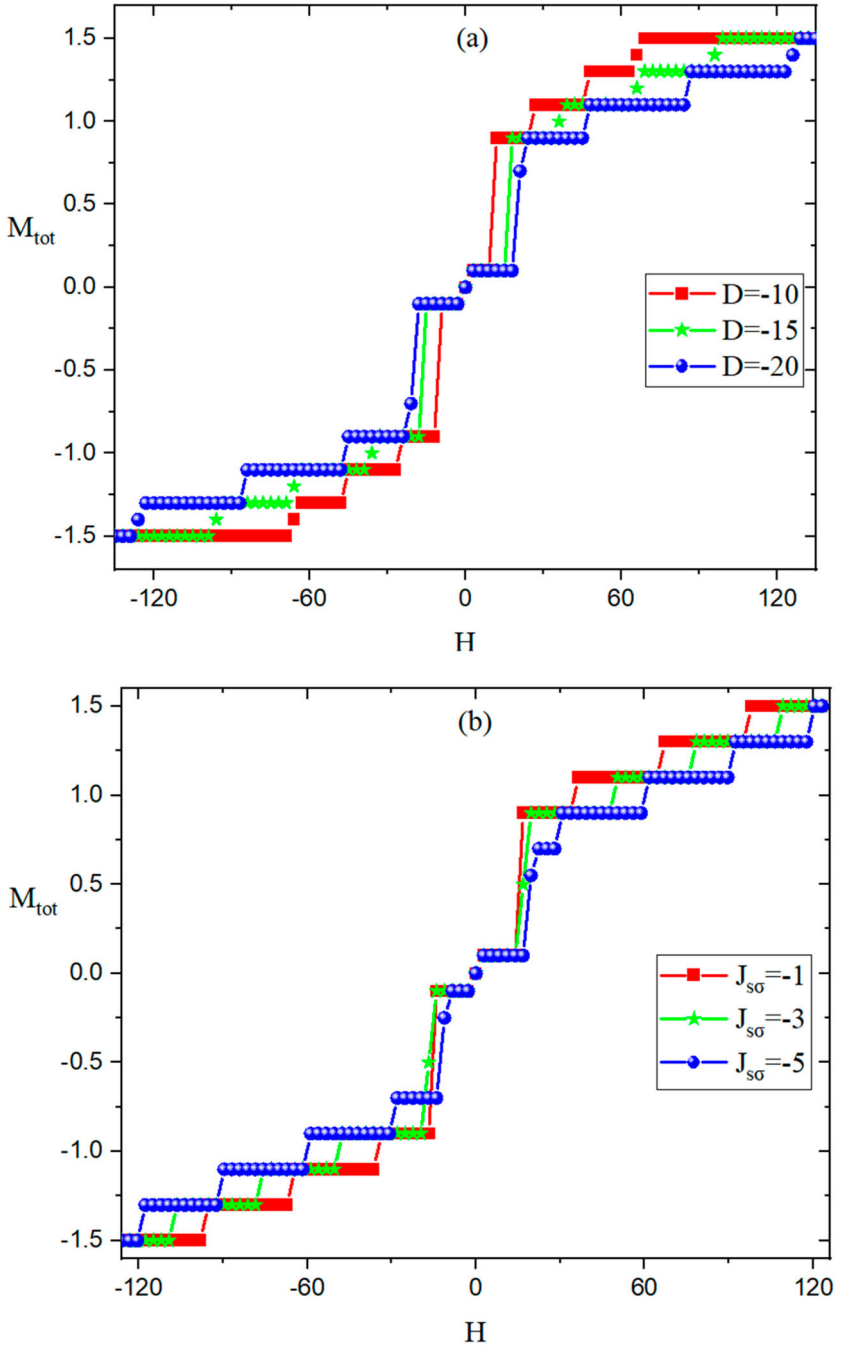

Figure 4. Total magnetisation plateaus at $T = 0.01$: (a) obtained by varying D while keeping $J_{S\sigma}$ constant at − 1, (b) by varying $J_{S\sigma}$ with D held constant at −15.

as the nanosystem nears full spin alignment, where the interactions grow more complex.

The saturation field H_S, which represents the point at which all spins were completely aligned with the external magnetic field, also shows considerable sensitivity to changes in

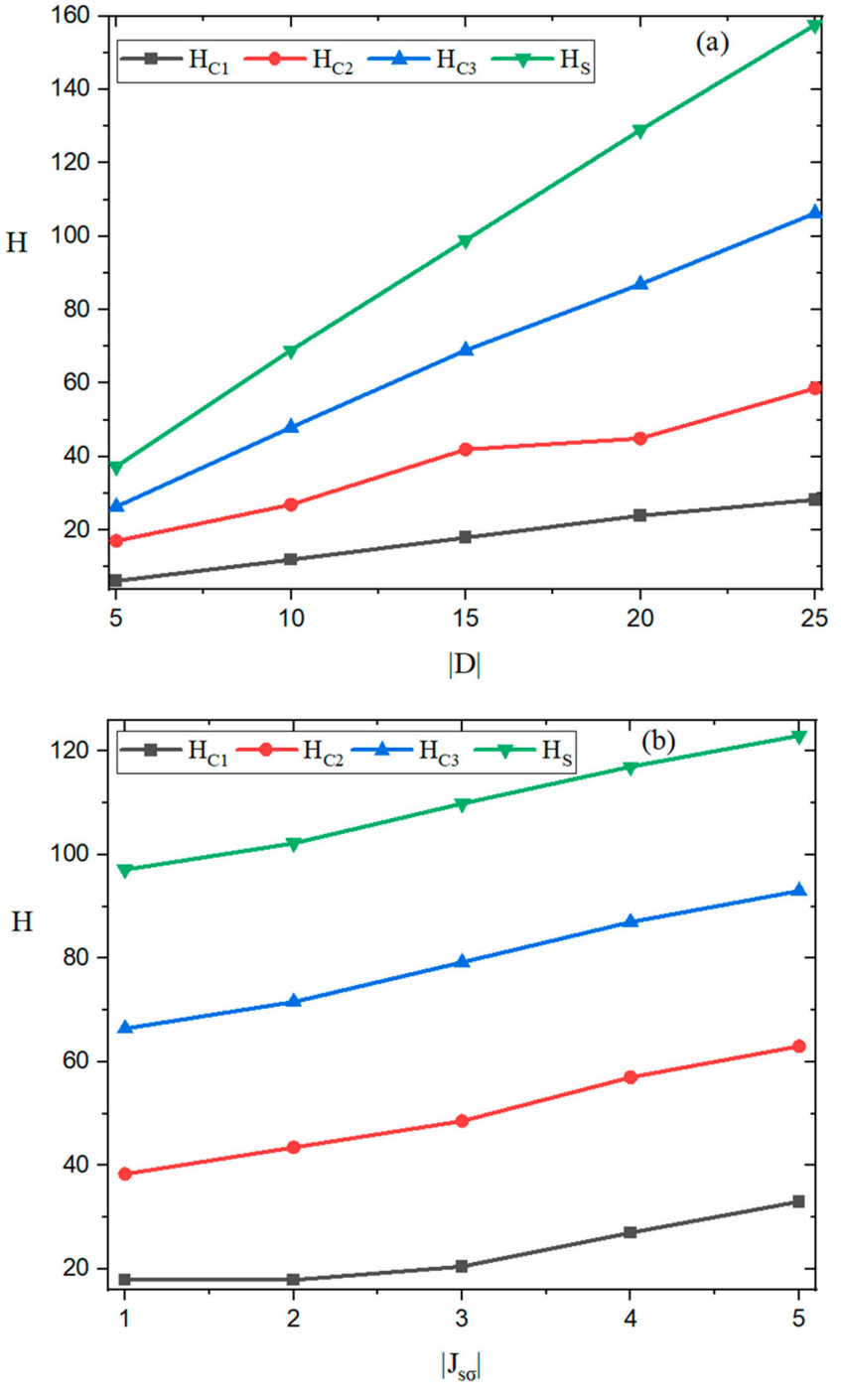

Figure 5. Behaviour of critical and saturation fields at $T = 0.01$: (a) for varying D with $J_{S\sigma}$ kept at -1, and (b) for varying $J_{S\sigma}$ while D is held at -15.

both $|D|$ and $|J_{S\sigma}|$. As these parameters increase, the energy required to fully align the spins also increases, showing further the influence of the crystal field and coupling strength on the magnetic behaviour of the nanosystem.

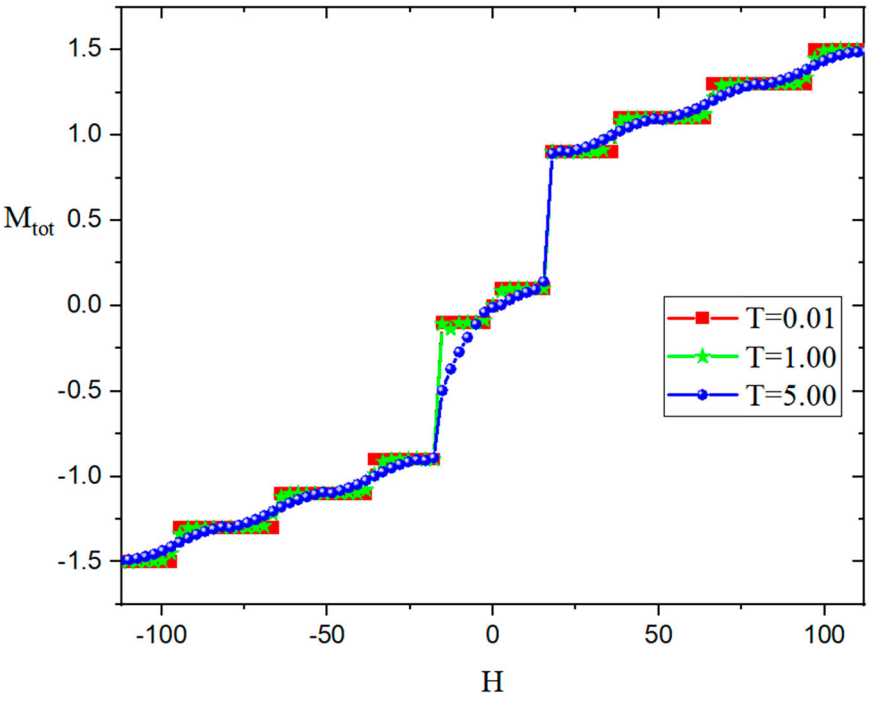

Figure 6. Total magnetisation plateaus obtained by varying T, while keeping $J_{S\sigma}$ at −1 and D at −15.

In order to conclude the study of magnetisation plateaus, it is necessary to consider the effect of temperature. Figure 6 depicts total magnetisation plateaus at different temperatures, with $J_{S\sigma} = -1$ and $D = -15$. The findings show that these plateaus emerge only at extremely low temperatures and become more prominent as the temperature approaches zero. This was because, at low temperatures, thermal fluctuations were limited, allowing spins to settle into stable, quantised states that resist further alignment by the external magnetic field.

As the temperature rises, thermal agitation destroys these stable spin configurations, causing plateaus to gradually disappear. Higher temperatures provide enough energy for spins to transition between states, resulting in a more continuous and disordered magnetisation response. Thus, extremely low temperatures were critical for the creation of magnetisation plateaus, but higher temperatures cause them to dissipate due to thermal randomness.

These findings on magnetisation plateau behaviour, observed under the variation of key parameters such as the crystal field strength D, the ferrimagnetic coupling $J_{S\sigma}$, and temperature T, align closely with the well-established patterns documented in previous studies. The observed plateaus, characterised by discrete and stable magnetisation states, are consistent with theoretical predictions and observations reported in earlier works that study similar systems, including zigzag graphene nanoribbon structures, nano-graphene bilayer structures, the TbB_4 system, honeycomb nanostructures, hexagonal decorated nanoparticles, bi-layer graphyne-like structures, and nano-graphene with sandwich-like structures using Monte Carlo simulations [25–31]. For instance, the influence of the crystal field D on stabilising specific magnetic phases, the role of ferrimagnetic coupling

$J_{S\sigma}$ in modulating interlayer interactions, and the temperature-dependent transitions between plateau states all corroborate findings from prior investigations. This consistency not only validates the reliability of the Monte Carlo simulations employed in this study but also reinforces the broader understanding of magnetisation dynamics in low-dimensional systems. Such alignment with existing literature underscores the robustness of the observed phenomena and highlights the potential of CrI_3-inspired nanostructure as a tuneable platform for exploring magnetic states in van der Waals materials, with implications for spintronics, quantum computing, and high-density data storage technologies.

5. Conclusions

Motivated by recent advances in the study of magnetisation plateaus and their relevance to nanotechnology applications, this research successfully employed Monte Carlo simulations using the Metropolis algorithm, with the Blume-Capel model, to explore the phase diagrams and magnetisation behaviour in a CrI_3-inspired nanostructure at very low temperatures. Our study reveals that the system exhibits 16 stable configurations, symmetrically distributed around the zero magnetic field, a characteristic of ferrimagnetic systems. The D crystal field plays a crucial role in determining the stability of these configurations, favouring negative values for its contribution. In addition, the study highlights the appearance of magnetisation plateaus for sublattices and total magnetisation, reflecting the quantised steps that emerge when the external magnetic field was varied. The magnetisation behaviour of the CrI_3-inspired nanostructure was strongly influenced by crystal field D, ferrimagnetic coupling $J_{S\sigma}$ and temperature T. Increasing $|D|$ and $|J_{S\sigma}|$ increases the critical and saturation fields, reflecting higher energy barriers between the magnetisation states. The sensitivity of the system intensifies at higher critical fields as it approaches full spin alignment. Magnetisation plateaus were prominent at very low temperatures, where thermal fluctuations were minimal. As the temperature rises, these plateaus fade due to increased thermal agitation. These results provide a better understanding of the magnetisation behaviour of CrI_3-inspired nanostructure, with potential applications in spintronics, in agreement with established theoretical models.

Acknowledgements

The authors acknowledge and appreciate the Ongoing Research Funding Program (ORF-2025-1118), King Saud University, Riyadh, Saudi Arabia.

Disclosure statement

No potential conflict of interest was reported by the author(s).

Funding

This research was supported by the Ongoing Research Funding Program (ORF-2025-1118), King Saud University, Riyadh, Saudi Arabia. Also, this research was supported by the Basic Science Research Program through the National Research Foundation of Korea (NRF) funded by the Ministry of Education (2020R1I1A3052258) and the support of the '2024 System Semiconductor Technology Development Support Project' of Chungbuk Technopark.

References

[1] A.K. Katiyar, A.T. Hoang, D. Xu, J. Hong, B.J. Kim, S. Ji, and J.H. Ahn, *2D materials in flexible electronics: recent advances and future prospectives*. Chem. Rev. 124(2) (2023), pp. 318–419.

[2] S.J. Kim, K. Choi, B. Lee, Y. Kim, and B.H. Hong, *Materials for flexible, stretchable electronics: graphene and 2D materials*. Ann. Rev. Mater. Res. 45(1) (2015), pp. 63–84.

[3] Y.P. Feng, L. Shen, M. Yang, A. Wang, M. Zeng, Q. Wu, and C.R. Chang, et al., *Prospects of spintronics based on 2D materials*. Wiley Interdiscip. Rev.: Comput. Mol. Sci. 7(5) (2017), pp. e1313.

[4] E.C. Ahn, *2D materials for spintronic devices. npj 2D*. Mater. Appl. 4(1) (2020), pp. 17.

[5] E. Marchiori, L. Ceccarelli, N. Rossi, L. Lorenzelli, C.L. Degen, and M. Poggio, *Nanoscale magnetic field imaging for 2D materials*. Nat. Rev. Phys. 4(1) (2022), pp. 49–60.

[6] C. Chang, W. Chen, Y. Chen, Y. Chen, Y. Chen, and F. Ding, et al., *Recent progress on two-dimensional materials*. Wuli Huaxue Xuebao/Acta Phys.-Chim. Sin 37(12) (2021), Article No. 2108017.

[7] H.H. Kim, B. Yang, S. Li, S. Jiang, C. Jin, Z. Tao, and A.W. Tsen, et al., *Evolution of interlayer and intralayer magnetism in three atomically thin chromium trihalides*. Proc. Natl. Acad. Sci. 116(23) (2019), pp. 11131–11136.

[8] N. Richter, D. Weber, F. Martin, N. Singh, U. Schwingenschlögl, B.V. Lotsch, and M. Kläui, *Temperature-dependent magnetic anisotropy in the layered magnetic semiconductors Cr I 3 and CrB r 3*. Phys. Rev. Mater. *2*(2) (2018), pp. 024004.

[9] B. Zhai, R. Cheng, W. Yao, L. Yin, C. Shen, C. Xia, and J. He, *Using ferroelectric polarization to regulate and preserve the valley polarization in a HfN 2/CrI 3/In 2 Se 3 heterotrilayer*. Phys. Rev. B 103(21) (2021), pp. 214114.

[10] M. Gibertini, M. Koperski, A.F. Morpurgo, and K.S. Novoselov, *Magnetic 2D materials and heterostructures*. Nat. Nanotechnol. *14*(5) (2019), pp. 408–419.

[11] J. Xu, W. Li, and Y. Hou, *Two-dimensional magnetic nanostructures*. Trends Chem. 2(2) (2020), pp. 163–173.

[12] N. Sethulakshmi, A. Mishra, P.M. Ajayan, Y. Kawazoe, A.K. Roy, A.K. Singh, and C.S. Tiwary, *Magnetism in two-dimensional materials beyond graphene*. Mater. Today 27 (2019), pp. 107–122.

[13] S.D. Bader and S.S.P. Parkin, *Spintronics*. Annu. Rev. Condens. Matter Phys. 1(1) (2010), pp. 71–88.

[14] I. Žutić, J. Fabian, and S.D. Sarma, *Spintronics: fundamentals and applications*. Rev. Mod. Phys. 76(2) (2004), pp. 323.

[15] G. Reiss and A. Hütten, *Applications beyond data storage*. Nat. Mater. 4(10) (2005), pp. 725–726.

[16] M. Wuttig and N. Yamada, *Phase-change materials for rewriteable data storage*. Nat. Mater. 6(11) (2007), pp. 824–832.

[17] A. Steane, *Quantum computing*. Rep. Prog. Phys. 61(2) (1998), pp. 117.

[18] R. Rietsche, C. Dremel, S. Bosch, L. Steinacker, M. Meckel, and J.M. Leimeister, *Quantum computing*. Electron. Mark. 32(4) (2022), pp. 2525–2536.

[19] C. Herrmann, G.C. Solomon, and M.A. Ratner, *Organic radicals as spin filters*. J. Am. Chem. Soc. 132(11) (2010), pp. 3682–3684.

[20] S.J. Kim and J.S. Lee, *Flexible organic transistor memory devices*. Nano Lett. 10(8) (2010), pp. 2884–2890.

[21] Z. Zhu, Y. Guo, and Y. Liu, *Application of organic field-effect transistors in memory*. Mater. Chem. Front. 4(10) (2020), pp. 2845–2862.

[22] M.C. Lemme, L.J. Li, T. Palacios, and F. Schwierz, *Two-dimensional materials for electronic applications*. MRS Bull. 39(8) (2014), pp. 711–718.

[23] M. Takigawa and F. Mila, *Magnetization plateaus*, in *Introduction to Frustrated Magnetism: Materials, Experiments, Theory*, C. Lacroix, P. Mendels and F. Mila, eds., Springer, Berlin, Heidelberg, 2010, pp. 241–267.

[24] H. Kikuchi, Y. Fujii, M. Chiba, S. Mitsudo, T. Idehara, T. Tonegawa, and H. Ohta, et al., *Experimental observation of the 1 / 3 magnetization plateau in the diamond-chain compound* $Cu_3\ (CO_3)_2\ (OH)_2$. Phys. Rev. Lett. 94(22) (2005), pp. 227201.
[25] W. Wang, Q. Li, D. Lv, R.J. Liu, Z. Peng, and S. Yang, *Monte Carlo study of magnetization plateaus in a zigzag graphene nanoribbon structure*. Carbon. N. Y. *120* (2017), pp. 313–325.
[26] W. Wang, Q. Li, M.Z. Wang, Y. Ma, A.B. Guo, and T. Huang, *Magnetization plateaus behaviors in a nano-graphene bilayer structure: A Monte Carlo study*. Phys. E: Low-dimens. Syst. Nanostruct. 111 (2019), pp. 63–74.
[27] W.C. Li, Z.Q. Liu, D. Xie, Z.X. Deng, and Y.W. Yao, *Magnetocaloric effect and magnetization plateaus in* TbB_4*: The Monte Carlo simulation*. J. Supercond. Nov. Magn. 37(3) (2024), pp. 573–578.
[28] Z. Fadil, A. Mhirech, B. Kabouchi, L. Bahmad, and W.O. Benomar, *Dilution effect on magnetization plateaus of honeycomb nanostructure at low temperature: Monte Carlo simulations*. Int. J. Thermophys. 43(2) (2022), pp. 20.
[29] K.L. Shi, Z. Wang, and W. Jiang, *Monte Carlo simulation of magnetic and thermodynamic properties of hexagonal decorated nanoparticle in a magnetic field*. J. Mater. Sci. 58(18) (2023), pp. 7620–7641.
[30] Z. Fadil, A. Mhirech, B. Kabouchi, L. Bahmad, and W.O. Benomar, *Monte Carlo study of magnetization plateaus of a bi-layer graphyne-like structure*. Integr. Ferroelectr. 213(1) (2021), pp. 146–157.
[31] D. Lv, Y. Ma, X.H. Luo, W. Jiang, F. Wang, and Q. Li, *Monte Carlo study of magnetization plateaus and thermodynamic properties of a nano-graphene with a sandwich-like structure in a longitudinal magnetic field*. Phys. E: Low-dimens. Syst. Nanostruct. 116 (2020), pp. 113721.

Philosophical Magazine

ISSN: 1478-6435 (Print) 1478-6443 (Online) Journal homepage: www.tandfonline.com/journals/tphm20

Magnetic response of zigzag graphene vs. borophene nanoribbons: a Monte Carlo investigation

Hussein Sabbah, Z. Fadil, A. Samih, Chaitany Jayprakash Raorane, Seong Cheol Kim, Mohammad Ajmal Ali, Khalid Mashay Al-Anazi & E. Salmani

To cite this article: Hussein Sabbah, Z. Fadil, A. Samih, Chaitany Jayprakash Raorane, Seong Cheol Kim, Mohammad Ajmal Ali, Khalid Mashay Al-Anazi & E. Salmani (2026) Magnetic response of zigzag graphene vs. borophene nanoribbons: a Monte Carlo investigation, Philosophical Magazine, 106:1, 82-102, DOI: 10.1080/14786435.2025.2547357

To link to this article: https://doi.org/10.1080/14786435.2025.2547357

Published online: 08 Sep 2025.

PHILOSOPHICAL MAGAZINE
2026, VOL. 106, NO. 1, 82–102
https://doi.org/10.1080/14786435.2025.2547357

Taylor & Francis
Taylor & Francis Group

Magnetic response of zigzag graphene vs. borophene nanoribbons: a Monte Carlo investigation

Hussein Sabbah[a], Z. Fadil[b], A. Samih[b], Chaitany Jayprakash Raorane[c], Seong Cheol Kim[c], Mohammad Ajmal Ali[d], Khalid Mashay Al-Anazi[e] and E. Salmani[b]

[a]College of Engineering and Technology, American University of the Middle East, Egaila, Kuwait; [b]Laboratoire de Matière Condensée et Sciences Interdisciplinaires (LaMCScI), Faculty of Sciences, URL-CNRST, Mohammed V University in Rabat, Rabat, Morocco; [c]School of Chemical Engineering, Yeungnam University, Gyeongsan, Republic of Korea; [d]Department of Botany and Microbiology, College of Science, Riyadh, Saudi Arabia; [e]Department of Zoology, College of Science, Riyadh, Saudi Arabia

ABSTRACT

By applying Monte Carlo simulations alongside the Blume-Emery-Griffiths model, this study compares the magnetic behaviour of zigzag graphene and zigzag borophene nanoribbons, focusing on the blocking temperature (T_B) under different physical parameters including temperature (T), external magnetic field (H), linear coupling (J) and biquadratic coupling (K). The zigzag borophene nanoribbon shows higher sensitivity to variations in all parameters compared to the zigzag graphene nanoribbon, which is attributed to borophene's more adaptable atomic structure. These findings underscore key elements that can aid in the advancement of nanoscale magnetic devices, particularly for spintronics, magnetic sensors and memory storage systems. Borophene's greater sensitivity to external conditions makes it a promising candidate for tunable magnetic materials, while graphene's stability is advantageous in applications requiring robust performance under varying external conditions.

ARTICLE HISTORY
Received 30 January 2025
Accepted 7 August 2025

KEYWORDS
Zigzag graphene nanoribbon; Zigzag borophene nanoribbon; magnetic characteristics; Monte Carlo simulations; blocking temperature

1. Introduction

Two-dimensional (2D) materials, defined by their atomic-scale thickness and planar structure, have garnered significant attention in condensed matter physics because of their unique mechanical, electrical and optical properties. Due to their distinctive mechanical, electrical and optical properties. The discovery of graphene in 2004 [1,2] marked a pivotal moment in the exploration of two-dimensional (2D) materials. Since then, researchers have delved into the properties of a multitude of among 2D materials are transition metal dichalcogenides (TMDs) [3–5], hexagonal boron nitride (h-BN) [6,7] and black phosphorus [8,9]. The distinctive properties of these materials are a

CONTACT Z. Fadil fadilzakaria604@gmail.com Laboratoire de Matière Condensée et Sciences Interdisciplinaires (LaMCScI), Faculty of Sciences, URL-CNRST, P.O. Box 1014, Mohammed V University in Rabat, Rabat, Morocco; Chaitany Jayprakash Raorane chaitanyaraorane22@ynu.ac.kr School of Chemical Engineering, Yeungnam University, Gyeongsan 38541, Republic of Korea; Seong Cheol Kim sckim07@ynu.ac.kr School of Chemical Engineering, Yeungnam University, Gyeongsan 38541, Republic of Korea

This article has been corrected with minor changes. These changes do not impact the academic content of the article.

consequence of their unique atomic interactions and electronic band structures, which indicate potential applications in a range of fields, including next-generation electronics [10,11], energy storage [12,13] and quantum computing [14]. The discovery of graphene [1], a single-layered material composed of carbon atoms arranged in a hexagonal lattice, represents a pivotal advancement within the scope of research on 2D materials. Due to its exceptional electron mobility [15–17], high thermal conductivity [18–21] and remarkable mechanical strength [22,23], graphene has the potential as a transformative material across a number of industries, including flexible electronics [24], energy storage [25] and biomedical devices [26,27]. The synthesis of graphene can be achieved through a number of techniques, including chemical vapour deposition (CVD) [28–30] and mechanical exfoliation [31–33]. Additionally, borophene [34], a two-dimensional allotrope of boron, has garnered substantial research interest [34] due to its elevated carrier mobility [35], mechanical flexibility [36,37] and ultrahigh thermal conductivity [38,39], which make it comparable to graphene. The synthesis of borophene, achieved through methods such as chemical vapour deposition [40,41] and liquid-phase exfoliation [42,43], has enabled its exploration in areas including energy storage [44] and sensing applications [45]. Furthermore, borophene's high adsorption capacity and moderate binding energy for hydrogen make it a promising material for hydrogen storage [46], with an efficiency that surpasses that of traditional metal hydrides [47]. Among the special structures of two-dimensional materials, zigzag graphene nanoribbons [48] (ZGNRs) and zigzag borophene nanoribbons [49] (ZBNRs) are of particular interest due to their distinctive edge-dependent electronic and magnetic properties. ZGNRs, with their distinctive zigzag edge configuration, display localised edge states, which contribute to a tunable bandgap [50]. They also exhibit temperature-dependent Pauli susceptibility, with Curie-like behaviour at low temperatures, indicating the presence of strong edge effects [51]. This edge configuration can also result in ferromagnetic configuration [52], which makes ZGNRs promising candidates for spintronic [53–55] and quantum computing [51,56] applications where spin state control is of paramount importance. Similarly, ZBNRs exhibit unique electronic characteristics. In contrast to the semiconductor nature of line edge borophene nanoribbons, zigzag configurations in ZBNRs demonstrate metallic behaviour [57,58]. The structure is highly sensitive to the ribbon width, which results in fluctuations in conductivity and magnetism [59]. Moreover, Borophene nanoribbons can demonstrate half-metallicity and significant spin-dependent transport phenomena [60], including negative differential resistance (NDR) in specific configurations [61]. The fascinating properties of graphene and borophene and their prospective applications in various fields have motivated extensive theoretical research employing the Monte Carlo Simulation method to investigate the properties of these materials. In this context, reports indicate that borophene has a higher blocking temperature (T_B) than graphene [62], with T_B marking the changeover between the ferrimagnetic/ferromagnetic to the superparamagnetic phases [63,64]. Furthermore, the zigzag graphene nanoribbon was found to display interesting magnetisation plateau behaviours, which were attributed to the edge effects [65]. Furthermore, the Monte Carlo method was employed to examine the phase transitions and magnetic characteristics of zigzag triangular nanographenes [66], as well as the magnetic characteristics of a bi-layer borophene system [67] with RKKY (Ruderman-Kittel-Kasuya-Yoshida) interactions.

In this study, we examined the magnetic behaviours of zigzag graphene and zigzag borophene nanoribbons in this study by performing Monte Carlo simulations with the Metropolis algorithm [68] and the Blume-Emery-Griffiths model [69], a widely studied lattice model in statistical physics, particularly for investigating phase transitions and critical phenomena in magnetic systems. The BEG model, which was introduced in 1971 [69], extends the classical Ising model by incorporating a third spin state.

Moreover, the magnetic properties of 2D materials, particularly density functional theory (DFT). DFT methods are used to explore edge-induced magnetism and strain effects in borophene nanoribbons, while magnetism in graphene nanostructures is studied with a focus on edge states and defects [70–73]. Additionally, recent first-principles studies have investigated vacancy-induced magnetism in β_{12}-borophene nanosheets [74], magnetism enhancement and spin transport in edge-passivated zigzag borophene nanoribbons [75], electronic and magnetic properties of twisted graphene nanoribbons and Möbius strips [76], as well as graphene nanoribbons on Ni(111) substrates [77]. These DFT studies provide a complementary theoretical framework that supports and enriches the understanding of magnetic behaviours explored in our Monte Carlo simulations.

The choice of graphene and borophene is based on their two-dimensional structure and exceptional physical properties. Graphene exhibits high electron mobility and ferromagnetic edge states in zigzag nanoribbons (ZGNRs), making it attractive for spintronic applications. Borophene, on the other hand, offers high thermal conductivity, mechanical flexibility and variable magnetic behaviour depending on its geometry. While graphene is characterised by a flat, highly stable honeycomb structure, borophene exhibits a buckled atomic arrangement, which introduces greater structural flexibility and anisotropy. This buckled nature of borophene plays a crucial role in enhancing its sensitivity to external parameters such as magnetic field, exchange interactions and crystal field. Previous studies have emphasised that this geometric distinction endows borophene with unique electronic and magnetic behaviours not present in its planar counterparts [78,79]. In contrast, graphene's rigidity makes it less responsive but offers robustness desirable for certain applications. By comparing the two, we aim to explore how these structural differences manifest in their magnetic behaviour under various thermodynamic conditions.

Borophene, a two-dimensional allotrope of boron, also exhibits high charge carrier mobility, exceptional mechanical flexibility and excellent thermal conductivity. Borophene zigzag nanoribbons (ZBNRs), in particular, exhibit metallic behaviour and width-dependent magnetic effects, offering a promising platform for spin-dependent transport devices. This additional state was specifically designed to represent multi-component systems and order–disorder transitions. The model permits each spin at a lattice site to assume one of three values. The possible values of the spin variable are +1, 0 and –1. These states account for binary interactions (such as ferromagnetic or antiferromagnetic coupling) and an additional 'zero' state, which can signify the absence of a particle, vacancy, or phase separation in certain physical contexts. Therefore, the BEG model can be successfully applied to describe phase separation and coexistence in liquid mixtures, critical behaviour in magnetic systems, and complex spin arrangements under external fields [80,81]. This approach elucidates the differentiating magnetic characteristics between these two intriguing nanoribbons, focusing on the blocking temperature (T_B)

under varying physical parameters, including temperature (T), external magnetic field (H), linear coupling (J), and biquadratic coupling (K). These findings underscore key elements that can aid in the advancement of nanoscale magnetic devices, which can be utilised in various applications such as spintronics, data storage devices and high-sensitivity magnetic sensors. The paper is organised as follows: Section 2 describes the model and method, while Section 3 provides the results of the Monte Carlo simulations, and Section 4 offers the concluding remarks.

2. Model and method

The magnetic behaviour of the Zigzag Graphene and Zigzag Borophene nanoribbons, each composed by $N_{T(graphene)} = 54$ and $N_{T(borophene)} = 48$ atoms respectively, were compared in this study, as illustrated in Figure 1. The analysis considers atoms with a spin-1 in the context of free boundary conditions. The effective width of nanoribbons is determined by the number of atomic chains in the transverse direction. As shown in Figure 1, the graphene nanoribbon (Figure 1a) has 6 zigzag chains of hexagons, while the borophene nanoribbon (Figure 1b) has 6 rows of atoms in a triangular lattice. This width was chosen to balance physical accuracy and computational cost, ensuring stable simulations and accounting for significant edge effects. Moreover, the investigation applied Monte Carlo simulations governed by the Metropolis algorithm using the Blume-Emery-Griffiths model. Monte Carlo simulations were carried out using the Metropolis algorithm, performing 5×10^6 Monte Carlo steps per spin (MCSS). To ensure system equilibration, the first 5×10^5 steps were ignored (thermalisation). Thermodynamic averages were calculated from the remaining data.

Hamiltonian for Zigzag Graphene and Zigzag Borophene nanoribbons:

$$H = -J \sum_{\langle i,j \rangle} S_i S_j - K \sum_i (S_i S_j)^2 - H \sum_i S_i \tag{1}$$

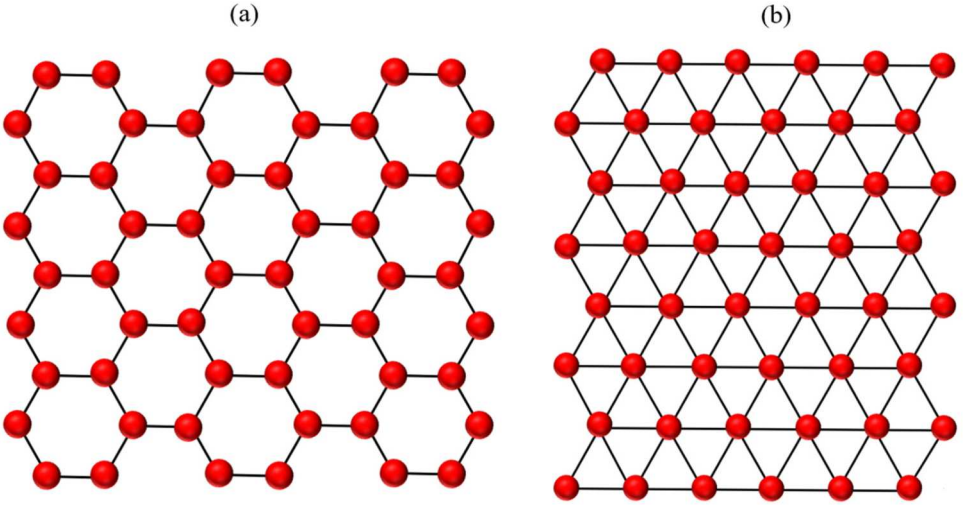

Figure 1. Illustration of the Zigzag Graphene (a) and Zigzag Borophene (b) nanoribbons. Each atom in both nanoribbons is composed of spin-1 atoms.

In this context, J and K represent the interactions arising from linear and biquadratic exchange between the nearest neighbor atoms in the plane, specifically between atoms S_i and S_j with the summation index $\langle i, j \rangle$. In addition, both nanoribbons are subjected to an external magnetic field, denoted H, which represents the external magnetic field applied along the longitudinal z-direction.

where $S_i \in \{-1,0,+1\}$ represents the spin-1 variable at site i, suitable for describing systems with magnetic and nonmagnetic states. J is the bilinear exchange interaction between nearest-neighbor spins, controlling the ferromagnetic coupling. K is the biquadratic exchange interaction, which captures higher-order spin correlations. $\langle i, j \rangle$ denotes the sum over nearest-neighbor pairs on the lattice. H is the external magnetic field applied in the longitudinal (z-axis) direction, influencing the net magnetisation along the nanoribbon.

Internal energy at each site:

$$E = \frac{1}{N_{T(graphene)}} \mathcal{H}, \tag{2}$$

$$E = \frac{1}{N_{T(borophene)}} \mathcal{H}, \tag{3}$$

Magnetisation and susceptibility expressions for Zigzag Graphene and Zigzag Borophene nanoribbons:

$$M_{graphene} = \frac{1}{N_{T(graphene)}} \sum_i S_i, \tag{4}$$

$$M_{borophene} = \frac{1}{N_{T(borophene)}} \sum_i S_i. \tag{5}$$

$$\chi_{graphene} = \beta \left(\left\langle M_{(graphene)}{}^2 \right\rangle - < M_{(graphene)} >^2 \right) \tag{6}$$

$$\chi_{borophene} = \beta \left(\left\langle M_{(borophene)}{}^2 \right\rangle - < M_{(borophene)} >^2 \right) \tag{7}$$

Defined as $\beta = \frac{1}{K_B T}$, with the Boltzmann constant k_B set to 1 for easiness, and T is used to represent the absolute temperature. We adopt a dimensionless approach by setting the Boltzmann constant to unity, k_B =1. This convention is commonly used in numerical studies in statistical physics, particularly in Monte Carlo simulations. Consequently, the temperature T is expressed in reduced (dimensionless) units, meaning it is technically T/k_B, but since k_B=1, it simply becomes T. Similarly, other quantities such as the magnetic susceptibility χ are also expressed in reduced, unitless form.

In our approach, all parameters are kept constant except one, which is intentionally varied between 1 and 5 to examine its specific influence on magnetic properties, particularly the blocking temperature and spin configuration. This parametric method is commonly used in the literature (see, for example, Refs. [62–66]) to isolate and analyse the individual effects of each parameter.

3. Findings from Monte Carlo simulations

This section uses Monte Carlo simulations to analyse and compare the magnetic properties of zigzag graphene and zigzag borophene nanoribbons, focusing on key physical parameters as defined in Hamiltonian Eq. (1). Figure 2 presents the temperature-dependent variations of magnetisation (a) and susceptibility (b) for both types of nanoribbons, considering a linear coupling interaction of $J = 1$, biquadratic coupling $K = 0$, and an external magnetic field $H = 1$. When analysed individually, the spin-up ($Si = +1$) and spin-down ($Si = -1$) states for each configuration. At low temperatures, graphene and borophene nanoribbons exhibit a strong predominance of spin-up states aligned with the external magnetic field, resulting in a total magnetisation close to 1. As the temperature increases, thermal fluctuations gradually favour the emergence of spin-down states, leading to a clear decrease in magnetisation. The results highlight that the magnetic behaviour of zigzag borophene nanoribbons differs from that of graphene nanoribbons. Both nanoribbons show a decrease in magnetisation as the temperature increases, resulting in a phase transition from the ferromagnetic to the superparamagnetic state. This transition is marked by the blocking temperature (T_B), where susceptibility peaks. For temperatures below T_B, both nanoribbons remain in the ferromagnetic phase, while above T_B, they transition into the superparamagnetic phase. Interestingly, the zigzag borophene nanoribbon exhibits a higher blocking temperature than the zigzag graphene nanoribbon, suggesting that graphene is more sensitive to temperature changes. Since both nanoribbons were analysed using the same method, spins, and physical parameters, this difference in behaviour was attributed to their distinct geometries, which influence their magnetic properties. Our analysis shows that borophene nanoribbons exhibit a higher blocking temperature than graphene, indicating better magnetic stability over a wider temperature range. This is due to the particular atomic geometry of borophene, which enhances its magnetic properties. Thus, while both materials are suitable for magnetic studies, borophene offers a more robust magnetic response, making it promising for spintronics and nanoscale magnetic sensing applications.

Figure 3 examines the magnetisation (a, c) and susceptibility (b, d) behaviour with temperature for both zigzag nanoribbons by varying H at $J = 1$ and $K = 0$. As H increases, both nanoribbons experience delayed phase transitions, leading to a rise in the blocking temperature T_B. This is because H helps maintain order in the nanoribbons, requiring higher temperatures to disrupt this order and transition to the superparamagnetic phase. Accordingly, T_B increases as the external magnetic field intensifies. An important observation is that T_B was more significantly affected in the borophene structure than in graphene when increasing H. For borophene, T_B shifts from 5.77 at $H = 1$–12.44 at $H = 3$. In contrast, for graphene, T_B increases from 9.77 at $H = 1$–23.55 at $H = 3$. This suggests that borophene was more sensitive to changes in H compared to graphene.

Figure 4 explores the behaviour of magnetisation (a, c) and susceptibility (b, d) with temperature for both zigzag nanoribbons, varying J at $H = 1$ and $K = 0$. As J increases, both nanoribbons exhibit delayed phase transitions, resulting in a higher blocking temperature (T_B) due to the enhanced ordering effect of the linear coupling, which necessitates elevated temperatures to trigger the transition to the superparamagnetic phase. Notably, T_B in borophene increases more significantly than in graphene as J rises, indicating that borophene is more sensitive to changes in the linear coupling interaction J. Due to this

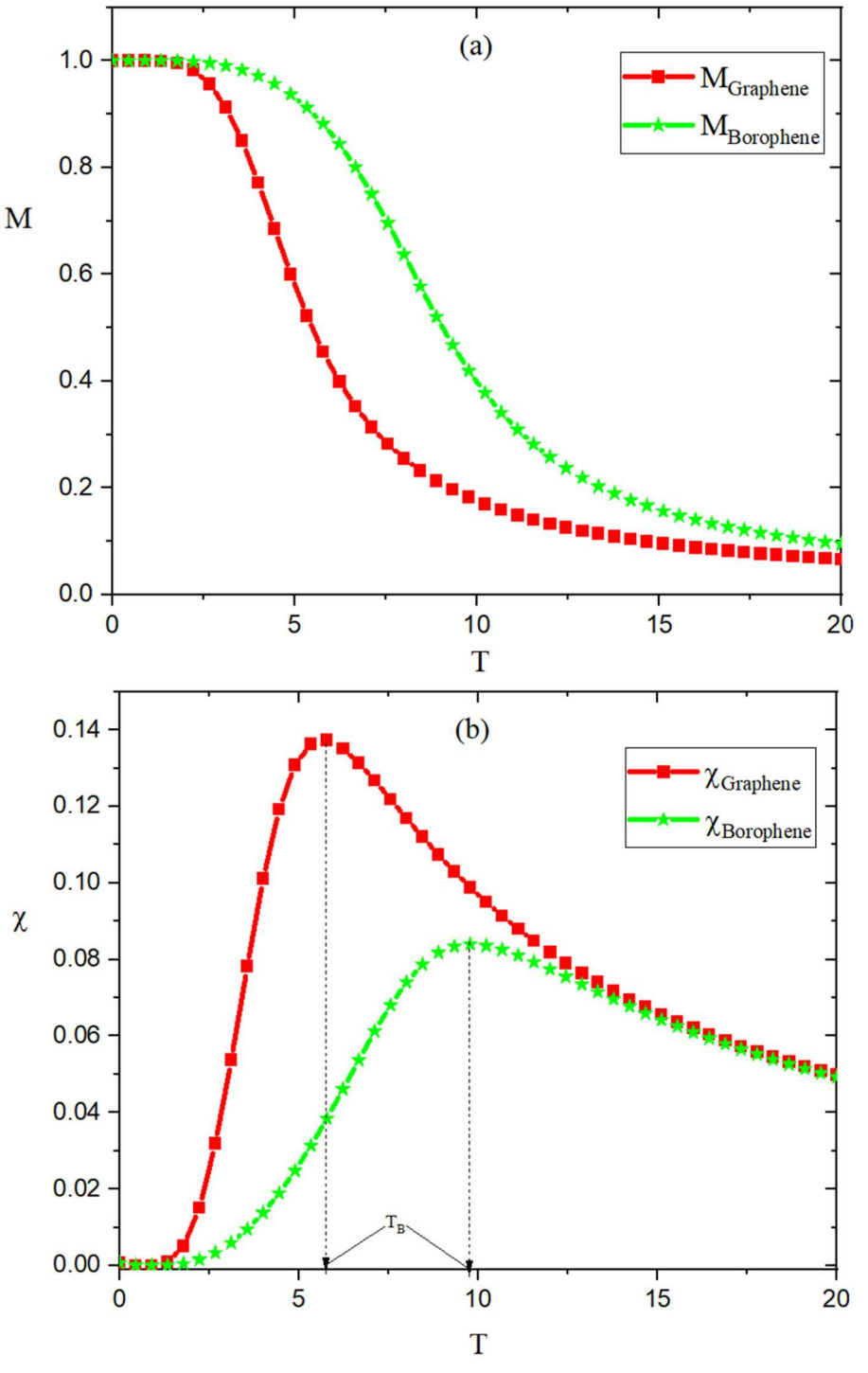

Figure 2. Variations of magnetisation (a) and susceptibility (b) with temperature at $J = 1$, $K = 0$ and $H = 1$.

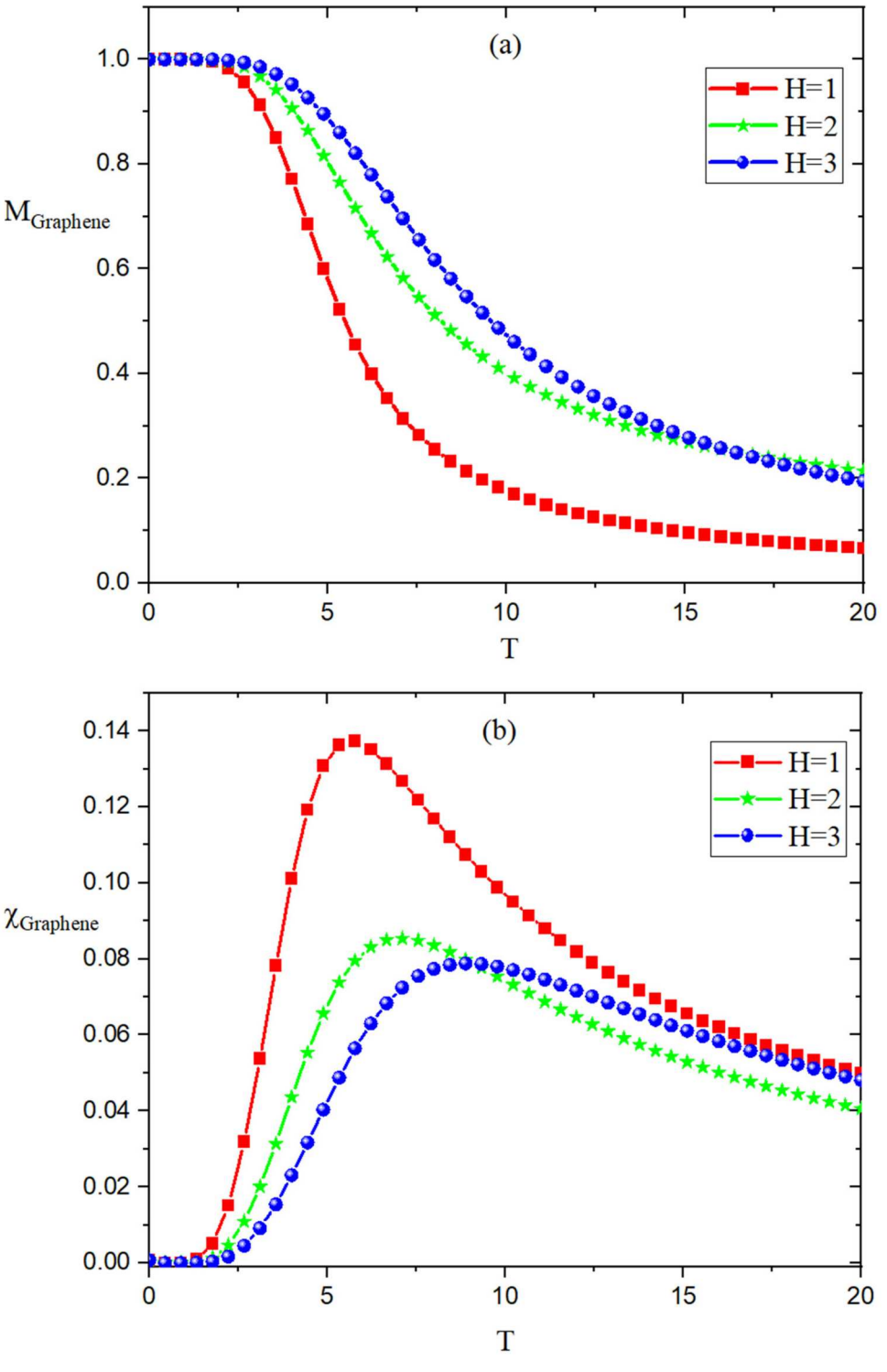

Figure 3. Variations of magnetisation (a, c) and susceptibility (b, d) with temperature by varying H at $J = 1$ and $K = 0$.

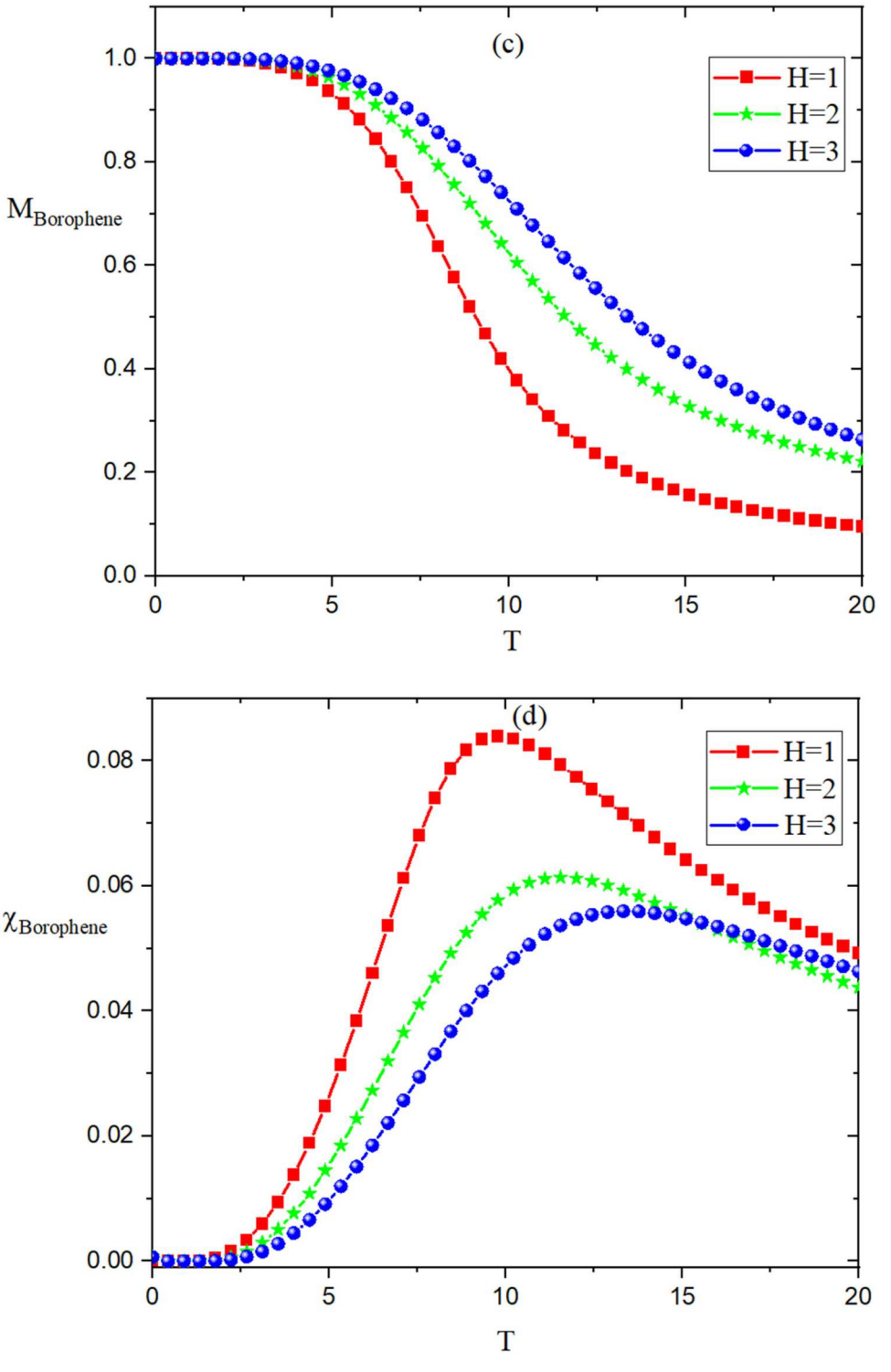

Figure 3 *Continued*

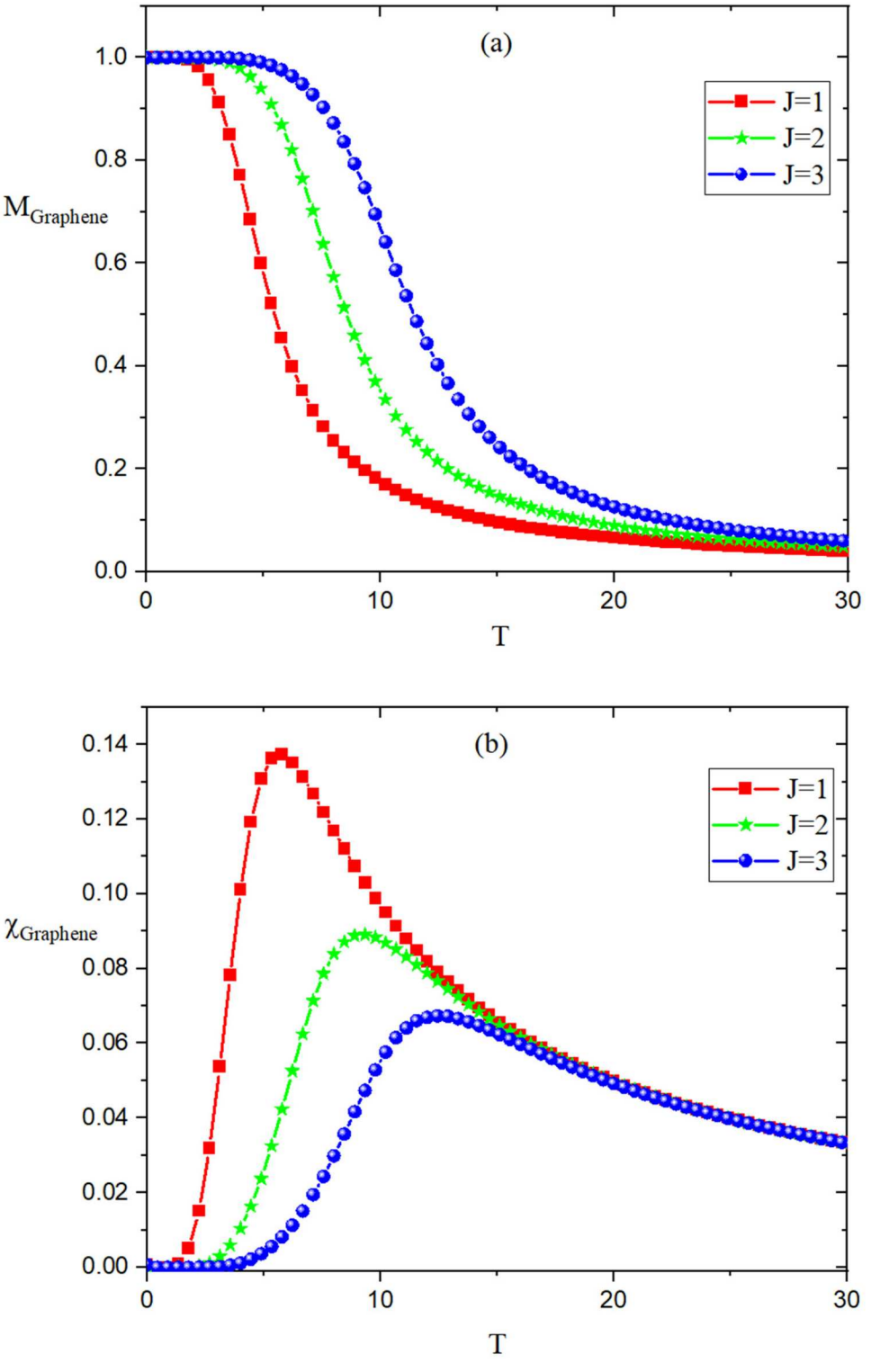

Figure 4. Variations of magnetisation (a, c) and susceptibility (b, d) with temperature by varying J at $H = 1$ and $K = 0$.

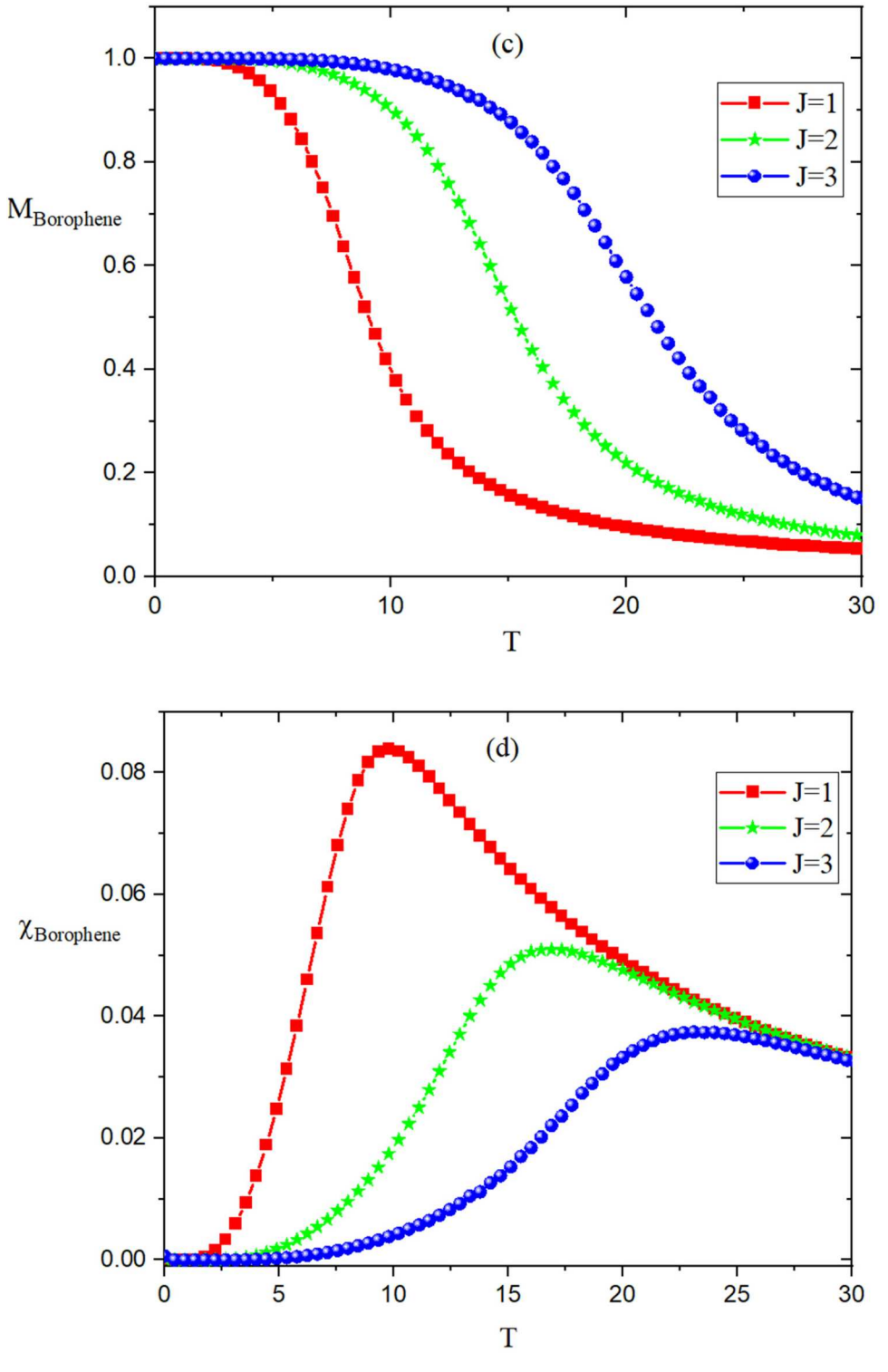

Figure 4 *Continued*

increased sensitivity, changes in J have a greater impact on the ordered state of borophene, which raises the blocking temperature more noticeably. Graphene, on the other hand, is less sensitive to these changes due to its more homogeneous and rigid structure, which produces less noticeable impacts from the same fluctuations in J.

Figure 5 examines the magnetisation (a, c) and susceptibility (b, d) response to temperature for both zigzag nanoribbons, as K was varied while keeping $H = 1$ and $J = 1$. As K increases, both nanoribbons experience delayed phase transitions, resulting in a higher blocking temperature (T_B) due to the strengthening of the ordering effect caused by the biquadratic coupling. This ordering necessitates elevated temperatures to trigger the transition to the superparamagnetic phase. Particularly, borophene's blocking temperature rises more significantly than graphene's with increasing K, suggesting that borophene is more sensitive to changes in the biquadratic coupling interaction. This increased sensitivity means that fluctuations in K have a more pronounced effect on borophene's ordered state, leading to a greater increase in the blocking temperature. In contrast, graphene's more uniform and rigid structure makes it less affected by the same variations in K.

Finally, in Figure 6, the blocking temperature T_B for both zigzag nanoribbons were analysed with respect to different parameters: varying H at $J = 1$ and $K = 0$ (a); varying J at $H = 1$ and $K = 0$ (b); and varying K at $H = 1$ H = 1 and $J = 1$ (c). Increasing H, J and K results in an almost linear increase in T_B for both types of nanoribbons. It was noted that the parameter K has a more substantial effect on T_B compared to H and J. Additionally, variations in all parameters affect the zigzag borophene nanoribbon more significantly than the zigzag graphene nanoribbon, due to borophene's more flexible and adaptable atomic structure, which responds more sensitively to changes in external parameters, while graphene's rigid structure dampens these effects. Furthermore, although a direct experimental validation of the results obtained for the studied systems is not available, there is a significant body of theory, notably based on Monte Carlo simulations, exploring the magnetic properties of 2D graphene and 2D borophene, such as those observed in the borophene trilayer structure[72], the Ising-ladder graphene nanoribbon[73] or the graphene nanoisland bilayer[74]. These works, which examine the blocking temperatures and transitions under similar parameters, are in agreement with the behaviours observed in our study. In the absence of specific experimental data, these theoretical studies therefore provide an indirect but credible validation of our results. We acknowledge the challenges related to experimental validation, notably the difficulties in observing the fine magnetic properties of nanostructures at the experimental scale. Future research should aim to develop experimental methods to test these predictions and to compare the obtained trends with simulation results to improve the understanding of the magnetic properties of these systems. Moreover, the quasi-linear increase in the blocking temperature T_B as a function of the parameters H, J and K for zigzag nanoribbons of graphene and borophene (Figure 6) is in good agreement with several previous works on two-dimensional materials. For instance, Behzad and Chegel [82] showed that the magnetic susceptibility $\chi(T)$ increases with temperature in graphene nanoribbons (GNRs) and boron nitride nanoribbons (BNNRs), with a more pronounced susceptibility in GNRs [82], which corresponds to our observation that graphene, due to its rigid structure, responds less strongly to variations in external parameters. Similarly, Chegel [83] highlighted the significant impact of the magnetic field

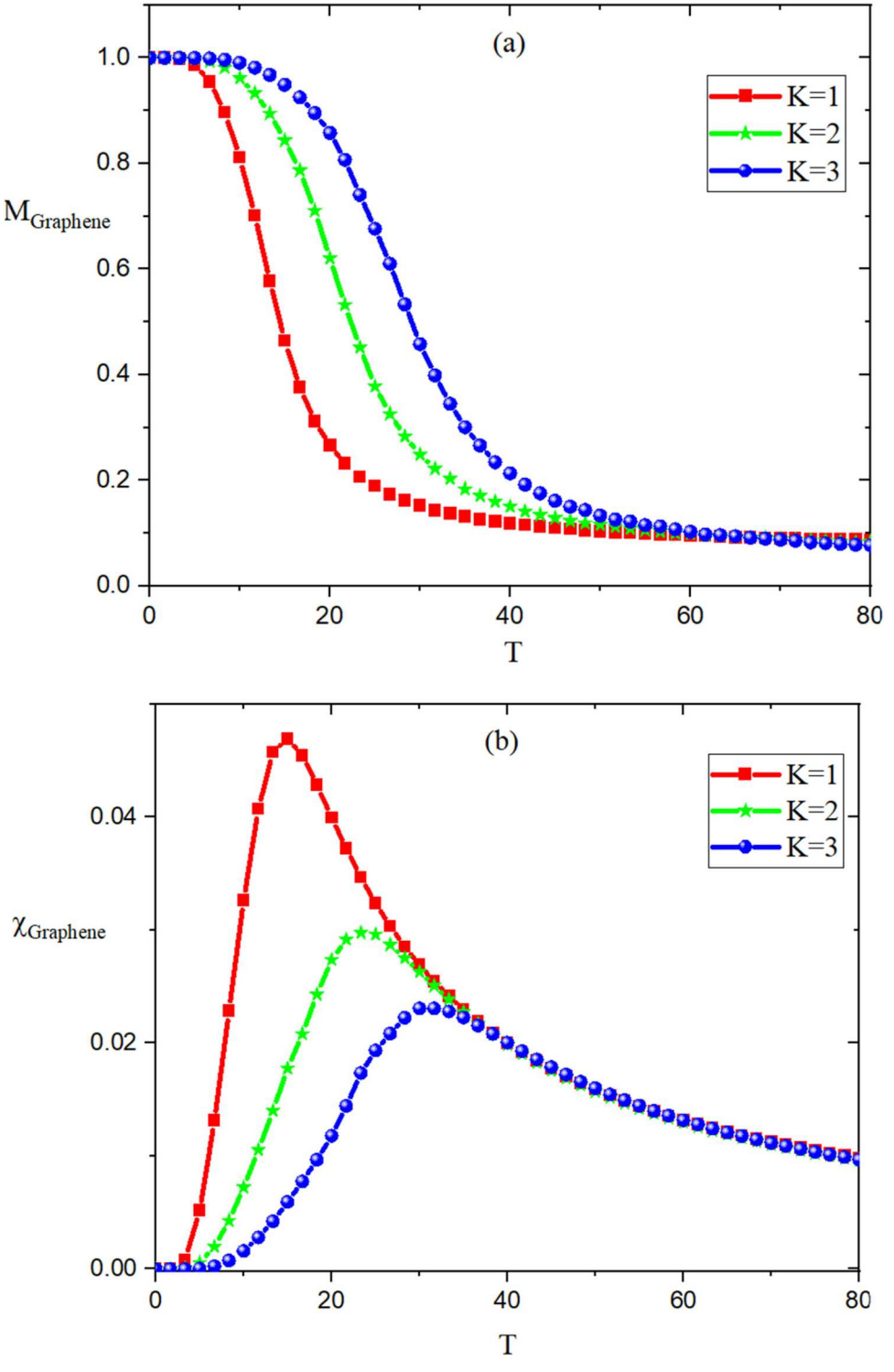

Figure 5. Variations of magnetisation (a, c) and susceptibility (b, d) with temperature by varying K at $H = 1$ and $J = 1$.

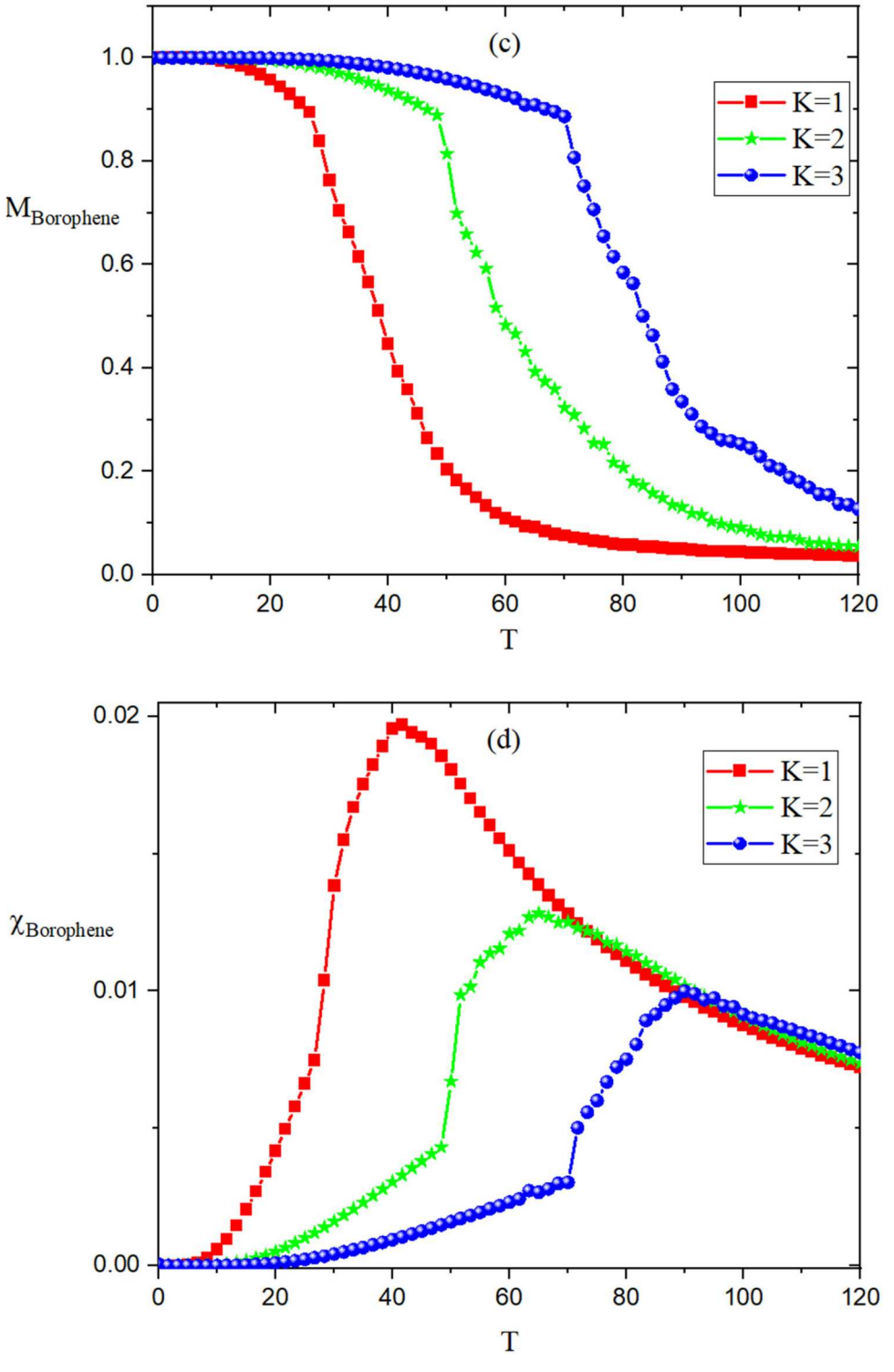

Figure 5 *Continued*

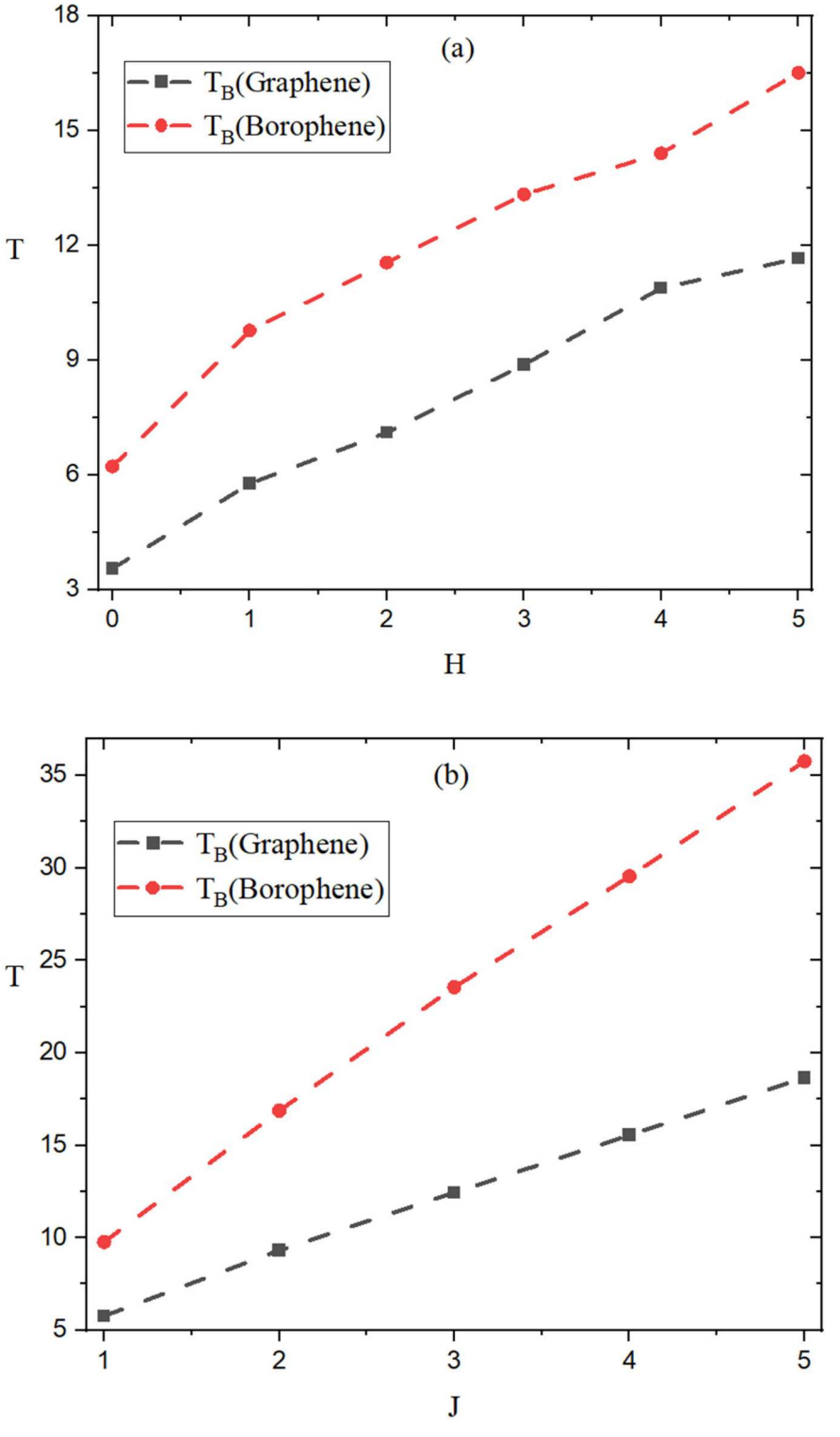

Figure 6. Blocking temperature T_B variations: with H at $J = 1$ and $K = 0$ (a); with J at $H = 1$ and $K = 0$ (b); with K at $H = 1$ and $J = 1$ (c).

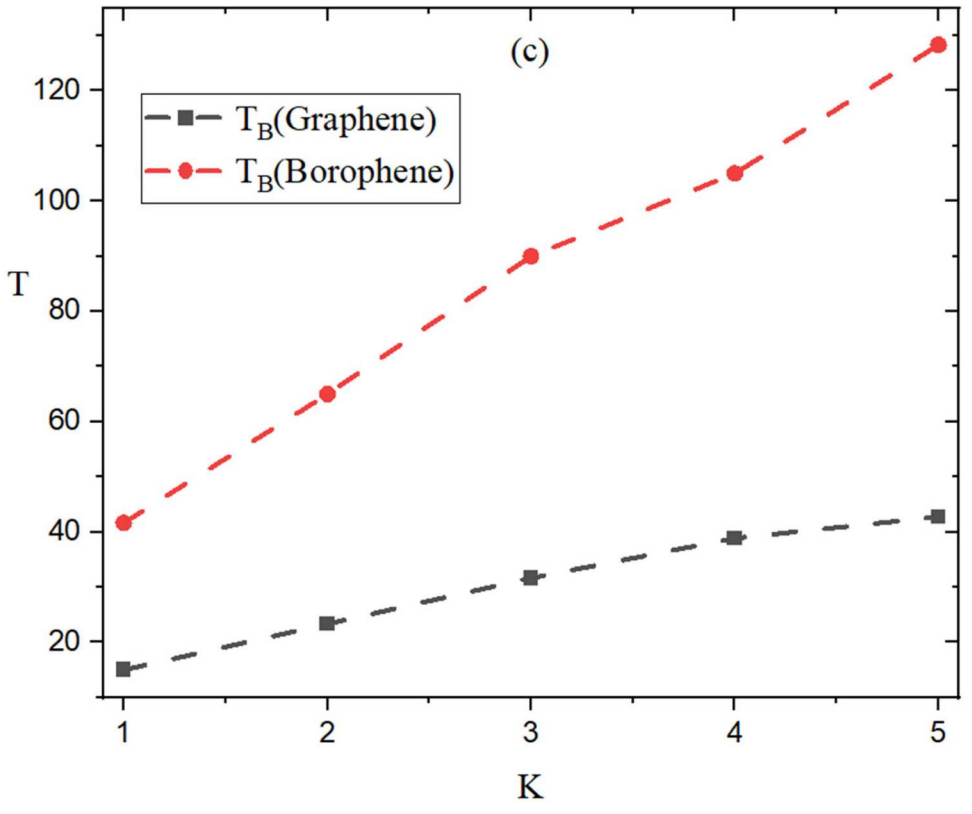

Figure 6 *Continued*

on the thermodynamic properties of doped S-graphene, notably revealing Schottky anomalies and field-dependent peaks in $\chi(T)$ [83], which supports our finding that borophene exhibits a more sensitive response due to its more flexible atomic structure. Finally, the study by Chegel et al. [70] on tetragonal silicene shows that electric and magnetic fields strongly influence thermal conductivity through modifications of the electronic structure[77], reinforcing the idea that materials with flexible structures, such as borophene, offer better adaptability to external fields compared to graphene. These comparisons underscore borophene's strong potential for applications in field-sensitive magnetic devices.

4. Conclusions

Using Monte Carlo simulations Monte Carlo simulations alongside the Blume-Emery-Griffiths model, this research examined the magnetic behaviour of zigzag graphene and zigzag borophene nanoribbons, revealing that both structures exhibited an increase in blocking temperature (T_B) as physical parameters including temperature (T), external magnetic field (H), linear coupling (J) and biquadratic coupling (K) increased. Remarkably, the parameter K exerted a more important influence on T_B than the other parameters. Additionally, the zigzag borophene nanoribbon displayed a higher sensitivity

to variations in all parameters compared to the zigzag graphene nanoribbon, which was attributed to borophene's more adaptable atomic structure. These findings underscored key elements that could aid in the advancement of nanoscale magnetic devices, particularly for spintronics, magnetic sensors and memory storage systems. Borophene's greater sensitivity to external conditions made it a promising candidate for tunable magnetic materials, while graphene's stability was advantageous in applications requiring robust performance in response to changing external factors.

Acknowledgements

The authors extend their appreciation to the Ongoing Research Funding program (ORF-2025-306), King Saud University, Riyadh, Saudi Arabia.

Disclosure statement

No potential conflict of interest was reported by the author(s).

Funding

This research was supported by the Basic Science Research Program through the National Research Foundation of Korea (NRF) funded by the Ministry of Education (2020R1I1A3052258). This research was funded by the Ongoing Research Funding program (ORF-2025-306), King Saud University, Riyadh, Saudi Arabia.

Data and code availability

All simulations were implemented in-house using custom Fortran code, validated against known benchmarks for the BEG model. Data analysis and plotting were performed using OriginLab.

References

[1] K.S. Novoselov, A.K. Geim, S.V. Morozov, D.E. Jiang, Y. Zhang, S.V. Dubonos, and A.A. Firsov, *Electric field effect in atomically thin carbon films*. Science 306(5696) (2004), pp. 666–669.
[2] A.K. Geim, *Graphene: status and prospects*. Science 324(5934) (2009), pp. 1530–1534.
[3] G. Pippia, D. Van Hamme, B. Martín-García, M. Prato, and I. Moreels, *A colloidal route to semiconducting tungsten disulfide nanosheets with monolayer thickness*. Nanoscale. 14(42) (2022), pp. 15859–15868.
[4] H. Chen, C. Chen, Y. Li, and X. Fang, *Monolayer-molybdenum-disulfide-based nano-optomechanical transistor and tunable nonlinear responses*. J. Semicond. 37(11) (2016), pp. 114004.
[5] J. Luo, C. Li, J. Liu, Y. Liu, W. Xiao, R. Zheng, and J. Zhu, *Spectroscopy of monolayer and multilayer tungsten disulfide under high pressure*. Appl. Phys. Lett. 124(3) (2024), pp. 033104.
[6] K. Zhang, Y. Feng, F. Wang, Z. Yang, and J. Wang, *Two dimensional hexagonal boron nitride (2D-hBN): synthesis, properties and applications*. J. Mater. Chem. C 5(46) (2017), pp. 11992–12022.
[7] A.F. Khan, D.A. Brownson, E.P. Randviir, G.C. Smith, and C.E. Banks, *2D hexagonal boron nitride (2D-hBN) explored for the electrochemical sensing of dopamine*. Anal. Chem. 88(19) (2016), pp. 9729–9737.

[8] M. Luo, T. Fan, Y. Zhou, H. Zhang, and L. Mei, *2D black phosphorus – based biomedical applications*. Adv. Funct. Mater. 29(13) (2019), pp. 1808306.
[9] J.B. Smith, D. Hagaman, and H.F. Ji, *Growth of 2D black phosphorus film from chemical vapor deposition*. Nanotechnology 27(21) (2016), pp. 215602.
[10] A. Pal, S. Zhang, T. Chavan, K. Agashiwala, C.H. Yeh, W. Cao, and K. Banerjee, *Quantum-engineered devices based on 2D materials for next-generation information processing and storage*. Adv. Mater. 35(27) (2023), pp. 2109894.
[11] J. Kang, W. Cao, X. Xie, D. Sarkar, W. Liu, and K. Banerjee, *Graphene and beyond-graphene 2D crystals for next-generation green electronics*, in *Micro-and Nanotechnology Sensors, Systems, and Applications VI*, Baltimore, MD, USA, Vol. 9083, Zongyu H., Thomas S. S. W. H. S., ed., SPIE, 2014, June, pp. 20–26.
[12] X. Zhang, L. Hou, A. Ciesielski, and P. Samorì, *2D materials beyond graphene for high-performance energy storage applications*. Adv. Energy. Mater. 6(23) (2016), pp. 1600671.
[13] R. Sahoo, A. Pal, and T. Pal, *2D materials for renewable energy storage devices: outlook and challenges*. Chem. Commun. 52(93) (2016), pp. 13528–13542.
[14] S. Ren, Q. Tan, and J. Zhang, *Review on the quantum emitters in two-dimensional materials*. J. Semicond. 40(7) (2019), pp. 071903.
[15] K.I. Bolotin, K.J. Sikes, Z. Jiang, M. Klima, G. Fudenberg, J. Hone, and H.L. Stormer, *Ultrahigh electron mobility in suspended graphene*. Solid State Commun. 146(9-10) (2008), pp. 351–355.
[16] S.H. Alwan, A.A. Omran, D.K. Naser, and M.F. Ramadan, *A mini-review on graphene: exploration of synthesis methods and multifaceted properties*. Eng. Proc. 59(1) (2024), pp. 226.
[17] S. Bruzzone and G. Fiori, *Ab-initio simulations of deformation potentials and electron mobility in chemically modified graphene and two-dimensional hexagonal boron-nitride*. Appl. Phys. Lett. 99(22) (2011).
[18] N.E. Safie, M.A. Azam, R.N.A.R. Seman, and A. Takasaki, *Graphene-based materials for energy production, conversion, and storage*, in *Materials for Energy Production, Conversion, and Storage*, Jenitta J.M., Nisa S., Sabu T., ed., CRC Press, Boca Raton, FL, 2024. pp. 89–103.
[19] A.A. Balandin, S. Ghosh, W. Bao, I. Calizo, D. Teweldebrhan, F. Miao, and C.N. Lau, *Superior thermal conductivity of single-layer graphene*. Nano Lett. 8(3) (2008), pp. 902–907.
[20] X. Huang, C. Zhi, Y. Lin, H. Bao, G. Wu, P. Jiang, and Y.W. Mai, *Thermal conductivity of graphene-based polymer nanocomposites*. Mater. Sci. Eng. R Reports 142 (2020), pp. 100577.
[21] Z. Guo, D. Zhang, and X.G. Gong, *Thermal conductivity of graphene nanoribbons*. Appl. Phys. Lett. 95(16) (2009), pp. 163103.
[22] D.G. Papageorgiou, I.A. Kinloch, and R.J. Young, *Mechanical properties of graphene and graphene-based nanocomposites*. Prog. Mater. Sci. 90 (2017), pp. 75–127.
[23] H. El Etri. Graphene: A State-of-the-Art Review of Types, Properties and Applications in Different Sectors.
[24] T.H. Han, H. Kim, S.J. Kwon, and T.W. Lee, *Graphene-based flexible electronic devices*. Mat. Sci. Eng. R Reports 118 (2017), pp. 1–43.
[25] R. Raccichini, A. Varzi, S. Passerini, and B. Scrosati, *The role of graphene for electrochemical energy storage*. Nat. Mater. 14(3) (2015), pp. 271–279.
[26] C. Chung, Y.K. Kim, D. Shin, S.R. Ryoo, B.H. Hong, and D.H. Min, *Biomedical applications of graphene and graphene oxide*. Acc. Chem. Res. 46(10) (2013), pp. 2211–2224.
[27] H. Shen, L. Zhang, M. Liu, and Z. Zhang, *Biomedical applications of graphene*. Theranostics 2(3) (2012), pp. 283.
[28] S.H. Alwan, A.A. Omran, D.K. Naser, and M.F. Ramadan, *A mini-review on graphene: exploration of synthesis methods and multifaceted properties*. Eng. Proc. 59(1) (2024), pp. 226.
[29] R. Munoz and C. Gómez-Aleixandre, *Review of CVD synthesis of graphene*. Chem. Vap. Deposition 19(10-11-12) (2013), pp. 297–322.
[30] X. Wang, H. You, F. Liu, M. Li, L. Wan, S. Li, and J. Cheng, *Large-scale synthesis of few-layered graphene using CVD*. Chem. Vap. Deposition 15(1-3) (2009), pp. 53–56.
[31] S. Asghar, T.M. Al-Qoyyim, M.H. Diarta, and A. Doyan. Graphene: The Revolutionary 2D Material, 2023.

[32] J.H. Lee, D.W. Shin, V.G. Makotchenko, A.S. Nazarov, V.E. Fedorov, Y.H. Kim, and J.B. Yoo, *One-step exfoliation synthesis of easily soluble graphite and transparent conducting graphene sheets*. Adv. Mater. 21(43) (2009), pp. 4383.
[33] M. Yi and Z. Shen, *A review on mechanical exfoliation for the scalable production of graphene*. J. Mater. Chem. A 3(22) (2015), pp. 11700–11715.
[34] P. Kumar, G. Singh, R. Bahadur, Z. Li, X. Zhang, C.I. Sathish, and A. Vinu, *The rise of borophene*. Prog. Mater. Sci. 140 (2024), pp. 101331.
[35] X. Yan, S. Wang, Y. Sun, Y. Liu, Y. Wang, and G. Yang, *Semiconducting bilayer borophene with high carrier mobility*. J. Phys. Chem. Lett. 14(43) (2023), pp. 9698–9704.
[36] Z. Zhang, Y. Yang, E.S. Penev, and B.I. Yakobson, *Elasticity, flexibility, and ideal strength of borophenes*. Adv. Funct. Mater. 27(9) (2017), pp. 1605059.
[37] A.J. Mannix, Z. Zhang, N.P. Guisinger, B.I. Yakobson, and M.C. Hersam, *Borophene as a prototype for synthetic 2D materials development*. Nat. Nanotechnol. 13(6) (2018), pp. 444–450.
[38] Y. Yin, Y. Hu, S. Li, G. Ding, S. Wang, D. Li, and G. Zhang, *Abnormal thermal conductivity enhancement in covalently bonded bilayer borophene allotrope*. Nano Res. 15 (2022), pp. 1–7.
[39] H. Zhou, Y. Cai, G. Zhang, and Y.W. Zhang, *Superior lattice thermal conductance of single-layer borophene. npj 2D*. Mater. Appl. 1(1) (2017), pp. 14.
[40] G.J. Adekoya, O.C. Adekoya, M. Muloiwa, E.R. Sadiku, W.K. Kupolati, and Y. Hamam, *Advances In borophene: synthesis tunable properties, and energy storage applications*. Small 2403656 (2024).
[41] G. Bilgiç, *Review of properties, synthesis, and energy applications of borophene, a novel boron-based 2D material*. J. Boron 9(2) (2024), pp. 82–95.
[42] U. Rajput, M.F. Akhtar, V. Walve, I. Mulani, G. Vyas, S. Bhowmick, and A. Deshpande, *Liquid phase exfoliated borophene on Au (111)*. J. Phys. Chem. C 128(9) (2024), pp. 4104–4110.
[43] K.P.P. Najiya, R. Konnola, T.S. Sreena, S. Solomon, and K.G. Gopchandran, *Liquid phase exfoliation of few-layer borophene with high hole mobility for low-power electronic devices*. Inorg. Chem. Commun. 168 (2024), pp. 112962.
[44] C. Li, A.K. Tareen, J. Long, M. Iqbal, W. Ahmad, M.F. Khan, ... K. Khan, *Two dimensional borophene nanomaterials: recent developments for novel renewable energy storage applications*. Prog. Solid State Chem. 33 (2023), pp. 100416.
[45] A. Rahman, M.T. Rahman, M.A. Chowdhury, S.B. Ekram, M.K. Uddin, M.R. Islam, and L. Dong, *Emerging 2D borophene: synthesis, characterization, and sensing applications*. Sens. Actuators, A 359 (2023), pp. 114468.
[46] K. Ledwaba, S. Karimzadeh, and T.C. Jen, *Emerging borophene two-dimensional nanomaterials for hydrogen storage*. Materials Today Sustainability 22 (2023), pp. 100412.
[47] N.A.A. Rusman and M. Dahari, *A review on the current progress of metal hydrides material for solid-state hydrogen storage applications*. Int. J. Hydrogen Energy 41(28) (2016), pp. 12108–12126.
[48] E.J. Kan, Z. Li, J. Yang, and J.G. Hou, *Half-metallicity in edge-modified zigzag graphene nanoribbons*. J. Am. Chem. Soc. 130(13) (2008), pp. 4224–4225.
[49] Y. Liu, Y.J. Dong, Z. Tang, X.F. Wang, L. Wang, T. Hou, and Y. Li, *Stable and metallic borophene nanoribbons from first-principles calculations*. J. Mater. Chem. C 4(26) (2016), pp. 6380–6385.
[50] F. Xiang, Y. Gu, A. Kinikar, N. Bassi, A. Ortega-Guerrero, Z. Qiu, and R. Fasel. Zigzag Graphene Nanoribbons with Periodic Porphyrin Edge Extensions, 2024.
[51] X.D. Tan, J.Q. Han, and L. Zhang, *Pauli susceptibility of zigzag graphene nanoribbons*. Micro and Nanostructures 184 (2023), pp. 207687.
[52] G.W. Semenoff, *Boundary ferromagnetism in zigzag edged graphene*. J. Math. Phys. 64(7) (2023), pp. 071901.
[53] E.J. Kan, Z. Li, J. Yang, and J.G. Hou, *Half-metallicity in edge-modified zigzag graphene nanoribbons*. J. Am. Chem. Soc. 130(13) (2008), pp. 4224–4225.

[54] F.J. Owens, *Electronic and magnetic properties of armchair and zigzag graphene nanoribbons*. J. Chem. Phys. 128(19) (2008), pp. 194701.
[55] O. Hod, V. Barone, J.E. Peralta, and G.E. Scuseria, *Enhanced half-metallicity in edge-oxidized zigzag graphene nanoribbons*. Nano Lett. 7(8) (2007), pp. 2295–2299.
[56] G.P. Guo, Z.R. Lin, T. Tu, G. Cao, X.P. Li, and G.C. Guo, *Quantum computation with graphene nanoribbon*. New J. Phys. 11(12) (2009), pp. 123005.
[57] Y. Liu, Y.J. Dong, Z. Tang, X.F. Wang, L. Wang, T. Hou, and Y. Li, *Stable and metallic borophene nanoribbons from first-principles calculations*. J. Mater. Chem. C 4(26) (2016), pp. 6380–6385.
[58] S. Kharwar and S. Singh, *The rise OF borophene and borophene nanoribbons: a potential quantum electronics material*. Surf. Rev. Lett. 29(05) (2022), pp. 2230005.
[59] C. Sun, X.F. Wang, L.P. Zhou, and Y.S. Liu, *The magnetism enhancement and spin transport in zigzag borophene nanoribbons edge-passivated by N atoms*. Appl. Nanosci. 10 (2020), pp. 29–35.
[60] F. Norouzi, M. Farokhnezhad, M. Esmaeilzadeh, and B. Szafran, *Controllable spin filtering and half-metallicity in β 12-borophene nanoribbons*. Phys. Rev. B 104(24) (2021), pp. 245431.
[61] J. Liu, J. Wu, C. Chen, L. Han, Z. Zhu, and J. Wu, *Negative differential resistance and magnetoresistance in zigzag borophene nanoribbons*. Int. J. Mod. Phys. B 32(04) (2018), pp. 1850033.
[62] Z. Fadil, C.J. Raorane, H. Sabbah, R. El Fdil, A.A. Ifseisi, R. Boopathiraja, and S.C. Kim, *Monte carlo exploration of magnetic properties: graphene and borophene comparison*. J. Magn. Magn. Mater. 594 (2024), pp. 171910.
[63] W. Jiang, Y.N. Wang, A.B. Guo, Y.Y. Yang, and K.L. Shi, *Magnetization plateaus and the susceptibilities of a nano-graphene sandwich-like structure*. Carbon. N. Y. 110 (2016), pp. 41–47.
[64] R. El Fdil, Z. Fadil, E. Salmani, C.J. Raorane, and H. Ez-Zahraouy, *Magnetic characteristics of the ferrimagnetic bilayer MXene-like nanostructure with interlayer exchange interactions: Monte Carlo study*. J. Magn. Magn. Mater. 580 (2023), pp. 170967.
[65] W. Wang, Q. Li, D. Lv, R.J. Liu, Z. Peng, and S. Yang, *Monte carlo study of magnetization plateaus in a zigzag graphene nanoribbon structure*. Carbon. N. Y. 120 (2017), pp. 313–325.
[66] A. Jabar, L. Bahmad, and A. Benyoussef, *Phase transitions and magnetic properties of zigzag triangular nanographenes: Monte Carlo simulation*. J. Supercond. Novel Magn. 36(1) (2023), pp. 111–118.
[67] Z. Fadil, M. Qajjour, A. Mhirech, B. Kabouchi, L. Bahmad, and W. Ousi Benomar, *Blume-Capel model of a borophene layers structure with RKKY interactions: Monte Carlo simulations*. Ferroelectrics 573(1) (2021), pp. 141–153.
[68] N. Metropolis, A.W. Rosenbluth, M.N. Rosenbluth, A.H. Teller, and E. Teller, *Equation of state calculations by fast computing machines*. J. Chem. Phys. 21(6) (1953), pp. 1087–1092.
[69] M. Blume, V.J. Emery, and R.B. Griffiths, *Ising model for the λ transition and phase separation in He 3-He 4 mixtures*. Phys. Rev. A 4(3) (1971), pp. 1071.
[70] R. Chegel, S. Behzad, and A.I. Ayesh, Tetragonal silicene: a study of field-dependent transport responses. Mater. Sci. Semicond. Process. 166 (2023), pp. 107711.
[71] T. Sahdane, R. Masrour, and A. Jabar, Magnetic properties of one defects on borophene trilayer structure: a Monte Carlo study. Phase Transitions 93 (2020), pp. 962–972.
[72] M. Yang, W. Wang, B.C. Li, H.J. Wu, S.Q. Yang, and J. Yang, Magnetic properties of an Ising ladder-like graphene nanoribbon by using Monte Carlo method. Physica A 539 (2020), pp. 122932.
[73] H.J. Wu, W. Wang, B.C. Li, M. Yang, S.Q. Yang, and F. Wang, Magnetic properties in graphene-like nanoisland bilayer: Monte Carlo study. Phys. E 112 (2019), pp. 86.
[74] Q. Lin, L. Miao, Z. Qian, Y. Sun, and R. Wang, *First-principles calculations on magnetism induced by vacancies in β12-borophene nanosheets: implications for property modulation*. ACS Applied Nano Materials 5(1) (2022), pp. 113–119.
[75] C. Sun, X.F. Wang, L.P. Zhou, and Y.S. Liu, *The magnetism enhancement and spin transport in zigzag borophene nanoribbons edge-passivated by N atoms*. Appl. Nanosci. 10 (2020), pp. 29–35.

[76] S.Y. Yue, Q.B. Yan, Z.G. Zhu, H.J. Cui, Q.R. Zheng, and G. Su, *First-principles study on electronic and magnetic properties of twisted graphene nanoribbon and Möbius strips*. . N. Y. 71 (2014), pp. 150–158.
[77] K. Sawada, F. Ishii, and M. Saito, *Magnetism in graphene nanoribbons on Ni (111): first-principles density functional study*. Phy. Rev. B 82(24) (2010), pp. 245426.
[78] A.J. Mannix, Z. Zhang, N.P. Guisinger, B.I. Yakobson, and M.C. Hersam, *Borophene as a prototype for synthetic 2D materials development*. Nat. Nanotechnol. 10 (2015), pp. 569–579.
[79] Z. Zhang, Y. Yang, and G. Gao, *Two-dimensional boron: structures, properties and applications*. Mat. Chem. Front. 1 (2017), pp. 768–783.
[80] D. Mukamel and M. Blume, *Ising model for tricritical points in ternary mixtures*. Phys. Rev. A 10(2) (1974), pp. 610.
[81] J.B. Santos-Filho and J.A. Plascak, *Monte Carlo simulations of the XY vectorial Blume-Emery-Griffiths model in multilayer films for He 3-He 4 mixtures*. Phys. Rev. E 96(3) (2017), pp. 032141.
[82] S. Behzad and R. Chegel, *Thermal conductivity, heat capacity and magnetic susceptibility of graphene and boron nitride nanoribbons*. Diamond Relat. Mater. 88 (2018), pp. 101–109.
[83] R. Chegel, *External magnetic field effects on the thermoelectric and thermodynamic properties of doped monolayer S-graphene: A theoretical study*. Phys. B 667 (2023), pp. 415177.

Philosophical Magazine

ISSN: 1478-6435 (Print) 1478-6443 (Online) Journal homepage: www.tandfonline.com/journals/tphm20

Re-entrant magnetic behaviour in core–shell nanotubes: a Monte Carlo study

Hussein Sabbah, M. Naziruddin Khan, Abdullah Almohammedi, A. Jabar, Z. Fadil, Abdulrahman A. Alsayyari, Chaitany Jayprakash Raorane & Seong-Cheol Kim

To cite this article: Hussein Sabbah, M. Naziruddin Khan, Abdullah Almohammedi, A. Jabar, Z. Fadil, Abdulrahman A. Alsayyari, Chaitany Jayprakash Raorane & Seong-Cheol Kim (2026) Re-entrant magnetic behaviour in core–shell nanotubes: a Monte Carlo study, Philosophical Magazine, 106:13-14, 1301-1317, DOI: 10.1080/14786435.2026.2619353

To link to this article: https://doi.org/10.1080/14786435.2026.2619353

PHILOSOPHICAL MAGAZINE
2026, VOL. 106, NOS. 13–14, 1301–1317
https://doi.org/10.1080/14786435.2026.2619353

Re-entrant magnetic behaviour in core–shell nanotubes: a Monte Carlo study

Hussein Sabbah[a], M. Naziruddin Khan[b], Abdullah Almohammedi[b], A. Jabar[c,d], Z. Fadil[e], Abdulrahman A. Alsayyari[f], Chaitany Jayprakash Raorane[g] and Seong-Cheol Kim[g]

[a]College of Engineering and Technology, American University of the Middle East, Egaila, Kuwait; [b]Department of Physics, Faculty of Science, Islamic University of Madinah, Madinah, Saudi Arabia; [c]Laboratory of Mechanics and High Energy Physics, Department of Physics, Faculty of Sciences Aïn Chock, University Hassan II, Casablanca, Morocco; [d]LPHE-MS, Science Faculty, Mohammed V University in Rabat, Morocco; [e]Laboratoire de Matière Condensée et Sciences Interdisciplinaires (LaMCScI), URL-CNRST, Faculty of Sciences, Morocco; [f]Department of Radiologic Technology, College of Applied Medical Sciences, Qassim University, Buraydah, Saudi Arabia; [g]School of Chemical Engineering, Yeungnam University, Gyeongsan, Republic of Korea

ABSTRACT

This study investigates the re-entrant magnetic behaviour in a core–shell nanotube structure using Monte Carlo simulations within the framework of the Metropolis algorithm. The system comprises mixed spins, modelled with Blume-Capel interactions under different physical conditions. The temperature dependence of magnetisation and susceptibility is systematically explored by varying the crystal field parameter, exchange couplings and external magnetic field. The results reveal a complex phenomenon of re-entrant magnetisation, where the total magnetisation reverses its sign with temperature changes. For specific values of crystal field and interlayer exchange coupling, the system exhibits multiple sign changes in the sublattice magnetisations and a noticeable compensation point. In addition, the application of a strong external magnetic field suppresses the re-entrant effect due to spin alignment stabilisation. These results highlight the tunability of magnetic properties in core–shell nanostructures, offering potential applications in magnetic storage, spintronics and nanoscale sensors.

ARTICLE HISTORY
Received 8 December 2025
Accepted 14 January 2026

KEYWORDS
Core–shell nanotube; Monte Carlo simulation; re-entrant magnetisation; blume-capel model; compensation temperature; nanostructured magnetism;

1. Introduction

The study of magnetism in low-dimensional systems has become an important new area of condensed matter physics and nanotechnology because of its significant implications in fundamental research and technological development [1]. Nanostructured materials, such as core–shell nanotubes [2-8], are worth investigating for their interesting magnetic

CONTACT Z. Fadil fadilzakaria604@gmail.com Laboratoire de Matière Condensée et Sciences Interdisciplinaires (LaMCScI), URL-CNRST, Faculty of Sciences, P.O. Box 1014, Mohammed V University in Rabat, Morocco; Chaitany Jayprakash Raorane chaitanyaraorane22@ynu.ac.kr School of Chemical Engineering, Yeungnam University, Gyeongsan, 38541, Republic of Korea; Seong-Cheol Kim seongcheol2025@gmail.com School of Chemical Engineering, Yeungnam University, Gyeongsan, 38541, Republic of Korea

properties arising from quantum confinement, reduced dimensions, and interfacial coupling.

The emerging classes of magnetic nanostructures are observed to exhibit exotic phenomena that are absent in bulk systems that include unusual coercivity, exchange bias and tuneable magnetic phase transitions; thus, they are possible candidates for advanced applications in high-capacity magnetic storage, spintronic devices, magnetocaloric devices, and nanoscale magnetic sensors [9, 10].

System is re-entrant magnetic behaviour, which has been an incredibly interesting and non-intuitive avenue of research. Re-entrant magnetism is characterised by a non-monotonous dependence of magnetisation on temperature [11, 12], often exhibiting a transition from an ordered magnetic state to a disordered or sometimes even a different ordered magnetic state with further cooling, or multiple magnetic phase transitions as a function of temperature. Re-entrant magnetism usually indicates that the magnet obeys competing magnetic interactions, spin frustration, or strong crystal field effects, which can provide interesting insights into the spin Hamiltonian and critical phenomena. The ability to induce, suppress, or control re-entrant transitions provides much potential for new functionalities for: advanced magnetic memories, future spintronic devices, and extremely sensitive nanoscale sensors.

Although magnetic nanostructures are of increasing interest, the re-entrant magnetic phases of mixed-spin core–shell nanotube structures have not yet received systematic attention [13-15]. The tubular geometry can impose additional constraints and symmetries to the spin ordering, and the inclusion of different spin values in the core and shell (mixed spins) along with crystal field effects is a further complication for the magnetic response [16, 17].

Despite extensive research on mixed spin Ising nanostructures, for core–shell nanowires [18-20], fullerene-like systems [21-24], and multilayer [25, 26] or bilayer systems [27-29], the particular impact of a core–shell structure and a tubular geometry on re-entrant magnetic phenomena has yet to be investigated. As in contrast to the geometries studied earlier, in a nanotube, the hollow cylindrical topology will affect the coordination number at the interfaces, which will further accentuate the effects of curvature and thus lead to a different influence on the interactions at the surfaces, core, and interfaces. Such geometries can lead to differences in the magnetism, which will be unlike what has been observed in nanowires, fullerenes, or planar geometries. On the basis of previous studies where the carbon atoms have been replaced with the same spin values to describe the basic magnetic properties of different nanostructures such as a core–shell nanotube [13], a biphenylene network [30], a C_{20} fullerene molecule [31], bi-layer graphene nanoribbons [32], a graphene-like monolayer [33], as well as the study of the stacking arrangement and bond dilution effect in a trilayer graphene system [34], the spin configuration $\sigma = 3/2$ and $S = 1$ was used in the study.

The increased value of the spin in the shell promotes sensitivity to the crystal-field interaction, besides having the $S = 0$ state in the core that favours the occurrence of higher thermal fluctuations with a strong competition among the sublattices. Inclusion of the nanotube structure promotes the formation of more complex re-entrant patterns, compensation points, and reversals of the magnetisation of the sublattices that are not encountered in mixed-spin Ising nanostructures with other geometries.

Therefore, what is new in this research is that it reveals the joint influence of the spin asymmetry (3/2, 1) and the nanotube core–shell structure on the re-entrant and compensation phenomena, which cannot be established on the basis of existing research on nanowires, fullerenic clusters, or bilayer structures.

The Monte Carlo simulation is an established and efficient approach to simulate complex magnetic systems, as evidenced in previous mixed-spin Ising systems. For instance, in the mixed-spin Ising model with a three-layer hexagonal lattice and mixed spins (1, 1/2, 1), compensation temperatures were shown to be parameter-dependent, accompanied by two-step hysteresis loop phenomena [25]. Also, rotating double-layer films with mixed spins (1/2, 1) manifested complex Néel temperature phases and hysteresis effects, such as triple-loop behaviour and superparamagnetism [35]. In inverse spinel-like Cu_2F_5 systems with spin interactions of (1/2, 1), it was evidenced that magnetic compensation is deeply related to thresholds of the exchange coupling and single-ion anisotropy constants [36].

In this paper, a comprehensive Monte Carlo analysis is carried out on a mixed-spin ($\sigma = 3/2$, $S = 1$) core–shell nanotube within the Blume-Capel Ising model [37-43]. This approach proved successful in a number of geometrically complex nano-scale systems, such as decorated triangular lattices [37], double fullerenes in core–shell systems [38], carbon-like nanotubes [39], and double-wall cubic metal nanotubes [40]. Rich magnetic phenomena, like hysteresis, compensation phenomena, and magnetisation plateaus, have also been observed in preceding works on core–shell nanowires [41], decorated lattices in high-spin representations [42], and in bilayer mixed-spin models [43]. Based on these established antecedents, in this paper, a critical examination is undertaken on temperature dependencies of total, as well as individual, magnetisations, as well as susceptibility under wide ranges of crystal field, intra- and interlayer interactions, and applied magnetic fields. Evident in these calculations are the re-entrance phenomena in magnetism, sharpness in the compensation points, and high tunability of magnetic states caused by the present asymmetry in spin values and nanotube geometry.

2. Methodology and method

The magnetic properties of a core/shell nanotube composite were investigated using Monte Carlo simulations with free boundary conditions, performed according to the Blume-Capel Ising model. The model includes 128 Ising spins distributed in two concentric nanotubes, with 64 σ-spins in the shell and 64 S-spins in the core (Figure 1). The S-spins in the core interact with core-site strengths that allow them to take on -1, 0, or $+1$ values, while σ-spins in the shell interact with shell-site strengths that enable them to take on $-3/2$, $-1/2$, $+1/2$, or $+3/2$ values. The size (128) represents a finite nanostructure that can effectively account for the effects due to surfaces, interfaces, as well as being computationally efficient. Thermal equilibrium was also obtained in a Monte Carlo step per spin (timesteps), discarding the first 2×10^5 Monte Carlo steps per spin; equilibration was checked using the time evolution of the total energy and total magnetisation. The statistical averages were calculated over 2×10^6 Monte Carlo steps per spin. Monte Carlo simulations were performed using the Metropolis algorithm. For each set of parameters, the system was

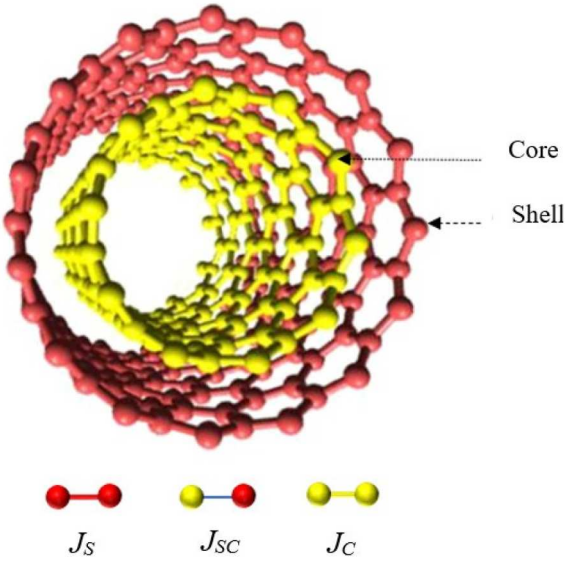

Figure 1. Schematic illustration of the core-shell nanotube structure composed of spin-3/2 (σ) atoms in the shell and spin-1 (S) atoms in the core.

balanced over 2×10^5 Monte Carlo steps per rotation, then a statistical average was calculated over $2 \times 10^5 - 2 \times 10^6$ steps. The simulations were repeated with different random seeds, and all quantities reported are ensemble averages. The approach for testing the obtained results consisted in the method described in Fabian & Leonhardt [44] in combination with Monte Carlo simulations [16].

The Hamiltonian governing the core–shell nanotube structure is given by the following formula:

$$H = -J_c \sum_{<i,j>} \sigma_i \sigma_j - J_S \sum_{<k,l>} S_k S_l - J_{SC} \sum_{<m,n>} S_m \, \sigma_n - H \left(\sum_i \sigma_i + \sum_j S_j \right) \\ -D_\sigma \sum_i (\sigma_i)^2 + D_s \sum_j (S_i)^2 \tag{1}$$

The exchange interactions J_C, J_S, and J_{CS} correspond to the spin couplings σ-σ, S-S, and σ-S, respectively. The system is influenced by an external magnetic field H and crystal field terms D_σ and D_S, representing the anisotropies of a single ion. For simplicity, we assume a uniform crystal field: $D = D_\sigma = D_S$.

For simplicity, dimensionless (reduced) parameters were employed: $j_C = J_C/J_S$, $j_{CS} = J_{CS}/J_S$, $t = T/J_S$, $h = H/J_S$ and $d = D/J_S$

The internal energy at each site can be expressed as follows:

$$E_{tot} = \frac{\langle \mathcal{H} \rangle}{N_\sigma + N_S} \tag{2}$$

The magnetisations and susceptibilities of the carbon bi-nanotube-like composite system

are defined as follows:

$$M_\sigma = \frac{1}{N_\sigma}\sum\nolimits_i \sigma_j \tag{3}$$

$$M_S = \frac{1}{N_S}\sum\nolimits_j S_j \tag{4}$$

$$M_{tot} = \frac{M_\sigma + M_S}{2} \tag{5}$$

$$\chi_{_\sigma} = \beta(< M_\sigma^2 > - < M_\sigma >^2) \tag{6}$$

$$\chi_S = \beta(< M_S^2 > - < M_S >^2) \tag{7}$$

$$\chi_{tot} = \frac{\chi_\sigma + \chi_S}{2} \tag{8}$$

The parameter β is formulated as $1/k_BT$, in energy discussions, where k_B is Boltzmann's constant and T is the absolute temperature.

Moreover, the model parameters are chosen based on physical considerations and explored systematically. Negative values of the crystal field control the stabilisation of the central non-magnetic state $S = 0$, while variations in exchange couplings probe the competition between center-shell and intra-layer interactions. This approach reveals general behaviours such as re-entry, magnetisation reversal, and compensation induced by spin asymmetry and nanotube geometry.

3. Magnetic characteristics

This section examines the thermal behaviour of magnetisation and susceptibility in the core–shell nanotube using Monte Carlo simulations with the Metropolis algorithm, under varying system parameters.

Figure 2 illustrates the temperature dependence of the magnetisations (a, c, e, g, i) and corresponding susceptibilities (b, d, f, h, j) for fixed values of $j_S = 1$, $j_{CS} = -1$, $h = 0$, while varying the crystal field parameter d.

The competition between the crystal field d, exchange interactions, and thermal fluctuations gives rise to the mentioned sublattice magnetisation reversals and to re-entrant magnetic behaviour. Indeed, when a negative crystal-field value favours the single-ion anisotropy of the core spins towards the nonmagnetic $S = 0$ state, there is a reduction in their effective magnetic contribution and a weakening of the core–shell coupling. This imbalance can trigger, for appropriate strength or sign of the interfacial exchange interaction, a reorientation of the sublattice magnetisations and induce sign changes in the core or shell magnetisation. Increasing temperature leads to a progressive reshaping of the effective free-energy landscape due to thermal fluctuations, which destabilises low-temperature ordered states and allows competing magnetic configurations to turn favourable with the subsequent emergence of re-entrant magnetic sequences.

Specifically, for $d = -1$ (Figure 2a,b), very low temperatures give sublattice magnetisations of $M_\sigma = +3/2$ and $M_S = +1$, leading to $M_{tot} = 1.25$ calculated using Equation 5, with

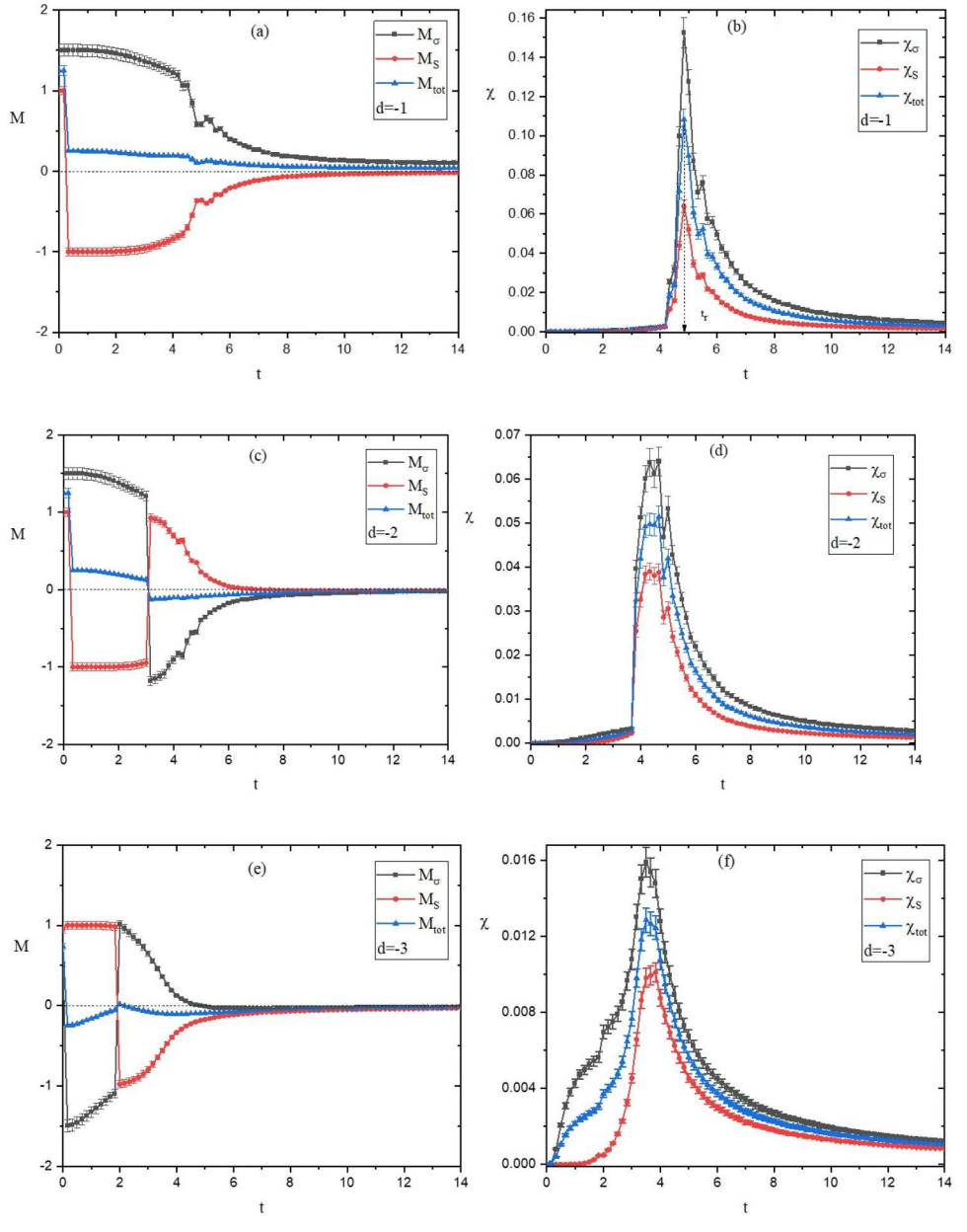

Figure 2. Temperature variation of magnetisations (a, c, e, g, i) and corresponding susceptibilities (b, d, f, h, j), for: $j_S = 1$, $j_{CS} = -1$, $h = 0$.

a transition temperature (t_r) of around 4.83, as indicated by the total susceptibility peak; for this configuration, re-entrant magnetisation behaviour is observed only for spin *S*.

For $d = -2$ (Figure 2c,d), similarly low temperatures give $M_\sigma = +3/2$ and $M_S = +1$, leading to $M_{tot} = 1.25$, and a t_r of around 4.33, marked by the total susceptibility peak; here, the re-entrant magnetisation phenomenon is evident as the *S* spin changes sign twice before cancelling, while the σ spin undergoes a single sign change before fading.

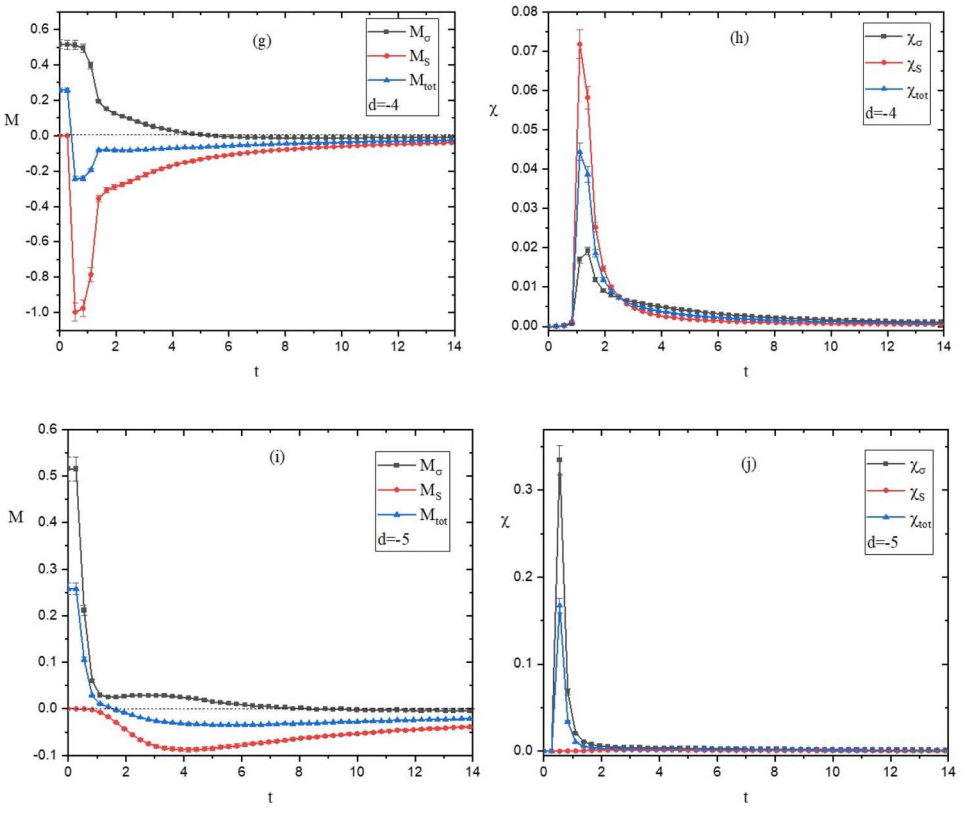

Figure 2. *Continued.*

Conversely, for $d = -3$ (Figure 2e,f), at very low temperature, $M_\sigma = +1/2$ and $M_S = +0.95$, giving $M_{tot} = 0.73$, with a t_r of around 3.66 identified by the susceptibility peak; in this case, the re-entrant magnetisation phenomenon is observed for spin σ with two sign changes before cancelling out, while spin S undergoes one sign change before becoming zero.

For $d = -4$ (Figure 2g,h), at very low temperature, $M_\sigma = 0$ and $M_S = +0.51$, leading to $M_{tot} = 0.25$, and a t_r of around 1.11, indicated by the susceptibility peak; while no sign change is observed for the partial magnetisations of the σ or S spins, the S spin exhibits a jump without sign change, which nevertheless influences the total magnetisation, showing re-entrant behaviour.

Finally, for $d = -5$ (Figure 2i,j), very low temperatures give $M_\sigma = 0$ and $M_S = +0.51$, with $M_{tot} = 0.25$, and a t_r of around 0.55 of the susceptibility peaks; as for $d = -4$, the re-entrant magnetisation phenomenon is not characterised by sign changes in the partial magnetisations, but a jump in the spin S value affects the total magnetisation, indicating re-entrant behaviour.

Figure 3 illustrates the temperature dependence of the magnetisations (a, c, e, g, i) and corresponding susceptibilities (b, d, f, h, j) for fixed values of $j_S = 1$, $d = -2$, $h = 0$, while varying the exchange coupling between the core and the shell parts j_{CS}.

For $j_{CS} = -1$ (Figure 3a,b), at very low temperatures, the sub-lattice magnetisations are $M_\sigma = +3/2$ and $M_S = +1$, giving a total magnetisation $M_{tot} = 1.25$, with a transition temperature $t_r \approx 4.33$, indicated by the susceptibility peak. For $j_{CS} = -2$ (Figure 3c,d), $M_\sigma =$

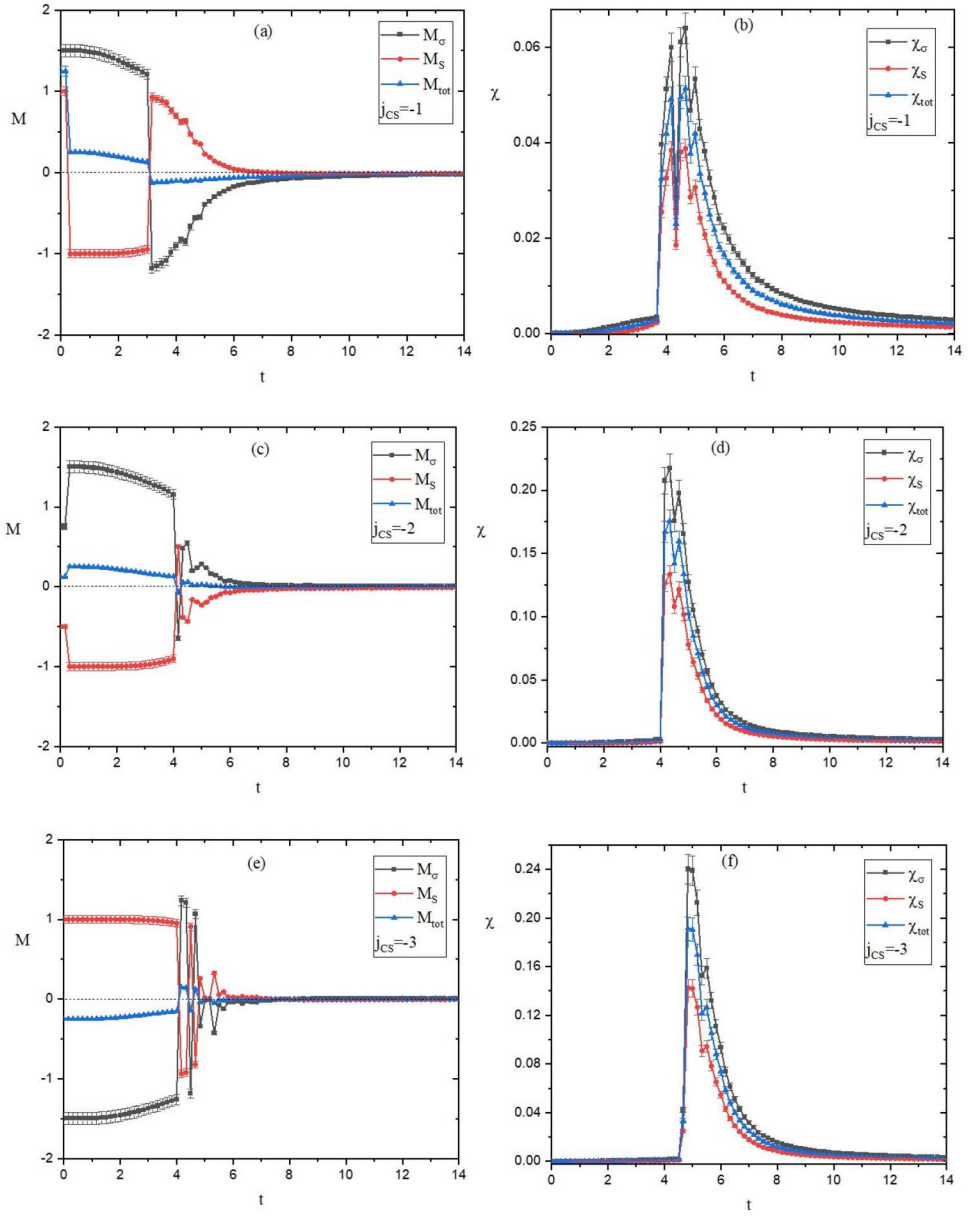

Figure 3. Temperature variation of magnetisations (a, c, e, g, i) and corresponding susceptibilities (b, d, f, h, j), for: $j_S = 1$, $d = -2$, $h = 0$.

+0.75 and $M_S = -0.50$, giving $M_{tot} = 0.12$, with $t_r \approx 4.5$. For $j_{CS} = -3$ (Figure 3f), $M_\sigma = 3/2$ and $M_S = +1$, giving $M_{tot} = -0.25$, with $t_r \approx 5.0$. For $j_{CS} = -4$ (Figure 3g/h), the values are $M_\sigma = +3/2$, $M_S = -1$, and $M_{tot} = 0.25$, with $t_r \approx 6.38$.

Finally, at $j_{CS} = -5$ (Figure 3i,j), the magnetisations are $M_\sigma = -1.32$ and $M_S = +0.87$, hence $M_{tot} = -0.22$, and $t_r \approx 5.83$.

Re-entrant magnetisation is only observed for $j_{CS} = -1$, characterised by a temperature-induced change in sign of total magnetisation. For $j_{CS} = -2$, -3, and -5, multiple

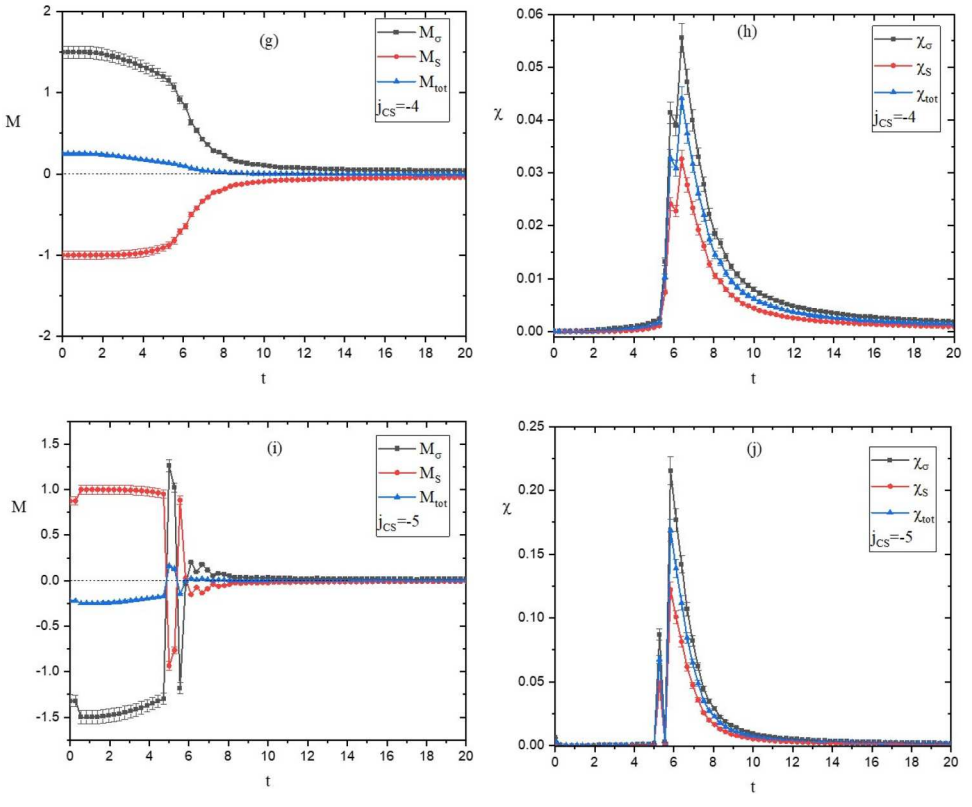

Figure 3. *Continued.*

thermal fluctuations appear near the transition temperature, highlighting competition between exchange interactions and thermal agitation.

Figure 4 illustrates the temperature dependence of the magnetisations (a, c, e, g, i) and corresponding susceptibilities (b, d, f, h, j) for fixed values of $j_{CS} = -1$, $d = -2$, $h = 0$, while varying the exchange coupling in the shell part j_S.

For $j_S = 1$ (Figure 4a,b), at very low temperatures, the sub-lattice magnetisations are $M_\sigma = +3/2$ and $M_S = +1$, giving a total magnetisation $M_{tot} = 1.25$, with a transition temperature $t_r \approx 4.33$, as indicated by the susceptibility peak. For $j_S = 2$ (Figure 4c,d), the same magnetisation values are observed, with $t_r \approx 5.5$. Similarly, for $j_S = 3$ (Figure 4e,f), $j_S = 4$ (Figure 4g,h), and $j_S = 5$ (Figure 4i,j), the magnetisations remain $M_\sigma = +3/2$, $M_S = +1$, and $M_{tot} = 1.25$, while the transition temperature (t_r) increases to around 7.0, 9.44, and 10.55, respectively. This steady increase in t_r with increasing j_S highlights the enhancement of magnetic order due to improved intra-nucleus coupling.

Re-entrant magnetisation is observed for all j_S values, characterised by a temperature-induced sign change in total magnetisation. For $j_S = 3$, 4 and 5, an additional phenomenon appears as temperature increases, namely the appearance of a compensation temperature after the re-entrant magnetisation behaviour.

Finally, Figure 5 illustrates the temperature dependence of the magnetisations (a, c, e, g, i) and corresponding susceptibilities (b, d, f, h, j) for fixed values of $d = -2$, $j_{CS} = -1$, $j_S = 1$, while varying the external magnetic field parameter h.

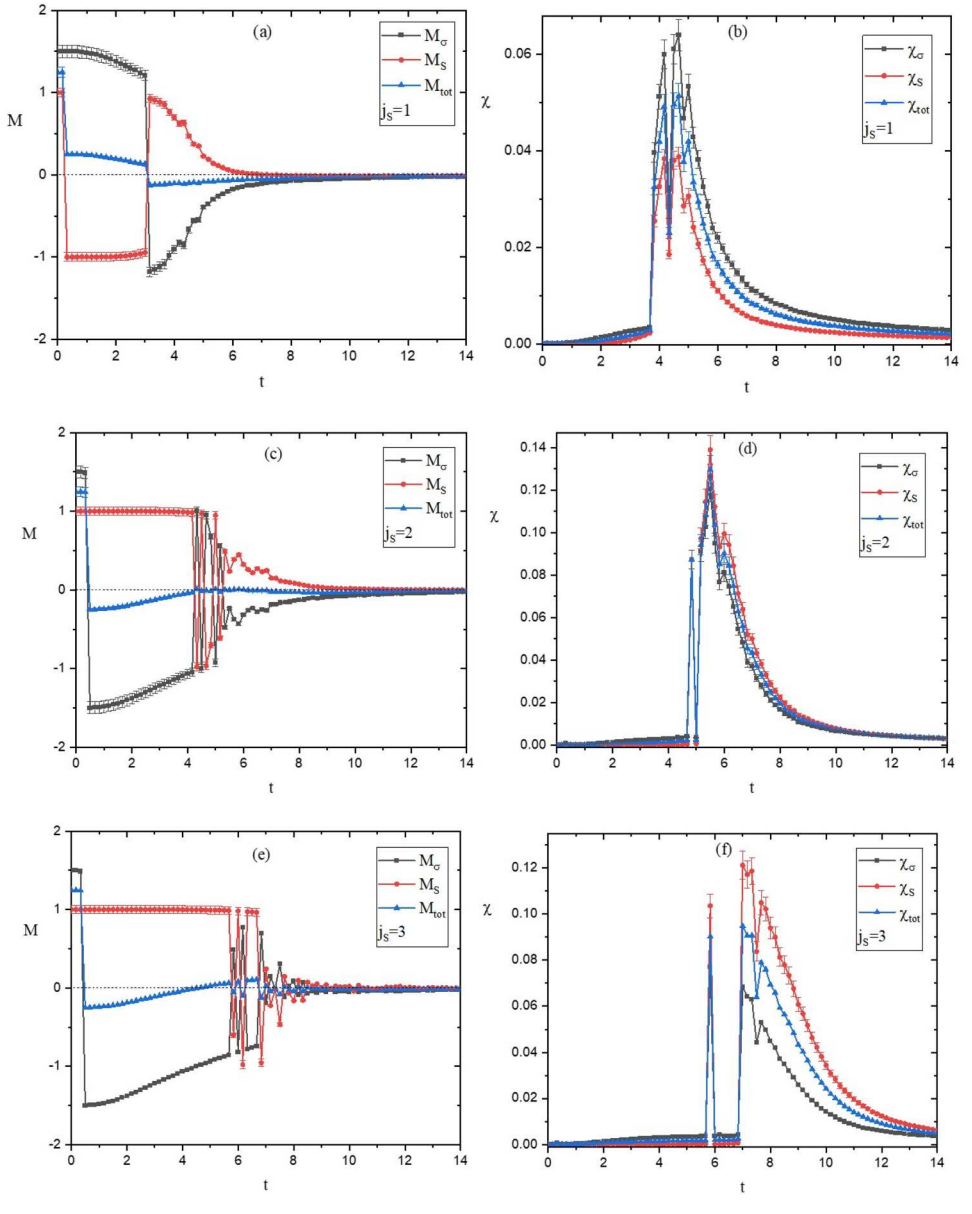

Figure 4. Temperature variation of magnetisations (a, c, e, g, i) and corresponding susceptibilities (b, d, f, h, j), for: $d = -2$, $j_{CS} = -1$, $h = 0$.

For $h = 1$ (Figure 5a,b), at very low temperatures, the sub-lattice magnetisations are $M_\sigma = +3/2$ and $M_S = +1$, giving a total magnetisation $M_{tot} = 1.25$, with a transition temperature $t_r \approx 4.5$, as indicated by the susceptibility peak. For $h = 2$ (Figure 5c,d), $M_\sigma = +3/2$ and $M_S = +1$, giving $M_{tot} = 1.25$, with $t_r \approx 5.5$. Similarly, for $h = 3$ (Figure 5e,f), the values remain $M_\sigma = +3/2$, $M_S = +1$, and $M_{tot} = 1.25$, with $t_r \approx 6.83$. For $h = 4$ (Figure 5g,h), the same magnetisation values are observed, with a higher transition temperature of $t_r \approx 8.05$. Finally, for $h = 5$ (Figure 5i,j), $M_\sigma = +3/2$, $M_S = +1$, and $M_{tot} = 1.25$, with $t_r \approx 10$.

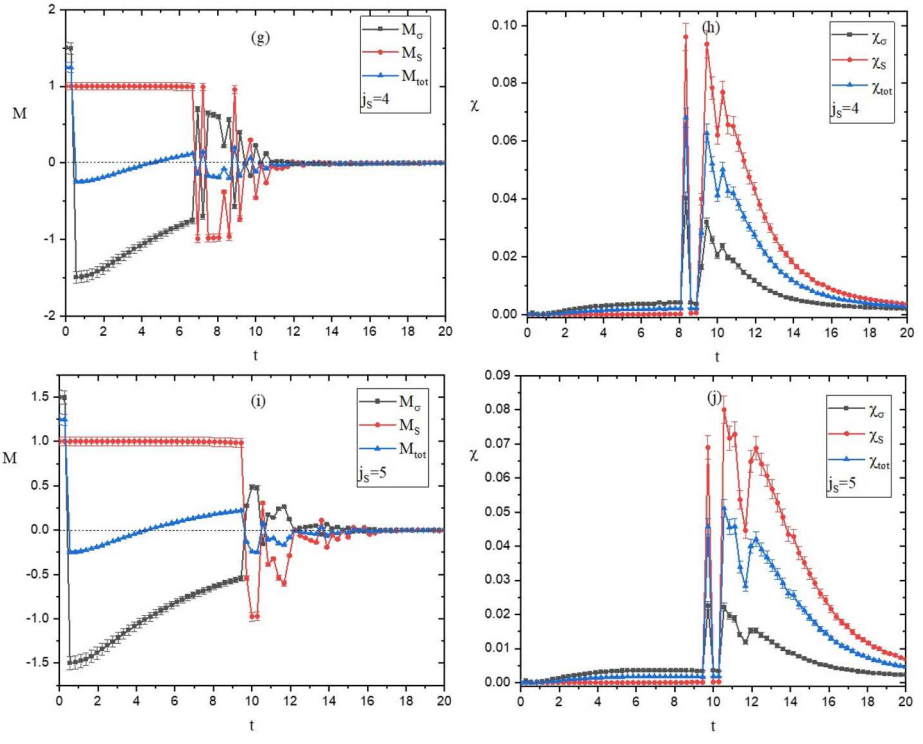

Figure 4. *Continued.*

Re-entrant magnetisation is only observed for external magnetic field $h = 1$, particularly in the magnetisation of S atoms, and is characterised by a temperature-induced change in sign of the total magnetisation. For $h > 2$, the re-entrant magnetisation disappears. The disappearance of re-entrant magnetisation at high h is due to the field-induced stabilisation of spin alignment, which prevents the system from undergoing spin reorientations that would normally cause re-entrance.

Moreover, our paper takes a theoretical and numerical predictive approach. However, the correctness of the chosen approach is justified by a number of existing studies that have all successfully applied the described Monte Carlo simulation method based on the Blume-Capel model to similar nanostructures with mixed spins [23, 26, 27, 31, 41, 45]. These studies, concerning fullerenes [23, 31, 38], graphenes [27–29, 32, 33], nanotubes [39, 40], as well as other core/shell systems [38, 41, 43], have all provided relevant data related to the main researched features like phase transition points, compensation effects, as well as effects caused by various parameters such as exchange constants, crystal fields, and external magnetic fields.

Finally, Figure 6 displays the evolution of transition temperature t_r versus crystal field $|d|$ (a), core–shell exchange coupling $|\ j_{CS}\ |$ (b), shell exchange coupling j_S (c), and external magnetic field h (d). It follows from the performed analysis that t_r is determined by the interplay between mechanisms, which stabilise magnetic orders and thermal fluctuations. The growth in the absolute value of the crystal field $|d|$ leads to an almost linear decrease in t_r, being this mechanism favours lower spin

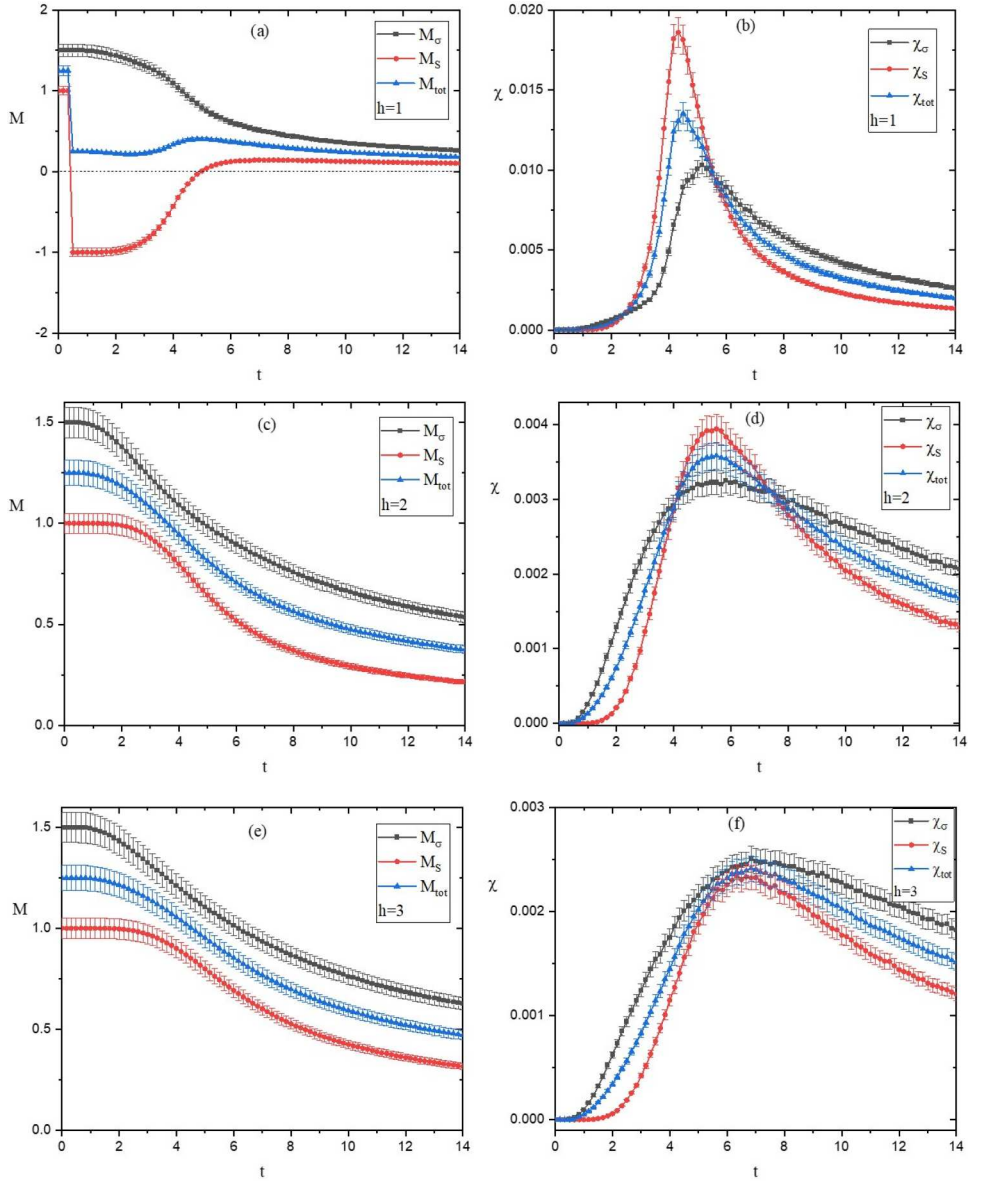

Figure 5. Temperature variation of magnetisations (a, c, e, g, i) and corresponding susceptibilities (b, d, f, h, j), for: $d = -2$, $j_{CS} = -1$, $j_S = 1$.

states and deteriorates ferrimagnetic stability. In turn, the rise in the absolute values of the exchange couplings $|\, j_{CS} \,|$ and j_S amplifies magnetic correlations, giving rise to an enhanced t_r, up to the point where saturation phenomenon occurs. The core–shell coupling exhibits a non-monotonic behaviour, with the optimal value occurring for $|\, j_{CS} \,| = 4$. Within this regime, the interfacial interaction strongly correlates core and shell spins, hence yielding maximum ferrimagnetic coherence. For large $|j_{CS}|$, the presence of antiferromagnetic coupling becomes excessively dominant, enhancing frustration at the interfacial region and making the spin sublattices stiffer against collective

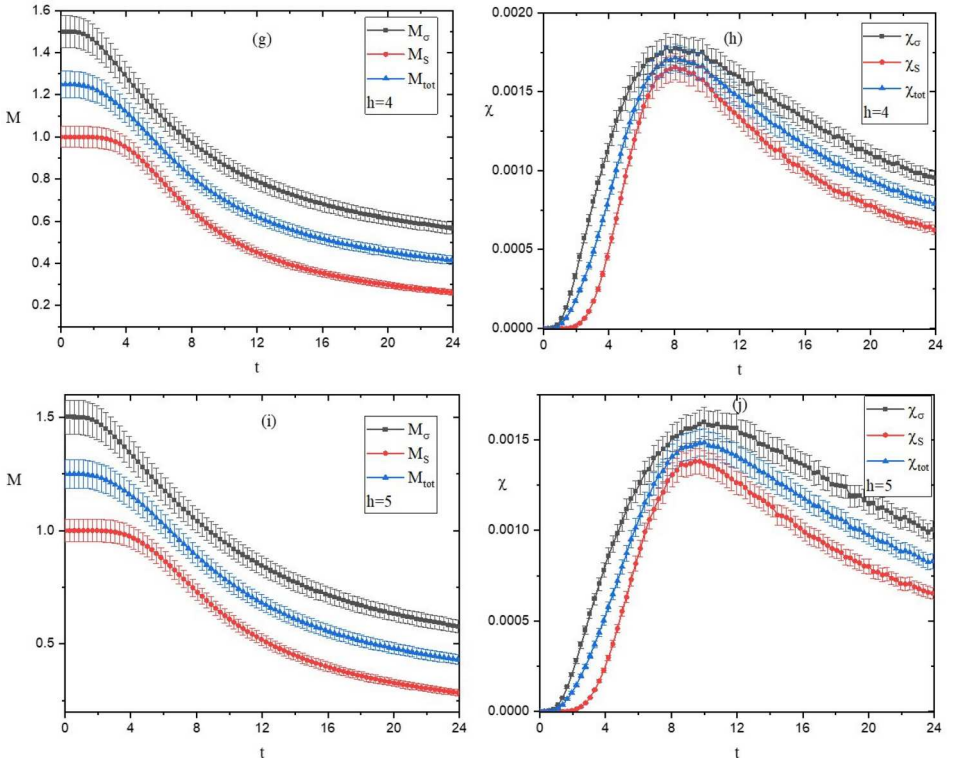

Figure 5. *Continued.*

responses to thermal excitation. At last, the presence of external magnetic fields h enhances spin alignment and contributes to a linear rise in the value of transition temperature.

4. Conclusions

In this work, we carried out a detailed Monte Carlo analysis of the magnetic properties of mixed-spin core–shell nanotube structures. The study focused on the impact of crystal field d variations, exchange interactions (j_{CS}, j_S) and external magnetic field h on thermal magnetisation and susceptibility. Simulations demonstrate the appearance of re-entrant magnetisation under specific conditions, in particular for weak interlayer coupling and low magnetic fields. An increase in $|d|$ linearly suppresses t_r by favouring lower spin states and weakening ferrimagnetic order. Conversely, stronger exchange couplings ($|j_{CS}|$ and j_S) enhance magnetic stability and raise t_r up to a saturation limit. Notably, $|j_{CS}|$ shows a non-monotonic trend, peaking at $|j_{CS}| = 4$, where core–shell correlation is optimal. Larger values introduce excessive antiferromagnetic frustration and spin rigidity, lowering t_r. Lastly, an external field h aligns spins and linearly increases t_r by supporting magnetic order against thermal fluctuations. In addition, for higher values of shell coupling, a compensation temperature appears after the re-entrant behaviour. The application of a strong external magnetic field aligns the spins and suppresses

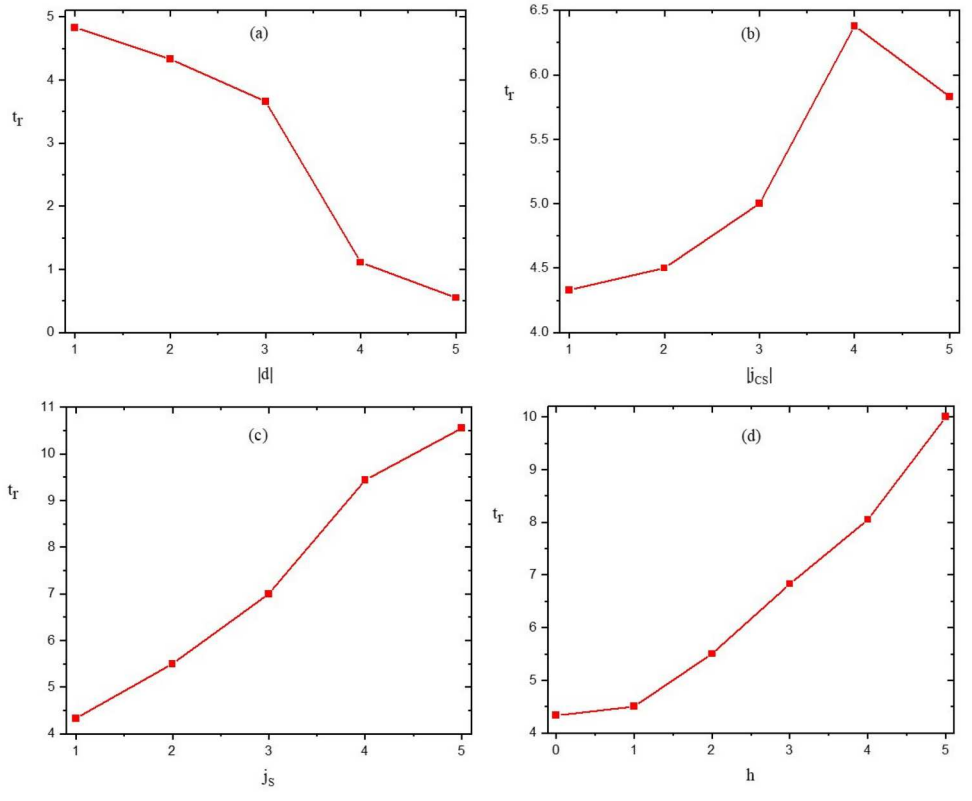

Figure 6. Transition temperature t_r as a function of parameters: crystal field | d | (a), core-shell coupling | j_{CS} | (b), shell coupling j_S (c), and external field h (d).

the re-entrant phenomenon. Overall, this work provides insight into the magnetic tunability of core–shell nanotubes, which could guide the development of advanced magnetic devices and nanotechnology applications.

Acknowledgements

The researchers also wish to extend their sincere gratitude to the Deanship of Scientific Research at the Islamic University of Madinah for the support provided to the Post-Publishing Program.

Disclosure statement

No potential conflict of interest was reported by the authors.

Funding

This work was supported by the National Research Foundation of Korea (NRF) grant funded by the Korea government (MSIT) (RS-2025-22222973) and also supported by the Regional Innovation System & Education (RISE) program through the Gyeongbuk RISE CENTER, funded by

the Ministry of Education (MOE) and the Gyeongsangbuk-do, Republic of Korea (2025-RISE-15-115).

Data and code availability

The investigation was conducted using Monte Carlo simulations employing the Metropolis algorithm through a Fortran code.

References

[1] S.D. Bader, *Magnetism in low dimensionality*. Surf. Sci. 500(1-3) (2002), pp. 172–188.
[2] H. Zou, Z. Luo, X. Yang, Q. Xie, and Y. Zhou, *Toward emerging applications using core–shell nanostructured materials: a review*. J. Mater. Sci. 57(24) (2022), pp. 10912–10942.
[3] L. Su, Y. Jing, and Z. Zhou, *Li ion battery materials with core–shell nanostructures*. Nanoscale. 3(10) (2011), pp. 3967–3983.
[4] Q. Zhang, I. Lee, J.B. Joo, F. Zaera, and Y. Yin, *Core–shell nanostructured catalysts*. Acc. Chem. Res. 46(8) (2013), pp. 1816–1824.
[5] A.M. El-Toni, M.A. Habila, J.P. Labis, Z.A. AlOthman, M. Alhoshan, A.A. Elzatahry, and F. Zhang, *Design, synthesis and applications of core–shell, hollow core, and nanorattle multifunctional nanostructures*. Nanoscale. 8(5) (2016), pp. 2510–2531.
[6] X. Ma, Y. Li, I. Hussain, R. Shen, G. Yang, and K. Zhang, Core–shell structured nanoenergetic materials: preparation and fundamental properties. Adv. Mater. 32(30) (2020), p. 2001291.
[7] K.C. Ho and L.Y. Lin, *A review of electrode materials based on core–shell nanostructures for electrochemical supercapacitors*. J. Mater. Chem. A 7(8) (2019), pp. 3516–3530.
[8] W. Li, A. Elzatahry, D. Aldhayan, and D. Zhao, *Core–shell structured titanium dioxide nanomaterials for solar energy utilization*. Chem. Soc. Rev. 47(22) (2018), pp. 8203–8237.
[9] C. Gong and X. Zhang, *Two-dimensional magnetic crystals and emergent heterostructure devices*. Science 363(6428) (2019), pp. eaav4450.
[10] G. Scheunert, O. Heinonen, R. Hardeman, A. Lapicki, M. Gubbins, and R.M. Bowman, A review of high magnetic moment thin films for microscale and nanotechnology applications. Applied Physics Reviews 3(1) (2016), p. 011301. Available at https://doi.org/10.1063/1.4941497.
[11] A. Majeed and H. Singh, Effect of the interface transparency and ferromagnetic thickness on the critical temperature of NbN/Gd/NbN hybrid structure. Physica C 602 (2022), p. 135412.
[12] Y. Sánchez-León, G. Attolini, F. Bolzoni, R. Vargas, and P. Silva, Exploring magnetic transitions in the FeIn2xCr2-2xS4 semiconductor system through electron spin resonance. J. Magn. Magn. Mater. 604 (2024), p. 172317. Available at https://doi.org/10.1016/j.jmmm.2024.172317.
[13] A. El Abbassi, M. Salama, E.B. Choubabi, N. Hachem, and M. El Bouziani, Hysteresis loops in a mixed-spin (3/2, 3) nanotube with core-shell structure. Appl. Phys. A 131(6) (2025), p. 464. Available at https://doi.org/10.1007/s00339-025-08443-4.
[14] M. Gharaibeh, S. Alqaiem, A. Obeidat, A. Al-Qawasmeh, S. Abedrabbo, and M.H. Badarneh, Magnetic properties of the ferrimagnetic triangular nanotube with core–shell structure: A Monte Carlo study. Physica A 584 (2021), p. 126394. Available at https://doi.org/10.1016/j.physa.2021.126394.
[15] M. Astaraki, M. Ghaemi, and K. Afzali, *Investigation of phase diagrams for cylindrical Ising nanotube using cellular automata*. Phys. Lett. A 382(19) (2018), pp. 1291–1297.
[16] A. Jabar and R. Masrour, Magnetic properties of an Olympicene structure: Monte Carlo simulations. Physica A 541 (2020), p. 123377. Available at https://doi.org/10.1016/j.physa.2019.123377.

[17] A. Jabar, R. Masrour, A. Benyoussef, and M. Hamedoun, *Magnetic properties of the mixed spin-1 and spin-3/2 Ising system on a bilayer square lattice: A Monte Carlo study*. Chem. Phys. Lett. 670 (2017), pp. 16–21.
[18] D. Lv, F. Wang, R.J. Liu, Q. Xue, and S.X. Li, *Monte Carlo study of magnetic and thermodynamic properties of a ferrimagnetic mixed-spin (1, 3/2) Ising nanowire with hexagonal core-shell structure*. J. Alloys Compd. *701* (2017), pp. 935–949.
[19] A. Feraoun and M. Kerouad, *Magnetic properties of a mixed spin Ising nanowire with inner core, inter core-shell and outer shell morphology*. Computational Condensed Matter *16* (2018), pp. e00297.
[20] B. Deviren, Nonequilibrium magnetic properties of the mixed spin (1/2, 1) Ising nanowire with core-shell structure. Phys. E 120 (2020), p. 114052. Available at https://doi.org/10.1016/j.physe.2020.114052.
[21] O. Abounachit, A. Jabar, S. Idrissi, and L. Bahmad, Investigation of the magnetic properties of the fullerene C_{30} with mixed spins: A Monte Carlo study. J. Magn. Magn. Mater. 589 (2024), p. 171604. Available at https://doi.org/10.1016/j.jmmm.2023.171604.
[22] M. Sabzevar, M. Solaimani, M.H. Ehsani, and D.H.T. Tehrani, The effect of vacancy-defects on the magnetic properties of Ising fullerene-like nano-structures: a Monte Carlo study. J. Magn. Magn. Mater. 502 (2020), p. 166573. Available at https://doi.org/10.1016/j.jmmm.2020.166573.
[23] W. Wang, B.C. Li, T.L. Wang, J. Liang, and F.G. Zhang, *Compensation characteristics and hysteresis loops of a fullerene-like (XY) 540: a Monte Carlo study*. J. Mater. Sci. *59*(20) (2024), pp. 8874–8893.
[24] W. Wang, B.C. Li, T.L. Wang, Q. Li, and F. Wang, Thermodynamic and magnetocaloric properties of an AnB60-n fullerene-like structure under the applied magnetic field. J. Magn. Magn. Mater. 553 (2022), p. 169292. Available at https://doi.org/10.1016/j.jmmm.2022.169292.
[25] A. Al-Qawasmeh, M. Badarneh, A. Obeidat, and M. Gharaibeh, Magnetic properties and phase diagrams of Ising mixed spin (1-1/2-1) multilayer's system with hexagonal structure: A Monte Carlo study. Phys. B 643 (2022), p. 414170. Available at https://doi.org/10.1016/j.physb.2022.414170.
[26] H. Saadi, A. Al-Rajhi, E.M. Jalal, O. Hachem, M. Madani, and M. El Bouziani, Monte Carlo simulation of the magnetic properties of a multilayer mixed-spin system (5/2, 3/2). Vacuum 232 (2025), p. 113781. Available at https://doi.org/10.1016/j.vacuum.2024.113781.
[27] R. Masrour, L. Bahmad, and A. Benyoussef, *Size effect on magnetic properties of a nano-graphene bilayer structure: A Monte Carlo study*. J. Magn. Magn. Mater. *324*(23) (2012), pp. 3991–3996.
[28] R. Masrour and A. Jabar, *Magnetic properties of bilayer graphene: a Monte Carlo study*. J. Comput. Electron. *16*(1) (2017), pp. 12–17.
[29] H.J. Wu, W. Wang, F. Wang, B.C. Li, Q. Li, and J.H. Xu, Monte Carlo study of an Ising nanoisland with bilayer graphene-like structure in a longitudinal magnetic field. J. Phys. Chem. Solids 136 (2020), p. 109174. Available at https://doi.org/10.1016/j.jpcs.2019.109174.
[30] M. Mouhib, A. El Fadl, S. Bri, M.D. Belrhiti, and H. Mounir, A Monte Carlo study of magnetic and hysteretic properties of a graphenic allotrope with a biphenylene network. The European Physical Journal B 98(11) (2025), p. 249. Available at https://doi.org/10.1140/epjb/s10051-025-00813-w.
[31] A. Jabar, S. Benyoussef, and L. Bahmad, Magnetic and magnetocaloric properties of a C_{20} fullerene structure: Monte Carlo study. J. Comput. Electron. 24(4) (2025), p. 128. Available at https://doi.org/10.1007/s10825-024-02263-y.
[32] M. Mouhib, A.E. Fadl, S. Bri, M.D. Belrhiti, and H. Mounir, The magnetic and hysteretic characteristics of bilayer graphene nanoribbons: a comparative study by the Monte Carlo method. Phys. Scr. 100(8) (2025), p. 085994. Available at https://doi.org/10.1088/1402-4896/ad67ec.
[33] S. Zouhair, H. Saadi, K. El Kihel, and M. El Bouziani, Critical Behavior and Compensation Phenomena in a Mixed Spin-(1, 5/2) Ising Ferrimagnetic Model on Graphene-like

Monolayer. J. Phys.: Condens. Matter 38(4) (2026), p. 045802. Available at https://doi.org/10.1088/1361-648X/ad9871.

[34] M. Mouhib, A.E. Fadl, S. Bri, M.D. Belrhiti, and H. Mounir, Magnetic properties dependence on stacking configurations of a trilayer graphene bond-diluted Ising model. J. Magn. Magn. Mater. 618 (2025), p. 173199. Available at https://doi.org/10.1016/j.jmmm.2024.173199.

[35] A. Obeidat, A. Almahmoud, and A. Al-Qawasmeh, Influence of rotation on magnetic properties of thin film. Physica A 655 (2024), p. 130179. Available at https://doi.org/10.1016/j.physa.2024.130179.

[36] A. Obeidat, S. Alqaiem, A. Al-Qawasmeh, M. Badarneh, and M.K. Qaseer, Magnetic properties of copper fluorides (Cu2F5 inverse spinel-like structure): A Monte Carlo study. Phys. B 654 (2023), p. 414698. Available at https://doi.org/10.1016/j.physb.2023.414698.

[37] A. Jabar and R.J.P.A.S.M. Masrour, Magnetic properties on a decorated triangular lattice: A Monte Carlo simulation. Physica A 538 (2020), p. 122959. Available at https://doi.org/10.1016/j.physa.2019.122959.

[38] H. Eraki, Z. Fadil, N. Maaouni, A. Mhirech, B. Kabouchi, L. Bahmad, and W.O. Benomar. Magnetization plateaus of a double fullerene core/shell like-nanostructure in an external magnetic field: Monte Carlo study. arXiv preprint arXiv:2109.01453, 2021.

[39] Z. Fadil, N. Saber, H. Eraki, A. Mhirech, B. Kabouchi, and L. Bahmad, *Study of the Blume–Emery–Griffiths model for mixed carbon-like nanotube: Monte Carlo study*. J. Low Temp. Phys. 210(1) (2023), pp. 285–296.

[40] A. Jabar, R. Masrour, A. Benyoussef, and M. Hamedoun, *Ferrimagnetic behaviors in a double-wall cubic metal nanotube: a Monte Carlo study*. J. Supercond. Novel Magn. 29(7) (2016), pp. 1953–1959.

[41] R. Masrour, A. Jabar, A. Benyoussef, M. Hamedoun, and L. Bahmad, *Hysteresis and compensation behaviors of mixed spin-2 and spin-1 hexagonal Ising nanowire core–shell structure*. Phys. B 472 (2015), pp. 19–24.

[42] R. Masrour, A. Jabar, A. Benyoussef, and M. Hamedoun, *Comparable studies of magnetic properties of Ising spins-5/2 and 3/2 systems on decorated square and triangular lattices*. J. Magn. Magn. Mater. 410 (2016), pp. 223–225.

[43] M. Qajjour, Z. Fadil, A. Mhirech, B. Kabouchi, L. Bahmad, and W. Ousi Benomar, *Magnetic properties of a Bi-layer borophene structure with mixed spins: Monte Carlo study*. J. Low Temp. Phys. 202(1) (2021), pp. 231–246.

[44] K. Fabian and R. Leonhardt, *Multiple-specimen absolute paleointensity determination: an optimal protocol including pTRM normalization, domain-state correction, and alteration test*. Earth Planet. Sci. Lett. 297(1-2) (2010), pp. 84–94.

[45] S. Zouhair, K. El Kihel, and M. El Bouziani, Magnetic properties, reentrant phenomenon, and phase diagrams in mixed half-integer spin (1/2, 5/2) Ising model under a random crystal field. Phys. B 723 (2025), p. 418080. Available at https://doi.org/10.1016/j.physb.2024.418080.

PHILOSOPHICAL MAGAZINE

Contact us

Editorial Department | digitaleditor@philosophicalmagazine.com

Taylor & Francis
by informa